

**COMPUTATIONAL INTELLIGENCE IN
PREDICTION OF WAVE TRANSMISSION
FOR HORIZONTALLY INTERLACED
MULTI-LAYER MOORED FLOATING
PIPE BREAKWATER**

Thesis

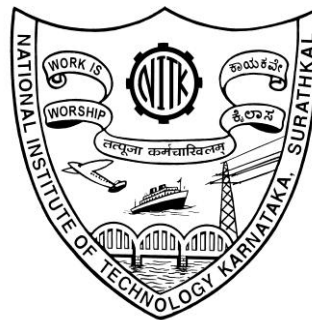
Submitted in partial fulfillment of the requirements for the degree of

DOCTOR OF PHILOSOPHY

by

PATIL SANJAY GOVIND

Register Number: AM07P01



DEPARTMENT OF APPLIED MECHANICS AND HYDRAULICS

NATIONAL INSTITUTE OF TECHNOLOGY KARNATAKA

SURATHKAL, MANGALORE –575 025

DECEMBER - 2012

DECLARATION

I hereby *declare* that the Research Thesis entitled “**Computational Intelligence in Prediction of Wave Transmission for Horizontally Interlaced Multi-layer Moored Floating Pipe Breakwater**” which is being submitted to the **National Institute of Technology Karnataka, Surathkal** in partial fulfillment of the requirements for the award of the Degree of **Doctor of Philosophy in Civil Engineering** is a *bonafide report of the research work carried out by me*. The material contained in this Research Thesis has not been submitted to any University or Institution for the award of any degree.

Register Number: AM07P01

Name of the Research Scholar: Patil Sanjay Govind

(Signature)

Department of Applied Mechanics and Hydraulics

Place: NITK- Surathkal

Date: 04.12.2012

CERTIFICATE

This is to *certify* that the Research Thesis entitled “**Computational Intelligence in Prediction of Wave Transmission for Horizontal Interlaced Multi-layer Moored Floating Pipe Breakwater**” submitted by **Patil Sanjay Govind** (Register Number: AM07P01) as the record of the research work carried out by him, is *accepted as the Research Thesis submission* in partial fulfillment of the requirements for the award of degree of **Doctor of Philosophy**.

Prof. Arkal Vittal Hegde
(Research Guide)

Dr. Sukomal Mandal
(Research Guide)

Prof. Subba Rao
(Chairman – DRPC)

DEPARTMENT OF APPLIED MECHANICS AND HYDRAULICS
NATIONAL INSTITUTE OF TECHNOLOGY KARNATAKA
SURATHKAL, MANGALORE –575 025

ACKNOWLEDGEMENTS

I express my deep sense of gratitude to my research supervisors Prof. Arkal Vittal Hegde, Professor, Department of Applied Mechanics and Hydraulics and Dr. Sukomal Mandal, Deputy Director, Ocean Engineering Division, National Institute of Oceanography for their encouraging, logical and critical suggestions during this work. The interaction and the time spent in discussions are imprinted in my memory permanently. Only with their moral support and guidance, this research work could be completed and I could publish my work in many international journals and conferences.

I express my deep sense of gratitude to the Director of National Institute of Technology Karnataka, Surathkal, for permitting me to carry out my research work and to make use of institutional infrastructure facilities.

I express my deep sense of gratitude to the Director of National Institute of Oceanography for permitting me to carry out my research work and to make use of institutional infrastructure facilities.

I am greatly indebted to Research Progress Appraisal Committee members, Prof. Ch. S. N. Murthy and Prof. Kasturi V. Bangera, for their useful suggestions during the progress of the work.

I sincerely acknowledge the help and support of Prof. M. K. Nagaraj, Head of the Department of Applied Mechanics and Hydraulics, NITK, Surathkal, for permitting me to use the departmental computing and laboratory facilities and his continuous support in completing the work.

I gratefully acknowledge the support and all help rendered by Mr. Amit S. Magadam Mr. Deepak J. Chandran, Mr. Jagdish Y. S. for the experimental data and I also thank Dr. Kiran Kamath for giving crucial insights on the performance characteristics of horizontally interlaced multi-layer moored floating pipe breakwater. I gratefully

acknowledge the support of Research Scholar Mr. Sachi Rajappa, Mr. Nagraj Gumageri, Mr. Harish and Mr. Srinivasulu during the research work.

I sincerely acknowledge the invaluable help rendered by my colleagues at Caledonian College of Engineering, Muscat, Oman, Mr. Srinivasan Alavandar; Senior Lecturer and Mr. Muruganandan; Lecturer.

I sincerely acknowledge Mr. B. Jagadish, Foreman, Department of Applied Mechanics and Hydraulics, and Mr. Balakrishna, Literary Assistant at NITK, Surathkal, for their support and help during the research work.

I express my heart felt gratitude to the authors of all those research publications which have been referred to in preparing this thesis.

Finally, I wish to express love and affection to my beloved family members, my Parents, my wife Rashmi for their continuous support and all the big and small sacrifices they had to make.

Sanjay Govind Patil

ABSTRACT

Energy dissipation process of Horizontally Interlaced Multi-layer Moored Floating Pipe Breakwater (HIMMFPB) depends on various factors like pipe interference effect, the spacing between the pipes and number of layers. As the effect of all these factors on transmission is not clearly understood, it will be extremely difficult to quantify them mathematically. Furthermore, it is a complex problem, and till now there has not been available a simple mathematical model to predict the wave transmission through HIMMFPB by considering all the boundary conditions, and hence one has to depend on physical model studies which are expensive and time consuming.

Computational Intelligence (CI) techniques, such as, Artificial Neural Network (ANN), Adaptive Neuro-Fuzzy Inference System (ANFIS), Support Vector Machine Regression (SVMR), Genetic Programming (GP) and Genetic Algorithm (GA) have been efficaciously proposed as an efficient tool for modelling and predictions in coastal/ocean engineering problems. For developing CI models in prediction of wave transmission for HIMMFPB, data set were obtained from experimental wave transmission of HIMMFPB using regular wave flume at Marine Structure Laboratory, National Institute of Technology, Karnataka, Surathkal, Mangalore, India. These data sets are divided into two groups, one for training and other for testing. The input parameters that influence the wave transmission (K_t) of floating breakwater, such as, relative spacing to pipes (S/D), relative breakwater width (W/L), ratio of incident wave height to water depth (H_i/d), incident wave steepness (H_i/L) are considered in developing CI models for prediction of wave transmission past HIMMFPB. In the present work, five layer pipes with S/D of 2, 3, 4 and 5 are considered.

The ANN model is developed for prediction of wave transmission for HIMMFPB. Two network models, ANN1 and ANN2 are constructed based on the parameters which influence the wave transmission of floating breakwater. The input parameters of ANN1 model are W/L , H_i/d and H_i/L . To study over a range of spacing of pipes

S/D on K_t , an input parameter, S/D is added to form ANN2 model. Training and testing of the network models are carried out for different hidden nodes and epochs. It is observed that the correlation (above 90%) between predicted wave transmission values by the network models and measured values are in good agreement.

Furthermore, to improve the result of prediction of wave transmission of HIMMFPB, recently developed technique such as SVMR is used. This technique works on structural risk minimization principle that has greater generalization ability and is superior to the empirical risk minimization principle as adopted in conventional neural network models. Support vector machines (SVMs) are based on statistical learning theory. The basic idea of support vector machines is to map the original data x into a feature space with high dimensionality through a non-linear mapping function and construct an optimal hyper-plane in new space. Six SVMR models are constructed using kernel functions. In order to study the performance of each kernel in predicting wave transmission of HIMMFPB, SVMR is trained by applying these kernel functions. Performance of SVMR is based on the best setting of SVMR and kernel parameters. Correlation Coefficient (CC) of SVMR (b-spline) model (CC Train = 0.9779 and CC Test = 0.9685) is considerably better than other SVMR models.

However, it is noticed that ANN model in isolation cannot capture all data patterns easily. Adaptive neuro-fuzzy inference system (ANFIS) uses hybrid learning algorithm, which is more effective than the pure gradient decent approach used in ANN. ANFIS models are developed to predict wave transmission of HIMMFPB. The performance of the ANFIS models in the prediction of K_t is compared with the measured values using statistical measures, such as, CC, Root mean Square Error ($RMSE$) and Scatter Index (SI). All the ANFIS models have shown CCs higher than or equal to 0.9510, with $RMSE$ less than or equal to 0.051074 and SI less than or equal to 0.102296. ANFIS5 model predictions are very realistic when compared with the measured values (CC Train = 0.9723, CC Test = 0.9635). It is also observed that an S/D plays an important role to train ANFIS5 model to map an input-output relation. Furthermore influence of input parameters is assessed using Principal

Component Analysis (PCA). It is observed that H_i/L is the least influential parameter. Based on the PCA study discarding the least influential parameters, ANFIS6 model is developed. It is observed that the ANFIS models yield higher CCs as compared to that of ANN models.

To improve the performance of SVMR and better selection of SVMR and kernel parameters, hybrid genetic algorithm tuned support vector machine regression (GA-SVMR) model is developed to predict wave transmission through HIMMFPB. Furthermore, parameters of both linear and nonlinear SVM models are determined by GA. The results are compared with ANN, SVMR and ANFIS models in terms of CC, *RMSE* and *SI*. Performance of GA-SVMR is found to be reliably superior.

CI models can be utilized to provide a fast and reliable solution in prediction of the wave transmission for HIMMFPB, thereby making GA-SVMR as an alternate approach to map the wave structure interactions of HIMMFPB.

Keywords: Floating Breakwaters; Wave Transmission; HIMMFPB; Artificial Neural Networks; Neuro-Fuzzy; ANFIS; SVMR; GA; GA-SVMR; Principal Component Analysis.

CONTENTS

ACKNOWLEDGEMENTS	i
ABSTRACT	iii
CONTENTS	vi
LIST OF FIGURES	ix
LIST OF TABLES	xii
LIST OF PLATES	xiv
LIST OF NOTATIONS	xv
CHAPTER 1 INTRODUCTION	1
1.1 GENERAL	1
1.2 BREAKWATERS	2
1.2.1 Rubble mound or heap breakwaters	3
1.2.2 Upright or vertical wall breakwaters	4
1.2.3 Mounds with superstructure or composite breakwaters	5
1.2.4 Special type breakwaters	6
1.3 FLOATING BREAKWATERS	7
1.3.1 Classification of floating breakwaters	8
1.3.2 Wave transmission of floating breakwaters	11
1.3.3 Advantages and disadvantages of floating breakwaters	12
1.4 SCOPE OF THE PRESENT INVESTIGATIONS	13
1.5 ORGANIZATION OF THE THESIS	14
1.6 SUMMARY	16
CHAPTER 2 LITERATURE REVIEW	17
2.1 GENERAL	17
2.2 REVIEW OF THEORETICAL ANALYSIS	18
2.3 REVIEW OF LITERATURE ON APPLICATIONS OF COMPUTATIONAL INTELLIGENCE IN COASTAL / OCEAN ENGINEERING	28

2.4	PROBLEM FORMULATION	45
2.5	OBJECTIVES OF THE PRESENT INVESTIGATIONS	46
2.6	SUMMARY	47
CHAPTER 3	EXPERIMENTAL MODEL SETUP AND DATA USED	48
3.1	GENERAL	48
3.2	EXPERIMENTAL SETUP	49
3.2.1	Wave flume	49
3.2.2	About experimental HIMMFPB model	52
3.2.3	Instrumentation used	54
3.3	EXPERIMENTAL PROCEDURE	54
3.4	EXPERIMENTAL DETAILS OF HIMMFPB	55
3.5	EXPERIMENTAL DATA OF HIMMFPB	56
3.6	SUMMARY	58
CHAPTER 4	RESEARCH METODOLOGY	59
4.1	GENERAL	59
4.2	ARTIFICIAL NEURAL NETWORK	60
4.2.1	Introduction	60
4.2.2	Architecture of a ANN	62
4.2.3	Feed forward back-propagation neural network	63
4.2.4	Levenberg-Marquardt method	66
4.2.5	Feed forward back-propagation neural network model for wave transmission prediction of HIMMFPB	67
4.3	ADAPTIVE NEURO FUZZY INFERENCE SYSTEM	70
4.3.1	Introduction	70
4.3.2	ANFIS architecture	70
4.3.3	Fuzzy logic approach for wave transmission prediction of HIMMFPB	74
4.4	SUPPORT VECTOR MACHINE REGRESSION	79
4.4.1	Introduction	79
4.4.2	Theoretical background of SVMR	80

4.4.3	Support vector machine regression for wave transmission prediction of HIMMFPB	84
4.5	GENETIC ALGORITHM FOR SELECTING PARAMETERS IN THE SVMR MODEL	86
4.6	THE PROPOSED GA-SVMR MODEL	89
4.7	SUMMARY	91
CHAPTER 5	RESULTS AND DISCUSSION	92
5.1	GENERAL	92
5.2	PERFORMANCE OF FEED FORWARD BACK-PROPAGATED NEURAL NETWORK MODEL (ANN)	92
5.2.1	Estimation of K_r by ANN2 Model	100
5.3	PERFORMANCE OF SUPPORT VECTOR MACHINE REGRESSION MODEL (SVMR)	102
5.4	PERFORMANCE OF ADAPTIVE NEURO FUZZY INFERENCE SYSTEM MODEL (ANFIS)	111
5.5	PERFORMANCE OF GENETIC ALGORITHM BASED SUPPORT VECTOR MACHINE REGRESSION (GA-SVMR)	124
5.6	SUMMARY	133
CHAPTER 6	CONCLUSIONS	134
6.1	GENERAL	134
6.2	CONCLUSIONS	134
6.3	SUGGESTIONS FOR FUTURE WORK	136
6.4	SUMMARY	137
APPENDIX I	MATLAB CODES FOR DEVELOPING CI MODELS	138
REFERENCES		159
LIST OF PUBLICATIONS FROM PRESENT WORK		173
RESUME		175

LIST OF FIGURES

Figure No.	Title	Page No.
1.1	Typical cross section of rubble mound breakwater (Fousert, 2006)	3
1.2	Conventional caisson breakwater with vertical front (Fousert, 2006)	4
1.3	Composite breakwater (Fousert, 2006)	5
1.4	Typical floating breakwater (Fousert, 2006)	7
1.5	Flexible assemblies type floating breakwater	9
1.6	Single prism-type floating breakwater	10
1.7	Catamaran type floating breakwater	10
1.8	A-frame floating breakwater	11
2.1	Fig. 2.1 Sketch showing floating breakwater to full depth of water as per Carr (1951)	19
3.1	Regular wave flume setup for the present investigations (Jagadisha, 2007)	51
3.2	Typical Experimental set up of HIMMFPB	52
3.3	Details of five layers of pipes	52
4.1	A biological nerve cell	59
4.2	Basic Neuron Model	60
4.3	Feed forward Back-propagation Network	62
4.4	ANFIS Structure	70
4.5	ANFIS procedure	74
4.6	Physical meaning of the parameters in the bell membership function	76
4.7	Initial membership functions of input parameters (x-axis) for ANFIS5 model	76
4.8	The loss margin setting corresponds to one-dimensional linear SV machine	81
4.9	Genetic Algorithm Procedure	86
4.10	Flow chart of GA-SVMR	89
5.1	Fig. 5.1 Comparison of predicted and measured K_t for ANN1	94

	model with $S/D = 2$	
5.2	Fig 5.2 Comparison of predicted and measured K_t for ANN1 model with $S/D = 3$	95
5.3	Comparison of predicted and measured K_t for ANN1 model with $S/D = 4$	96
5.4	Comparison of predicted and measured K_t for ANN1 model with $S/D = 5$	97
5.5	Comparison of predicted and measured K_t for ANN2 model	98
5.6	ANN2 structure with weights and biases	100
5.7	Comparison of predicted and measured K_t for SVMR (linear) model	104
5.8	Comparison of predicted and measured K_t for SVMR (polynomial) model	105
5.9	Comparison of predicted and measured K_t for SVMR (rbf) model	106
5.10	Comparison of predicted and measured K_t for SVMR (erbf) model	107
5.11	Comparison of predicted and measured K_t for SVMR (spline) model	108
5.12	Comparison of predicted and measured K_t for SVMR (b-spline) model	109
5.13	Final membership functions of input parameters (x-axis) for ANFIS5 model	110
5.14	Fuzzy rule architecture of the generalized bell membership function for ANFIS5 model	111
5.15	Comparison of predicted and measured K_t for ANFIS1 model	117
5.16	Comparison of predicted and measured K_t for ANFIS2 model	118
5.17	Comparison of predicted and measured K_t for ANFIS3 model	119
5.18	Comparison of predicted and measured K_t for ANFIS4 model	120
5.19	Comparison of predicted and measured K_t for ANFIS5 model	121

5.20	Comparison of predicted and measured K_t for ANFIS6 Model	122
5.21	Comparison of predicted and measured K_t for GA-SVMR (linear) model	126
5.22	Comparison of predicted and measured K_t for GA-SVMR (polynomial) model	127
5.23	Comparison of predicted and measured K_t for GA-SVMR (rbf) model	128
5.24	Comparison of predicted and measured K_t for GA-SVMR (erbf) model	129
5.25	Comparison of predicted and measured K_t for GA-SVMR (spline) model	130
5.26	Comparison of predicted and measured K_t for GA-SVMR (b-spline) model	131

LIST OF TABLES

Table No.	Title	Page No.
3.1	Details of the wave-specific and structure-specific parameters of HIMMFPB (Magadum, 2005; Deepak, 2006; Jagadisha, 2007)	55
3.2	Number of data points and input parameters used to train CI models	56
4.1	ANN models with input parameters	67
4.2	ANFIS models with input	73
4.3	Principal component analysis	78
4.4	Factor loading of principal components	78
4.5	Data used for training and testing the SVMR models with input parameters	83
4.6	Kernel Functions	84
4.7	Data used for training and testing the GA-SVMR models with input parameters	88
5.1	Correlation coefficient of K_t for ANN1 model with $S/D=2$	92
5.2	Correlation coefficient of K_t for ANN1 model with $S/D=3$	93
5.3	Correlation coefficient of K_t for ANN1 model with $S/D=4$	93
5.4	Correlation coefficient of K_t for ANN1 model with $S/D=5$	93
5.5	Correlation coefficient of K_t for ANN2 model	99
5.6	Correlation coefficients of K_t for two network models	99
5.7	SVMR models with statistical measures	102
5.8	Optimal parameters for SVMR models with different kernels	103

5.9	Premise parameters for ANFIS5 model	112
5.10	Fuzzy <i>IF – THEN</i> rules after training for ANFIS4 model	114
5.11	ANFIS models with statistical measures for train and test data	116
5.12	ANN and SVMR models with correlation coefficients of K_t	116
5.13	GA-SVMR models with statistical measures	123
5.14	Optimal parameters for GA-SVMR models with different kernels	123
5.15	ANN and ANFIS models with statistical measures	125

LIST OF PLATES

Plate No.	Title	Page No.
3.1	View of the experimental set up (Jagadisha, 2007)	50
3.2	View of the floating pipe breakwater model with five layers of pipes and $S/D = 5$ (Jagadisha, 2007)	53

LIST OF NOTATIONS

Symbol	Description
C	Capacity factor
D	Diameter of pipes
d	Still water depth
ε	Error in error tube
S/D	Relative spacing to pipes
W/L	Relative breakwater width
H_i/d	Ratio of incident wave height to water depth
H_i/L	Incident wave steepness
H_i	Incident wave height
K_r	Reflection coefficient
K_t	Transmission coefficient = H_t/H_i
L	Wavelength
l	Length of breakwater
n	Number of layers of pipes
nsv	Number of support vector
S	Centre-to-centre spacing between the pipes
W	Width of the breakwater measured along direction of wave propagation.
 Greek	
γ	Specific weight of water
σ	Standard deviation
η	Displacement of water surface from mean water level
μ	Dynamic viscosity
ρ	Mass density of water
 Abbreviations	
ANN	Artificial Neural Network
ANFIS	Adaptive neuro-fuzzy Inference system

CI	Computational intelligence
CC	Correlation coefficient
CERC	Coastal Engineering Research Centre
erbf	Exponential radial basis function
FIS	Fuzzy Inference System
GP	Genetic programming
GA	Genetic algorithm
GA-SVMR	Genetic algorithm based support vector machine regression
HIMMFPB	Horizontal Interlaced Multi-layer Moored Floating Pipe Breakwater
NITK	National Institute of Technology Karnataka
PCA	Principal component analysis
PVC	Polyvinyl Chloride
<i>RMSE</i>	Root mean square error
rbf	Radial basis function
<i>SI</i>	Scatter index
SWL	Still Water Level
SVM	Support vector machines
SVMR	Support vector machine regression
VLFS	Very Large Floating Structure

CHAPTER 1

INTRODUCTION

1.1 GENERAL

The environmental stress on the coastal zone is rapidly growing and there is a need to protect the coastal environment. The development of structures to provide protection against the destructive forces of the sea waves and to withstand the action of waves has been the constant challenge to coastal engineers. The coastal defense works such as seawalls, groins, offshore breakwaters, artificial nourishments have been tried to overcome the problem of erosion. Some of them have been successful while some others have failed to perform the job assigned for this purpose. The failure may be due to improper location and design or wrong choice of protective measures. The cause for the erosion is generally due to the concentration of wave energy at a specific location. Hence there is a need to dissipate the wave energy before it reaches coast. The use of breakwaters is one of the solutions to dissipate the wave energy. Breakwaters are constructed primarily to reduce or prevent wave action in an area which is to be sheltered. The waters directly behind the structure are protected from wave action and are comparatively calmer than the seaward waters.

The requirement of any port, harbor or marina is sheltered area, free from the sea waves. In the coastal areas where natural protection from waves is not available, the development of harbor requires an artificial protection for the creation of calm areas. For large harbors, where perfect tranquility conditions are required, large structures such as rubble mound breakwaters or vertical wall breakwaters are used. However, for small recreational harbors or fisheries harbor and marinas where large littoral drift and on-shore and off-shore sediment movement exists, floating breakwater are most suitable in such circumstances. In recreational harbors swimmers and surfers prefer to have acceptable wave conditions to suit their sporting activity and for fisheries harbor,

where high level of tranquility conditions are not necessary. In such cases expensive rubble mound or vertical wall breakwaters may not be the right choice.

In the last two decades, floating breakwaters (McCartney, 1985; Mani, 1991; Murali and Mani, 1997; Sannasiraj et al., 1998; Sundar et al., 2003; Deepak, 2006; Hegde et al., 2007; Jagadisha, 2007; Kamath, 2010) have generated a great interest in the field of coastal engineering, as floating breakwaters are less expensive compared to conventional type breakwaters. In addition, they have several desirable characteristics such as, comparatively small capital cost, adoption to varying harbour shapes and sizes, short construction time and freedom from silting and scouring. Floating breakwaters could also be utilized to meet location changes, extent of protection required or seasonal demand. They can be used as a temporary protection for offshore activities in hostile environment during construction, drilling works, salvage operation etc. In order to design a floating breakwater, it is necessary to study the motion characteristics of the structure. Hence, a study on wave transmission of the floating breakwater would provide a proper configuration to the structure. Several researchers have carried out experimental, analytical and numerical studies on floating breakwaters in the past but failed to give a simple mathematical model to predict the wave transmission through floating breakwaters by considering all the boundary conditions. It would be appropriate to discuss conventional breakwater in brief, types of floating breakwater and their relative merits over conventional breakwater.

1.2 BREAKWATERS

Breakwaters are barriers, either natural or artificial, that extend into the open water of a sea or a lake to break the force of the waves and provide calm water in a harbor. Natural breakwaters are offshore islands and promontories that shelter the shore from waves. Artificial breakwaters may be attached to the land or separated from it and are constructed in various shapes and sizes. They can be built of stones and rubble, of masonry, or of a combination of these. Since sea waves have enormous energy; the construction of structures to mitigate such energy is not easily accomplished. As these

structures need a considerable amount of initial investment, they should be properly aligned, designed and constructed.

An optimum breakwater from its hydraulic performance point of view should transmit and reflect wave energy as low as possible and dissipate the energy as high as possible. Various types of breakwaters are in use throughout the world. Research activities are in progress to study the performance characteristics of different types of breakwaters in order to recommend the most feasible one for a given prevailing environment. Breakwaters are classified mainly as:

- Rubble mound or heap breakwaters
- Upright or vertical wall breakwaters
- Mound with superstructure or composite breakwaters
- Special type of breakwaters

1.2.1 Rubble mound or heap breakwaters

Rubble mound breakwaters are the oldest form of harbor protection structure. They are simple to build and easier to maintain. Rubble components may be obtained from local sources or quarries near or far. Consequently, the variation in size and shape, mineral content, hardness, abrasion resistance and other physical property is extremely wide. They do not require skilled labour for construction. However, for

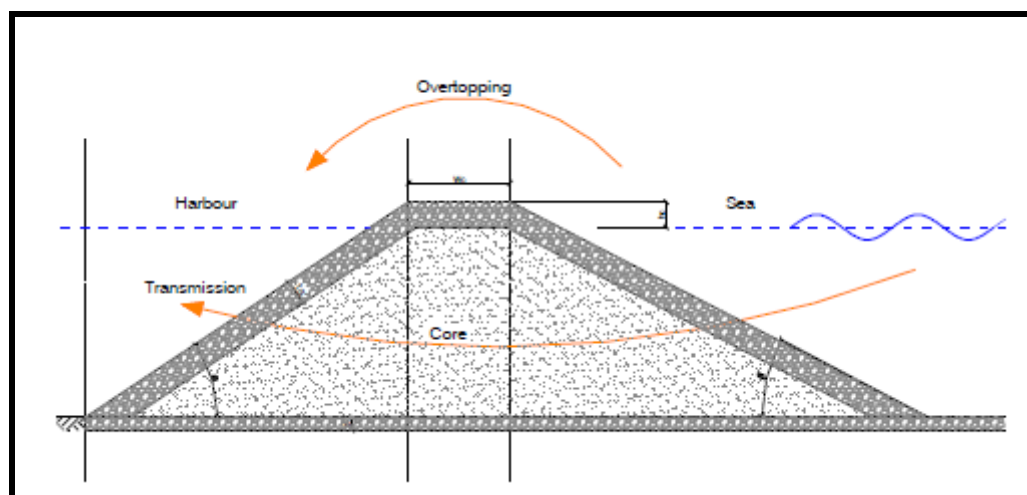


Fig. 1.1 Typical cross section of rubble mound breakwater (Fousert, 2006)

deep water sites and at locations having large tidal ranges, the quantity of stones required may be large, causing high expenditure. A rubble mound structure is normally composed of a bedding layer and a core of quarry-run stone covered by one or more layers of larger stone and an exterior layer of large quarry stone or concrete armor units. Typical rubble mound cross sections are shown in Fig. 1.1 (Fousert, 2006). The figure illustrates cross section features typical of designs for breakwaters exposed to waves on one side (seaward) and intends to allow minimal wave transmission to the other (leeward) side. Breakwaters of this type are usually designed with crest elevated to allow overtopping only in very severe storms with long return periods.

1.2.2 Upright or vertical wall breakwaters

These breakwaters are of types such as huge concrete blocks, gravity walls, concrete caissons, rock filled timber cribs and concrete or steel sheet pile walls as indicated in Fig. 1.2 (Fousert, 2006). Vertical wall structures are used as breakwaters, seawalls, and bulkheads in

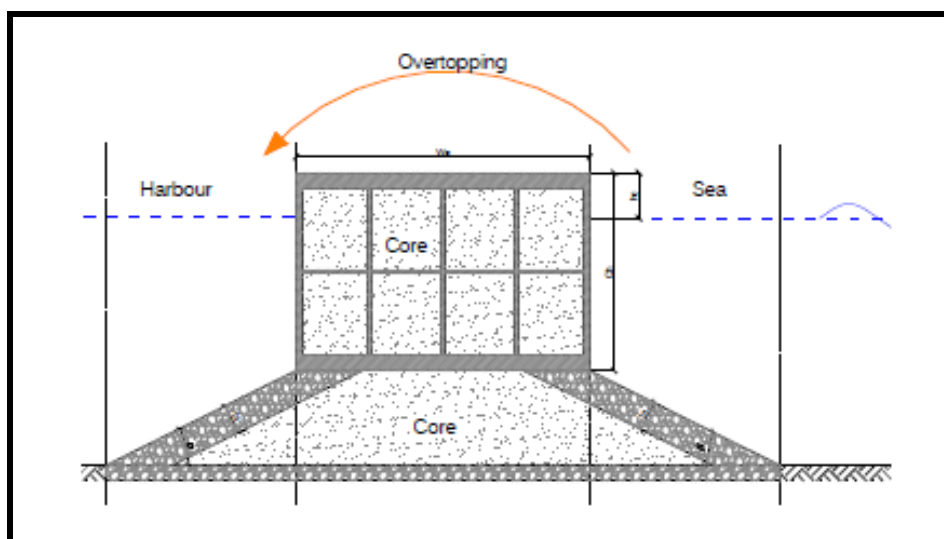


Fig. 1.2 Conventional caisson breakwater with vertical front (Fousert, 2006)

harbors. The vertical structure accommodates port activities because ships can be moored next to the structure to facilitate loading and unloading activities. Generally

vertical wall structures are designed to reflect the incident wave energy with little or no overtopping. The main disadvantage of vertical wall breakwater is that, it cannot be easily repaired and consequences of failures are always catastrophic. The failures are mainly because of the scour at toe of the structure. The construction of this type of breakwaters requires high technical knowledge, heavy construction equipment and skilled labor leading to heavy expenditure.

1.2.3 Mounds with superstructure or composite breakwaters

These structures usually combine a rubble mound base through part of water column, topped by a vertical monolithic structure as shown in Fig. 1.3 (Fousert, 2006). The rubble base of composite structure strengthens the foundation, and the vertical portion offers the mooring advantages of vertical structure. These are used in locations where either the depth of water is large or there is a wide tidal range and in such situations, the quantity of rubble stone required to construct a breakwater of the full height would be very large. In such conditions, a combination of rubble mound and vertical wall or other form of super structure is adopted.

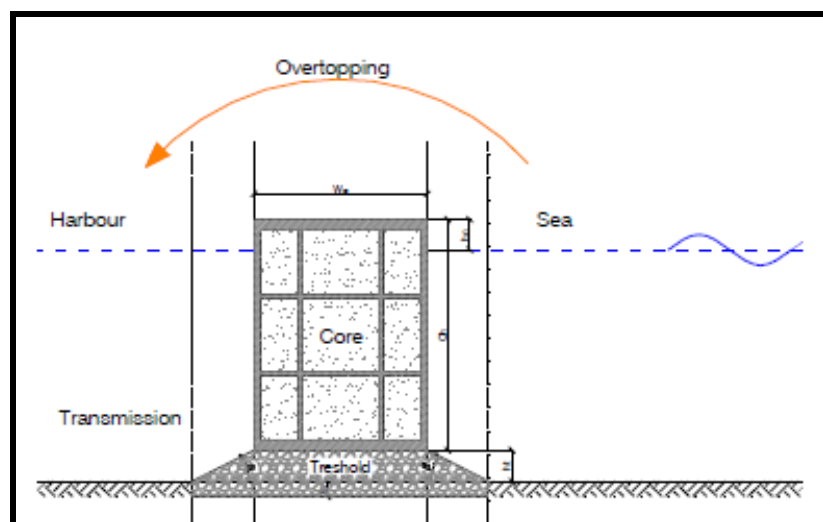


Fig. 1.3 Composite breakwater (Fousert, 2006)

Although the designs of the breakwaters differ from one another, a number of similarities can be identified. They are all built to block the incoming waves and to dissipate or reflect the wave energy. They are all fixed structures, designed for a

specific location. Bottom-founded structures are limited to a certain maximum water depth since these structures are not practical in deep water environments from a technical as well as an economical point of view.

1.2.4 Special type of breakwaters

Special type breakwaters are those employing some kind of special features and are not commonly used. Special type breakwaters can be divided into two kinds. One is the non-gravity type breakwaters such as pile type, floating, pneumatic etc. The other is the conventional breakwater with special features conceived to improve the functioning and stability of breakwater. Some special breakwaters are as follows:

- Curtain wall breakwater – commonly used as secondary breakwater to protect small craft harbors.
- Sheet pile walls – are used to break relatively small waves.
- Horizontal plate breakwater – can reflect and break waves and are supported by a steel jacket.
- Floating breakwater – very useful as breakwater in deep waters especially in places where the ground soil is poor for foundation
- The pneumatic breakwater – breaks the wave due to water current induced by air bubbles.

Breakwaters can further be classified into two categories based on their mobility. The first is permanent structure (immovable) and the second is a temporary structure (movable). Rubble mound, vertical wall and composite types of breakwaters are examples for the first type. The floating breakwater illustrates the second type. The permanent structure is desirable for harbors having intensive loading and unloading activities throughout the year. The cost of construction of permanent structures type breakwater increases rapidly for deeper waters. The floating breakwaters can be utilized for deeper waters, which have the following advantages. Its cost of construction does not increase rapidly with increase in depths. They do not offer obstruction to water circulation, fish migration and sediment transport beneath the

breakwater. They are mobile and can be relocated, if necessary. Their construction is less dependent on bottom soil conditions. The other features of the floating breakwater include short construction time, freedom from silting, scour and foundation problems and relatively small initial cost compared to conventional breakwaters.

1.3 FLOATING BREAKWATERS

A floating breakwater is a barrier floating at still water level Fig. 1.4 (Fousert, 2006).

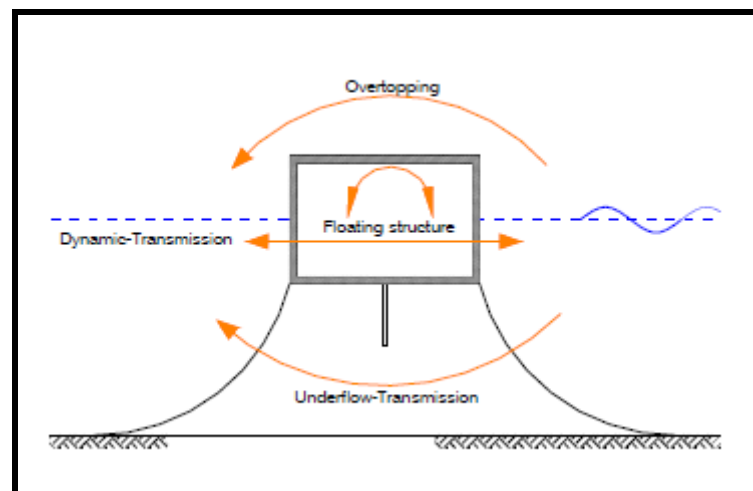


Fig. 1.4 Typical floating breakwater (Fousert, 2006)

In most of the engineering applications, situations frequently arise, where sheltering of areas, in the near shore and offshore regions are required for short time to carry out a specific task in the calm zone. These tasks could be creation of temporary harbors for many purposes including defense, short time commercial operations, summer recreational facilities and reclamation of sea as well as erection of structures on these lands. Advantages are that they can be fabricated at remote sites and deployed in deep water or where foundations are difficult for conventional breakwater constructions. They also allow better water circulation, have very less impact on sediment transport, and fish migration than the conventional breakwaters.

This type of breakwater is of transportable type, which can be effectively used at different places in and around sheltered areas wherever needed. Further, the classical and most effective way to prevent the spread of oil spilled in harbors or other areas of sea is by surrounding the spill with floating barriers. Due to its mobility, this breakwater can be used at any location where construction of conventional breakwater is ruled out in the view of their high cost, impossibility of their reuse and perhaps construction time.

1.3.1 Classification of floating breakwaters

In recent years research work on floating breakwater has given the ocean engineers a wide spectrum of choice for the types of breakwaters depending on the situation and purpose for which the breakwater is intended. Based on the types developed and tested so far the floating breakwaters can be categorized into the following types:

- Pneumatic and Hydraulic breakwaters
- Flexible floating structures
- Rigid floating structures

Pneumatic and hydraulic breakwaters

An artificial surface current can be produced by the air bubbles released from a compressed air manifold on the bed or by means of horizontal water jets from a pipe floating on the water surface. If the surface current is of sufficient magnitude and is directed towards the oncoming waves, the length of the wave is reduced and their height increased until instability occurs and the wave either breaks or is reflected.

When air is used, the device is termed as Pneumatic breakwaters and when water jets are used, they are referred to as hydraulic breakwaters. The principle of operation of such a system is based upon the development of the vertical current of water or air which rises to the structure and spreads out more or less horizontally in both the upstream and downstream directions of the breakwater system. Although such

breakwater seem appealing for its simplicity of operation it is imperative for generating the air bubbles or water jets that could demand exorbitant amount of fuel.

Flexible floating breakwater

Flexible type of breakwater is represented in Fig. 1.5. Most of the flexible breakwaters have reasonably good wave attenuation capacity if the ratio of length of the breakwater to the wavelength is larger than one (length measure parallel to the wave propagation).

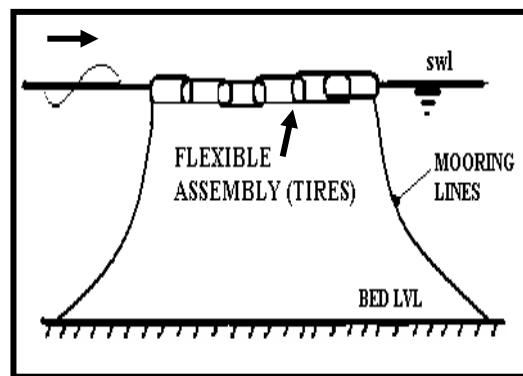


Fig. 1.5 Flexible assemblies type floating breakwater

Floating rigid breakwaters

Like the fixed rigid structure, the floating rigid breakwaters reduces wave transmission by dissipation through breaking, reflection, friction or by interaction of waves, so that the orbital motion of the water particles is reduced. They may be divided into pontoon type structures, either vertical or horizontal, perforated models and miscellaneous structures of specific shape. The prismatic forms offer the best prospect for multiple use i.e., walkways, boat slips etc. Kato et al. (1969) reported an interesting comparison of the rectangular and trapezoidal sections. The inverted shape yielded lower transmission coefficients, but developed higher anchor forces. This type of breakwater is shown in Fig. 1.6. One of the main advantages of these floating rigid

or a flexible structure is its indifference to tidal level changes. Although during the past, considerable work has been done on the evaluation performance characteristics of floating breakwater and many significant contributions have been made for its development, none has achieved perfection considering all factors.

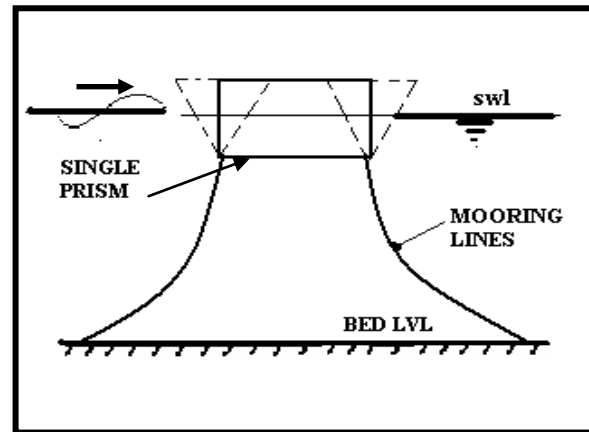


Fig. 1.6 Single prism-type floating breakwater

The Catamaran pontoon illustrates one way of distributing a given mass to achieve a longer roll period and potentially a more stable platform than would be achieved with a same mass of single prism as shown in Fig. 1.7. The extra corners provide additional

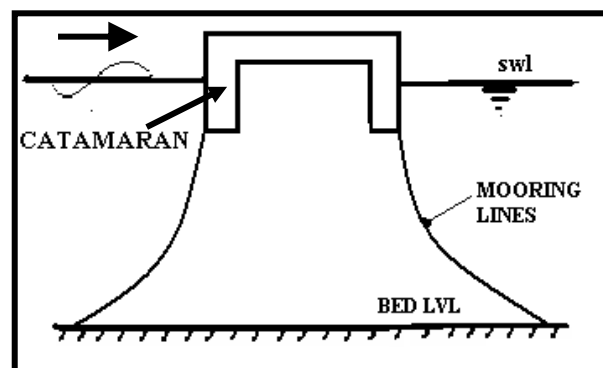


Fig. 1.7 Catamaran type floating breakwater

zones of energy loss, and the water mass between the hulls may add damping action, especially to sway (beam wise) excitation. The members of this group utilize combination of vertical walls as reflecting surfaces and outriggers for the stability to

develop a large roll period for a given weight. Brebner and Ofuya (1968) conducted extensive research on this type of breakwater. For the 'A' frame breakwater, they found that the range of effectiveness of a floating breakwater can be increased by large increase of its radius of gyration, involving only a slight increase of its mass. A-frame breakwater is indicated in Fig. 1.8.

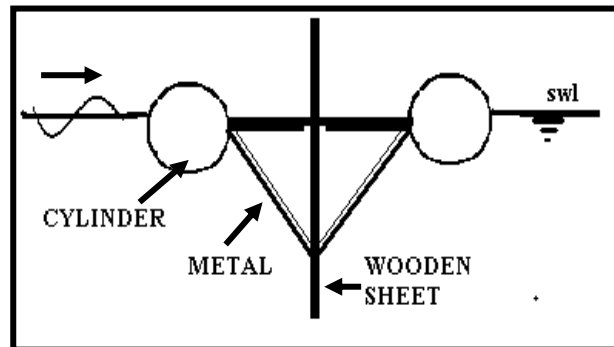


Fig. 1.8 A-frame floating breakwater

One restricting design parameter is the W/L (wavelength-to-breakwater width) ratio, McCartney (1985). As this value increases, the wave transmission coefficient, K_t , decreases. The wave transmission coefficient is the ratio of the wave height transmitted across the breakwater to the incident wave height.

1.3.2 Wave transmission of floating breakwater

The design of floating breakwater is based on the principle that the wave energy is concentrated at the surface in deep water and the same energy is concentrated at below the surface in shallow water, which is to be dissipated. Therefore different types of floating breakwaters like Box, Pontoon, Mat, Tethered float and Pipe are becoming popular. Morgan (1969) reported floating breakwaters attenuate wave heights by one or more of the following methods:

- Destruction of wave orbital motion – by the use of random placing of surface floats.
- Viscous damping – by the use of a thin membrane on the water surface.
- Dissipation of wave energy by breaking – by use of the floating slope.

- Out of phase damping – by using an air-filled flexible bag below the water surface.
- Wave reflection – which all floating breakwaters do to varying degrees.

The basic concept by which floating breakwater reduces wave energy include reflection, dissipation, interference and conversion of the energy into non-oscillatory motion. The prime factor in the construction of floating breakwater is to make the width of the breakwater in the direction of wave propagation greater than one-half the wavelength and preferably as wide as incident wavelength. Otherwise, the breakwater rides over the top of the wave without attenuating it. Pontoon and Box types of floating breakwaters belong to the category in which the wave attenuation is achieved by reflecting the wave energy. Mat and Tethered belong to the other category, in which wave energy dissipation is mainly due to drag from the resultant float in motion. Pipe breakwaters mainly dissipate the wave energy, and also partly reflect and transmit the waves. For effective reflection, the breakwater should remain relatively motionless and penetrate to a depth sufficient to prohibit appreciable wave energy from passing underneath.

1.3.3 Advantages and disadvantages of floating breakwaters

Over the years, many different types of floating breakwaters have been developed and many conclusions have been drawn. Some of the advantages of floating breakwaters include:

- Floating breakwaters are an economic alternative to fixed structures for use in deep waters (depths greater than 6000 mm).
- Poor soil conditions may make floating breakwaters the only option available.
- Floating breakwaters minimize the interference on water circulation and fish migration.
- If ice formation presents a problem, floating breakwaters can be removed from the site.

- Floating breakwaters are not obtrusive and can be more aesthetically pleasing than fixed structures.
- Floating breakwaters can easily be rearranged in a different layout or transported to another site for maximum efficiency.

Some of the disadvantages of floating breakwaters are:

- Floating breakwaters are ineffective in reducing wave heights for low steepness waves.
- Floating breakwaters are susceptible to structural failure during catastrophic storms.
- Relative to conventional fixed breakwaters, floating breakwaters require a high amount of maintenance.

1.4 SCOPE OF THE PRESENT INVESTIGATIONS

Several researchers in the past have carried out experimental, theoretical and numerical investigations on different types of floating breakwaters, such as, horizontal, sloping, A-type, Y-type, Cage, pontoon, tires, pipes etc., [Homma et al.(1964), Brebner and Ofuya (1968), Harris and Webber (1968), Kennedy and Marsalek (1968), Chen and Weigel (1970), Ito and Chiba (1972), Adee and Martin (1974), Seymour (1976), Arunachalam and Raman (1980), Yamamoto et al. (1980), Bishop (1982), Leach et al. (1985), Sastry et al. (1985), Muralikrishna et al. (1987), Mani and Venugopal (1987), Harms (1979), Mani (1991), Williams et al. (1991), Murali and Mani (1997), Williams and Azm (1997), Sannasiraj et al. (1998), Rao (2000), Briggs et al. (2002), Hermanson (2003), Liang et al. (2003), Sundar et al. (2003), Stiassnie and Drimer (2003), Li et al. (2005), Loukogeorgaki and Angelides (2005) Ruol et al. (2008)]. These studies are carried out considering a floating breakwater in basic form with some assumptions common in hydrodynamics, which shows less improvement. It is also found that most of the numerical methods have been attempted on simple box-type rectangular floating breakwaters or spar buoy

floating breakwaters. Till now, there has not been available a simple mathematical model to predict a wave transmission through floating breakwaters by considering all the boundary conditions.

A Horizontal Interlaced Multi-layer Moored Floating Pipe Breakwater (HIMMFPB) was developed at Marine Structure Laboratory of National Institute of Technology Karnataka, Surathkal, Mangalore, India to attenuate the wave transmission to the shore (Amit, 2005; Deepak, 2006; Jagadisha, 2007). The pipe breakwater is floating and intended to be economical as the material involved in its construction is poly-vinyl chloride (PVC) pipes, which are relatively inexpensive compared to other materials and also easily available in the market.

For floating pipe breakwaters, the energy dissipation process depends on various other factors like pipe interference effect, the spacing between the pipes and number of layers. As the effect of all these factors on transmission and forces in the moorings is not clearly understood, it will be extremely difficult to quantify them mathematically. Still it is a complex problem. From the literature review (chapter 2), it is found that, CI techniques, such as, ANN, fuzzy logic, ANFIS, SVMR, GA and genetic programming are successfully used to solve complex problems associated with coastal/ocean engineering. However, it is observed that there are hardly any applications of CI on the wave transmission of floating pipe breakwater and HIMMFPB.

1.5 ORGANIZATION OF THE THESIS

The thesis is presented in Six chapters.

- Chapter 1 - Introduction: Introduction to breakwaters and a short overview of the conventional breakwaters, special types of breakwaters, introduction to floating breakwaters, wave transmission of floating breakwaters, its advantages and disadvantages, scope of the present investigations has been discussed.

- Chapter 2 - Literature review: The literature review on theoretical and analytical studies specifically related to floating breakwaters, applications of computational intelligence in coastal/ocean engineering, problem formulation and objectives of present work have been discussed.
- Chapter 3 – Experimental setup and data used: Deals with the experimental investigations carried out in the regular wave flume at the department of applied mechanics and hydraulics, National Institute of Technology Karnataka (NITK), Surathkal, India, and it features the experimental model set up, and data used for developing CI models.
- Chapter 4 – Research Methodology: In this chapter, theoretical background of research methods used to developed CI models to predict wave transmission of HIMMFPB, such as, ANN, ANFIS, SVMR and GA has been discussed.
- Chapter 5 – Results and Discussion: The results obtained from the CI models, such as, ANN, ANFIS, SVMR and GA-SVMR in prediction of wave transmission of HIMMFPB are analyzed, interpreted and discussed. Also, the performance of these models is compared with each other.
- Chapter 6 – Conclusions: Conclusions drawn based on the results of CI models and suggestions for future work have been presented.
- Appendix I includes the MATLAB programs used to develop various CI models.
- The Appendix I is followed by references, list of publications based on the present work, and a brief resume of the researcher.

1.6 SUMMARY

The types of breakwaters that may be adopted have been discussed based on the situation and conditions, which includes different types of conventional breakwaters, such as, rubble mound breakwater, vertical wall breakwater, composite breakwater special type of breakwaters and floating breakwaters. Wave transmission of floating breakwaters, and its advantages and disadvantages over conventional type of breakwaters have been discussed. Moreover, the chapter highlights that most of the study on floating pipe breakwaters is experimental, numerical or theoretical in which researchers fails to give a simple mathematical model to predict wave transmission through floating breakwaters by considering all the boundary conditions. Still it is a complex problem. The scope of present investigations has been explained and the organization of the thesis is presented.

CHAPTER 2

LITERATURE REVIEW

2.1 GENERAL

Floating breakwaters are well accepted in recent years because of their basic advantages, such as, flexibility, easy mobilization, installation, and retrieval. The system can be fabricated in land, towed to the site, and installed along any desired alignment with ease. In addition, they have several desirable characteristics, such as, comparatively small capital cost, adoption to varying harbour shapes and sizes, short construction time and freedom from silting and scouring. Floating breakwaters could also be utilized to meet location changes, extent of protection required or seasonal demand. They can be used as a temporary protection for offshore activities in hostile environment during construction, drilling works, salvage operation, etc. Hence, it is necessary to study a detailed investigation of proposed floating breakwater. Proper formulation of the problem is necessary before carrying out any research work. For this purpose, an extensive literature review was carried out on floating breakwaters. Literatures on theoretical determination of transmission coefficient of floating breakwater have been discussed.

However, it is noticed that theoretical determination of transmission coefficient for a typical floating structure with all its coastal boundary and depth variation is extremely difficult. This is because of complexity and non-linearity associated with wave-structure interaction. Still it is a complex problem. Computational intelligence techniques are successfully used to solve complex problems, for this purpose, an extensive literature review was carried out on applications of computational intelligence such as, artificial neural networks, fuzzy logic, genetic programming, genetic algorithms, support vector machines, principal component analysis or

combinations of these techniques in coastal/ocean engineering in the following section.

2.2 REVIEW OF THEORETICAL ANALYSIS

Several researchers have carried out analytical and numerical studies on floating breakwaters in the past, and some of them are discussed below:

Carr (1951) as reported by Ippen (1966) has considered two dimensional case of floating breakwater, which extends over full depth of fluid. Shallow water waves are considered and the pressure distribution is therefore hydrostatic. Applying the equation of conservation of energy to the system, Carr (1951) determined reflection coefficient K_r and the transmission coefficient K_t for freely floating breakwater.

The equation for transmission coefficient K_t is given as:

$$K_t = \frac{1}{\sqrt{1 + \left(\frac{\pi W}{\gamma L h}\right)^2}} \quad (2.1)$$

Equation 2.1 applies to a freely floating structure as indicated in Fig. 2.1. For the case of moored system in which the restoring force acting on the breakwater is proportional to the displacement from its mean position, the transmission coefficient is given by,

$$K_t = \frac{1}{\sqrt{1 + \left(\frac{\pi W}{\gamma L h}\right)^2 \left[\left(\frac{T}{T_n}\right)^2 - 1\right]^2}} \quad (2.2)$$

Carr (1951) has presented a simpler formula for shallow water wave conditions for $h/L < 0.04$.

$$K_t = \frac{1}{\sqrt{1 + \left[\left(\frac{\pi B}{L} \right) \left(1 + \frac{D}{h-D} \right) \right]^2}} \quad (2.3)$$

In the above expressions,

L : Wave length,

W : Breakwater weight per unit length (in direction parallel to wave crests),

B : Breakwater width,

D : Draught of breakwater,

γ : Density of water,

h : Depth of water,

T : Time period of wave and

T_n : Natural period of the breakwater system.

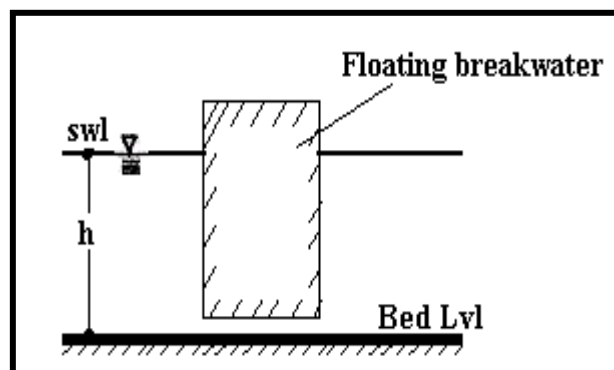


Fig. 2.1 Sketch showing floating breakwater to full depth of water as per Carr (1951)

Macagno (1953) as reported by Headland (1995) presented an analytical formula for computing the wave transmission coefficient K_t of rectangular breakwater of width B , draft D , rigidly moored in water depth h , and subjected to incident waves having a period T , and wave length L ;

$$K_t = \frac{1}{\sqrt{1 + \left[\frac{\pi B \sinh\left(\frac{h}{L}\right)}{L \cosh\left(2\pi \frac{(h-d)}{L}\right)} \right]^2}} \quad (2.4)$$

In the above equation the assumption is that the breakwaters are rigidly held. Since, the breakwaters have some motion the above equation should not be expected to provide accurate predictions. Regardless of the shortcomings of Macagno (1953) theoretical equation 2.1, it predicts remarkably close to the measured results for wave periods of 3 sec or higher.

The equations 2.2 to 2.4 assume the breakwater to be rigidly held and equation 2.4 assumes shallow water wave conditions. Hence, any mathematical equation derived is as good as the assumptions made while formulating them. If the assumed conditions are simulated properly then the predicted values match fairly well with the experimental values.

Kennedy and Marsalek (1968) devised an empirical equation compatible with wave theory for floating layer of logs. They reported that a floating layer of logs reflects comparatively little of the wave energy but dissipates a large portion of it. The equation devised was;

$$K_t = [1 - 0.5(PE + KE)]^{0.5} \quad (2.5)$$

Where, PE and KE are the proportion of the potential energy and kinetic energy lost as waves passes through the breakwater. It is assumed that the potential energy loss would be related to d/H (d = draft and H = incident wave height), and x/L (width of breakwater by wave length).

The expression developed was;

$$PE = 1.0 - \left[1.0 - 0.42(d/H)^{0.7} (x/L)^{0.67} \right]^2 \quad (2.6)$$

It was assumed that the kinetic energy dissipation would be related to x/L also and that it would be proportional to the fraction of total kinetic energy present in the top layer of water, which could be affected, by log layer. The fraction of kinetic energy present in a top layer of specified thickness z , for a wave of given dimension was designated as $R(KE)$ and eventually the equation evolved was;

$$R(KE) = 1.47 R(KE) (x/L)^{0.5} \quad (2.7)$$

For numerical evaluation of $R(KE)$, the following expression was employed

$$R(KE) = \left[1 - \frac{\sinh 2kS}{\sinh 2kh} \right] \times 100 \quad (2.8)$$

In the above equation,

h : Total depth of water.

$$S = h - z - d \quad (2.9)$$

$$z = 0.025 H^{0.60} L^{0.1} \quad (2.10)$$

By evaluating the equations from 2.5 to 2.10, it is possible to predict the transmission coefficient through a flexible breakwater. Kennedy and Marsalek (1968) showed that the experimental, and the values predicted by the above equation match fairly well for a floating breakwater with layer of logs.

Ito and Chiba (1972) presented a numerical model for determining the wave transmission characteristics of a rectangular floating breakwater. The model is two dimensional and accounts for breakwater response in heave, sway, and roll motion.

A simple mathematical model to determine transmission coefficient K_t for floating tire breakwater was developed by Harms (1979) as given in equation 2.11. The mathematical model was based on the assumption that the power required to propel a tire of negligible mass at instantaneous velocity unidirectionally through a viscous fluid at rest is still applicable when the tire is fixed. It is further assumed that the power associated with the drag and inertia terms represents the rate at which the energy is dissipated within the structure, and that this is the dominant mechanism causing a reduction in the transmitted wave energy.

$$K_t = \frac{H_t}{H_i} = \exp \left(- \frac{20\pi}{3} \frac{C_d}{P} \frac{\left(\frac{H_i}{L} \right)}{\left(\frac{L}{W} \right)} \right) \quad (2.11)$$

In equation 2.11,

H_t : Transmitted wave height,

H_i : Incident wave height,

C_d : Drag coefficient,

L : Wavelength,

W : Breakwater width and,

P : Porosity, which is proportional to volume of breakwater by volume of tires.

Arunachalam and Raman (1980) have presented a useful semi-empirical relation to evaluate the wave transmission characteristics and peak mooring forces of a floating breakwater system. This equation is used for predicting the transmitted wave height applicable only for deep-water waves. Besides, it is mentioned that the transmission coefficient is affected by relative draft (D/d) only “slightly”, (D is the draft of model and “ d ” is depth of water). They found by using a perforated floating breakwater in a two dimensional flume that transmission coefficient was influenced considerably by relative water depth and relative depth of projection of the reflected face of the breakwater.

Valioulis (1990) developed a mathematical model using three dimensional finite element techniques for the motion response and wave attenuation of two linked floating breakwaters moored to the ocean floor. The two-body interaction problem has been divided into a hydrodynamic problem and a motion response problem. The hydrodynamic problem has been dealt with the calculation of the wave-exciting, added mass, and damping forces on the two bodies induced by incident regular waves and the waves caused by the motion of the bodies. The motion response problem has been considered as a mechanical system subjected to the harmonic hydrodynamic forces and restrained by the mooring lines and the elastic links between the two bodies. The numerical model accounts for all three-dimensional effects, including the incidence of oblique waves, the interaction of the two breakwaters, their finite length-to-width ratio, the finite water depth, and the proximity of solid boundaries.

Drimer et al. (1992) studied the performance of a box-type floating breakwater by implementation of simplified assumptions concerning the flow beneath a pontoon-type floating breakwater, which led to an analytical solution of the two-dimensional linearized hydrodynamic problem. They compared the analytical results with a numerical solution of the full linear problem and found that there was good agreement over a wide range of parameters.

Vethamony (1995) conducted theoretical analysis to compute the wave attenuation characteristics of a tethered float system for various wave heights, wave periods,

water depths, depths of submergence of floats and float sizes. The results showed that transmission coefficient does not vary with changes in wave height or water depth. It was reported that the float velocity decreases with increase in float size and transmission coefficient increases with increase in float size. The influence of wave period on wave attenuation was remarkable when compared to other parameters. It is also reported that the theoretical results has been compared with experimental values and found that the theory overestimates wave attenuation, which may probably be due to various linearizations involved in the theoretical formulation.

Williams and McDougal (1996) developed an analytical solution to investigate the behavior of a submerged or surface-piercing, long tethered breakwater of rectangular cross section. They solved the equations of motion to provide the surge, heave, and pitch responses of the structure and calculated the wave reflection and transmission coefficients. They concluded that a reasonable agreement was found between theoretical and experimental values of the reflection and transmission coefficients.

Williams and Azm (1997) investigated theoretically the hydrodynamic properties of a dual pontoon floating breakwater consisting of a pair of floating cylinders of rectangular section, connected by a rigid deck. The structure was partially restrained by linear symmetric moorings fore and aft. The fluid motion was idealized as linearized two-dimensional potential flow and the equation of motion of the breakwater is taken to be that of a two-dimensional rigid body undergoing surge, heave and pitch motions.

Sannasiraj et al. (1998) conducted experimental and theoretical investigation of behaviour of pontoon-type floating breakwaters. A two dimensional finite element model was adopted to study the behaviour of pontoon-type floating breakwaters in beam waves. The stiffness coefficients of the slack moorings lines were idealized as the linear stiffness coefficients, which could be derived from basic catenary equations of the cable. The theoretical model was supported by experimental studies in wave flume. The comparison between the theoretical and experimental measurements showed good agreement except at the roll resonance frequency. The experimental

results showed a higher transmission coefficient for floating breakwater with cross moorings.

Azm and Gesraha (2000) examined theoretically the hydrodynamic properties of long rigid floating pontoon interacting with linear oblique waves in water of finite arbitrary depth. Assuming rigid body motions, dynamic responses of the moored structure was approximately calculated. They reported that the pontoons were convenient alternative for protection from waves in shallow water and the method of solution was found to be computationally efficient. They also reported that the results were comparable to those obtained through other techniques.

Williams et al. (2000) investigated theoretically the hydrodynamic properties of a pair of long floating pontoon breakwaters of rectangular section. The breakwater motions were assumed two dimensional, in surge, heave and pitch. The solution for the fluid motion has been obtained by the boundary integral equation method using an appropriate Green's function. Numerical results that illustrate the effects of the various wave and structural parameters on the efficiency of the breakwaters as barriers to wave action have been reported. They found that the wave reflection properties of the structures depend strongly on their width, draft, spacing and the mooring line stiffnesses, while their excess buoyancy was of lesser importance.

Liang et al. (2003) conducted experimental investigation on spar buoy floating breakwater to study the transmission and reflection characteristics, and mooring line tension induced by sea waves. They studied the variation of transmission coefficient with wave steepness for constant relative depth value. Theoretical predictions were made for multiple-layer fence system, the analytical solution was proposed linearly. The results show that the theoretical computations agree well with the experimental trends.

Stiassnie and Drimer (2003) derived an analytical solution of the flow field by interaction of linear shallow water wave with freely floating box. The relatively small drift forces obtained in this new solution indicated the advantage of porous structures

as floating breakwaters in future use. The studies were carried out with the simplification that the motion of the box was restricted to sway only and its draft was equal to the water depth. Graphs of transmission coefficient, reflection coefficient, and energy dissipation with wavelength to width of breakwater have been plotted. The results have been compared for a porous fixed box, porous free box, and impermeable free box.

Li et al. (2005) developed correction factor for the approximate numerical method proposed by Tsay and Liu (1983) to incorporate floating structure in 2D elliptical model. Since, Tsay and Liu (1983) model produced results that deviated considerably from the solution of the Laplace equations, a simple modification was developed. The modification approximately yielded improved results when compared with laboratory and theoretical results for a wide range of conditions.

Gesraha (2006) investigated analytically the reflection and transmission of incident waves interacting with a long rectangular breakwater with two thin sideboards protruding vertically downward shaped as the Greek letter Π . The numerical results were accurate through the energy conservation principle have been reported. The conclusions drawn were that the resulting wave transmission was lower within the range of incident wave frequency tested. Gunaydina and Kabdasli (2007) have conducted experimental investigation of Π -type floating breakwaters under regular and irregular waves. Based on the experimental results empirical expressions have been suggested to define the transmission, reflection and energy-dissipation coefficients for different immersion depths of solid and perforated breakwaters under regular and irregular waves. Moreover, performance of solid and perforated Π -type breakwaters were compared with that of solid and perforated U-type breakwaters investigated by Gunaydina and Kabdasli (2006) under regular and irregular waves.

Hong and Hong (2007) numerically evaluated the absorbed power, motion and drift force of a floating wave energy device with two oscillating water column within the scope of the linear wave theory. They reported the reflection and transmission

coefficients of the body by numerical analysis. They concluded that the floating wave energy devices might serve as a good floating breakwater having small drift force.

Tay et al. (2009) studied using numerical tool, the hydroelastic responses and hydrodynamic interactions of two large floating fuel storage modules placed side-by-side with the presence of floating breakwaters. These modules and breakwaters form the floating fuel storage facility (FFSF). The floating storage modules and breakwaters are modeled as plates and the linear wave theory has been used to model the water waves in the numerical model. The numerical model has been verified with existing numerical results and validated with experimental tests. Numerical simulations have been performed to determine the hydroelastic behavior and hydrodynamic interactions of floating storage modules placed adjacent to each other and enclosed by floating breakwaters under various incident wave angles. The effects of breakwaters, drafts, channel spacing formed by the two adjacent modules and water depth on the hydroelastic responses of the modules has been investigated by them.

From the review of literatures on theoretical determination of transmission coefficient of floating breakwater, it is found that theoretical treatment for floating breakwater type of structures is difficult, mainly because, it is strongly believed that the energy dissipation at the structure is basically due to the turbulence caused at the structure. The energy dissipation process is subjected to some complex phenomenon. Therefore, many researchers have adopted physical model study to quantitatively determine the parameters that influence the phenomenon. However, these physical model studies are time consuming. The general characteristics of floating breakwater problems related to complexity and non-linearity are outlined below:

- There exists vagueness associated with many of the governing variables and their effects on the performance of breakwater. Engineering judgments based on experience, subjectivity, confidence on model, and other factors are frequently used to deal with this non-statistical uncertainty.

- In order to derive mathematical model for prediction of performance of floating breakwaters researchers have introduced certain simplifying assumptions, since nonlinearity of ocean wave's behavior produces lots of difficulties in mathematical modeling.
- Most of floating breakwaters problems need to consider a large number of ocean wave parameters and dimension analysis of structure itself that affect the response of the systems. Thus, complexity is also an inherent feature of these problems.

Hence, developing computational intelligence models shall provide fast and reliable solution in predicting the performance characteristics of floating breakwaters.

2.3 REVIEW OF LITERATURE ON APPLICATIONS OF COMPUTATIONAL INTELLIGENCE IN COASTAL / OCEAN ENGINEERING

Several researchers have adopted computational intelligence to solve complexity and vagueness associated with coastal/ocean engineering problems and some of them are discussed below:

The first published paper in this area was by Mase et al. (1995). He applied neural network technique to predict the stability and damage level of rubble mound breakwater. According to them the neural network is an information-processing system, modeled on the structure of the human brain that is able to deal with information whose interrelation is not clear. They have considered six stability (input) parameters like Permeability of breakwater (P), Number of waves passing over breakwater (N), Damage level (S_d), Surf similarity parameter (ξ_m), dimensionless water depth (h/H_s), and spectral shape (SS). By adding spectral shape and dimensionless water depth parameters in the neural network model has shown improvement in the results. The predicted damage levels are matching well with the measured damage levels by Vander Meer's (1998) and Smith et al. (1992). The

agreement between the predicted stability numbers by neural network and measured ones is also good.

Deo and Naidu (1999) used previous wave heights to predict their future values. They found that the cascade correlation algorithm was superior to back-propagation in terms of accuracy and training time.

Mase and Kitano (1999) investigated the applicability of neural networks to predict weather impact wave force will act on the upright section of a composite breakwater. They fed four non-dimensional parameters to input layers i.e. h/L , H/h , d/h , and B_m/h . (h : the total water depth; L : the wavelength; H : the wave height; d : the water depth above the mound; and B_m : the horizontal distance from the shoulder of mound to the caisson). They found that neural network accurately predict whether impact wave force occurs on the upright section of a composite breakwater.

Remote sensing of waves often necessitates presentation of data in the form of wave height values grouped over large time intervals. This restricts their use to long-term applications only. Deo and Kumar (2000) used model-free neural network and model based statistical and numerical methods to derive the weekly mean significant wave heights from their monthly mean observations thus making it suitable for short-term usage in the field. They trained the network using error back propagation, conjugate gradient and cascade correlation algorithms. The technique of cascade correlation took minimum training time and showed better coefficient of correlation between observations and network output.

Deo et al. (2001) made an attempt to predict wave parameter using independent variables, rather than related measurement at earlier times or nearby locations. He predicted wave height and wave period by using wind speed over a previous period of times as inputs to multilayer perceptrons. They found that different ANNs were required for fair weather and monsoon conditions.

Mandal et al. (2001) developed back propagation neural network model for accurate prediction of tides which is reliably essential for human activities and construction cost in marine environment. This model predicts the time series of hourly tides using quick learning process called quick prop. The correlation coefficient between predicted tides and measured tides is found to be 0.998.

The harmonic tidal level is conventionally used to predict the tidal levels. The determination of tidal components using the spectral analysis requires a long-term tidal level record (more than one-year data), and for calculating the coefficient of tidal component by least squares method requires a large database of tide measurements. This problem is solved by Lee and Jeng (2002) using neural network model with less data set.

Ultsch and Roske (2002) used new method for predicting sea levels by employing self-organizing feature maps, these maps are transformed from an unsupervised learning procedure to supervised one. The prediction of sea levels is done by using neural network models. Self-organizing feature maps neural network predicted result is compared with other six models, such as, hydrodynamic, statistical, nearest neighbor, persistence model and verbal forecasts. Sea level prediction by self-organizing feature maps neural networks is better than all above-mentioned models.

Tsai et al. (2002) predicted wave heights and periods at one coastal station using values from series of other station within Taichung harbour, Taiwan. Similarly, Huang et al. (2003) used water level at a series of locations to predict tidal currents at an inlet of Long Island, New York. Both studies used basic multilayer perceptron. Londhe and Deo (2003) developed ANN model to obtain distribution of attenuated wave pattern at the entrance of the harbor involving dredged approach channel.

Deo and Jagdale (2003) develop neural network model for prediction of breaking waves. They trained the network by combining the existing deterministic relations with a random component, and then the network was validated with the help of fresh laboratory observations. The result shows that predicted breaking height and water

depth were more accurate than those obtained traditionally through empirical formulae.

Huang et al. (2003) developed regional neural network –water level (RNN-WL) using feed-forward back propagation neural network structure to enable coastal engineers to predict long term water levels in a coastal inlet, the network was trained using hourly data over one month period and validates for another one month based on the data obtained from US national oceanographic and atmospheric administration (NOAA). The model was then tested over year long periods. Results indicate that, despite significant changes in the amplitude and phases of the water levels over the regional study area, the RNN-WL model provides very good long term prediction of both tidal and non-tidal water levels at the regional coastal inlets. They also examine the effect of distance on the RNN_WL model performance. Satisfactory results indicate that the RNN_WL model is able to supplement long-term historical water level data at the coastal inlets based on the available data at remote NOAA stations in the coastal regions.

Tides can be conventionally predicted by harmonic analysis, which is the superposition of many sinusoidal constituents with amplitude and frequencies determined by a local analysis of the measured tide. However accurate predictions of tide levels could not be obtained without a large number of tide measurements by the harmonic method Lee (2004) developed a back propagation neural network model using short term on site tidal level data obtained from Taichung Harbor in Taiwan. Model predicted results were compared with conventional harmonic method which revealed that back propagation neural network efficiently predict the long term tidal levels.

Mohandes et al. (2004) used support vector machines and multilayer perceptron to predict wind speed. Mean daily wind speed data from Madina city, Saudi Arabia, is used for building and testing both models. Performance of support vector machine model is compared with multilayer perceptron. Statistical measure, such as root-mean square error between the actual and the predicted data indicate that support vector machine has shown favorably better predictions than multilayer perceptron model.

Makarynskyy et al. (2004) used feed forward neural network to predict hourly sea level variations for 1/2, 1, 5 and 10 days mean sea level. The results show the feasibility of sea level forecasts in terms of correlation coefficient between the ranges 0.7-0.9, root mean square error about 10% of tidal range and scatter index between the ranges 0.1-0.2.

When the performance of ANN alone is poor, Jeng et al. (2004) adopt the concept of genetic algorithm based training of ANN models in an effort to overcome the problems inherent in ANN training procedure. He used this new approach for determining maximum liquefaction depth in a real world application. In the proposed ANN model wave period, water depth, wave height, seabed thickness and degree of saturation are used as the input parameters, and liquefaction depth as output parameter.

Mandal et al. (2005) used back propagation neural network technique to estimate ocean wave parameters from theoretical pierson-moskowitz spectra and measured ocean wave spectra. They found that the ocean wave parameters estimation by back propagation neural network shows a very good correlation coefficient between measured and estimated ones. According to them the distribution of measured waves is not purely Gaussian distribution, but having multiple peaks with noise/spikes. Hence the correlation coefficients for training and testing field wave data are relatively less as compared to correlation coefficient for theoretical spectra. The correlation coefficients of neural network and scott spectra are comparable. According to them the ocean wave parameters can be directly obtained from the measured spectra using trained neural network.

Rao et al. (2005) used ANN approach to estimate the wave parameters from cyclone generated wind fields. Estimation of significant wave height (H_s) and periods is carried out using back propagation neural network with three updated algorithms, namely Rprop, Quick prop and superSAB. The predicted values using neural networks match well with those estimated using Young's model and a high

correlation coefficient of 0.99 is obtained. Similarly Karla et al. (2005) used feed forward back propagation neural network to obtain Hs at specified coastal site from the values sensed by a satellite at deeper locations.

Makarynskyy et al. (2005) used ANN technique to predict Hs and zero crossing wave periods (Tz). They achieved a higher accuracy of simulating the Hs and forecasting Tz using this technique. Naithani and Deo (2005) developed a neural network to estimate the wave surface density over a wide range of wave frequencies from average wave parameters of Hs, Tz, Spectral width and peakedness parameters They compare the neural network predicted values with the measured ones. Results are more satisfactory than those yields by PM, JONSWAP and Scott's spectra.

Kazeminezhad et al. (2005) used an Adaptive Network based Fuzzy Inference System (ANFIS) and Coastal Engineering Manual (CEM) methods to predict the ocean wave parameters. According to them, the results indicate that ANFIS outperforms CEM method in terms of prediction capability. Here the CEM method over estimates the Hs and under estimates the peak spectral period, while predictions by ANFIS models are more accurate.

Yagci et al. (2005) used neural network technique to predict the damage ratio of breakwater. According to them the accurate estimation of damage levels of breakwater is vital issue in design of breakwater. Network is constructed by considering input parameters like wave stiffness (Hs/Ls), significant wave period (Ts) and slope angle (α). They have used fuzzy logic system for mapping the inputs and output. The fuzzy model estimations of damage ratios were close to the predicted values by neural network methods. The employment of Artificial intelligence (AI) methods enables the consideration of wave period; wave stiffness, breakwater slope and wave height in estimating damage ratio. This application is useful especially when there is less number of laboratory data sets. The experimental data sets were plotted effectively using AI technique in order to generate more number of data sets.

Kim and Park (2005) have applied the artificial neural network method to design rubble mound breakwater. According to them the neural network technique gives more

accurate results than the conventional empirical model and the extent of accuracy can be affected by structure of neural network. They have constructed five-network model based on the parameters, which affect the stability of rubble mound breakwater. The following input parameters are considered in their study like permeability of breakwater (P), number of waves (Nw), damage level (Sd), surf similarity parameter (ξ_m), spectral shape (ss), slope of breakwater ($\cot \alpha$), wave stiffness (Hs/Ls) and relative water depth (h/Ls). They have shown that the trained neural network model could be embedded into Monte Carlo simulation technique to estimate the failure probability of breakwater. The neural network integrated reliability analysis gives more advanced results than by empirical model.

Bazartseren (2005) used ANN model to predict the near shore morphology. The ANNs are used for deriving certain relations such as sediment transport, seabed and suspended loads. According to him, the neural network with the number of neighboring points and time lags is to be considered for deriving the morphology development tendency. It is attempted to estimate the bed form movement tendencies based on the local neighboring features of bathymetry.

Mandal and Prabakaran (2006) used recurrent neural network with updated algorithm to forecast ocean waves. The recurrent neural network of 3, 6 and 12 hourly wave forecasting yields the correlation coefficient of 0.95, 0.90 and 0.87 respectively. According to them, the wave forecasting using recurrent neural network yields better results compared to previous neural network applications.

The marine structures in Taiwan suffer from typhoon attack every year. The earlier theoretical models are not properly predicting the typhoon waves. Chang and Chien (2006) developed ANN- multi trend-simulating transfer function model which accurately forecasts wave peak.

Rajasekaran et al. (2005 and 2006) used functional and sequential learning neural networks for accurate prediction of tides using very short-term observations. This method does not require harmonic parameters as used in conventional method. The

comparison between the measured and predicted tidal levels for 3 days and 1 month's prediction using 1 day's observation depicts the correlation coefficients 0.981 and 0.999 which are higher than the values obtained by Tsai and Lee (1999). It shows that the functional and sequential learning neural networks predict better values as compared to other conventional methods.

Chang and Lin (2006) present a tide generating neural network model (TGF-NN) for simulating tides at multi-points considering tide-generating forces. Harmonic method, response orthotide method, the NAO.99b model was also used to estimate the tides at single point. They have compared prediction accuracy of each method based on statistical measures, such as root mean square error and correlation coefficient in which TGF-NN model is efficient compare to harmonic method. Extended application of TGF-NN model to predicting tides at some points neighboring to an original interest point identifies more accurately simulating multi-point tides as compared to that of NAO.99b numerical model.

The storm tidal prediction using conventional methods requires a huge amount of tidal data and many other parameters like central pressure of typhoon, speed of typhoon, heavy rainfall data, coastal topography and local features. Lee (2006) used neural network technique to predict the storm surge with the help of four input parameters such as wind velocity, wind direction, wind pressure and harmonic analysis of tides. It is found that the network predicts reliable and better results of storm surges.

Browne et al. (2007) have carried out near shore swell estimation from a global wind wave model and compared with ANN model. The results revealed that the high correlations and relatively small standard-errors obtained by the ANN model on the validation data set indicates that 6-12 months of daily observations is sufficient to build a model that generalizes well.

Karla and Deo (2007) trained the data in an innovated manner to tackle the problem of modeling wind speeds that are always associated with very high variations in their magnitude. They used radial basis function neural network to project information on

wind speed and waves collected by the TOPEX satellite at deeper locations to a specified coastal site. They found that to train the network with sufficient flexibility it is necessary to combine network instead of separate one involving an input and output of all the three parameters, i.e. wave height, period and wind speed. They also found that network training based on statistical homogeneity of data sets is essential to obtain accurate results.

Mandal et al. (2007) used neural network technique to predict the stability number and damage levels of rubble mound breakwater. It is seen that a good correlation is obtained between network predicted stability numbers and estimated ones with less computational time compared to Mase et al. (1995) and Kim and Park (2005).

El-bisy (2007) investigated the scour phenomena at the toe of sea walls and the different parameters that affected it. He collected the data by conducting experiments using different wave steepness, bed material grain sizes, wall positions and inclinations. Using this data he prepared parametric plots of toe scour for smooth impermeable inclined seawalls were prepared. Also they developed a neural network model on the basis of experimental data and the model was validated. Results indicated that this model can be used in coastal engineering applications.

Bateni and Jeng (2007) develop adaptive neuro-fuzzy inference system (ANFIS) models for predicting scour depth as well as scour width for a group of piles supporting a pier. They used two combinations of input data. The first input combinations involves dimensionless parameters such as wave height, wave period and water depth, while the second combinations contain non-dimensional numbers including the Reynolds number, the keulegan-carpenter number, the shields parameter and the sediment number. The test results show that ANFIS perform better than the existing empirical formulae. They also found that the ANFIS predicts scour depth better when it is trained with the original (dimensional) rather than non-dimensional data. The depth of scour was predicted more accurately than its width.

Tseng et al. (2007) developed a typhoon-surge forecasting model with back-propagation neural network (BPN). The typhoon's characteristics, local meteorological conditions and typhoon surges at a considered tidal station at time (t-1) and (t) was used as input data. They developed four models to test and compared under the different composition of the above mentioned input factors. For models calibration and verification they have collected sixteen typhoon events and their corresponding typhoon surges and local meteorological conditions at K-feng Tidal Station in the coast of north-eastern Taiwan between 1993 and 2000. Twelve of them were used in models calibration while other four were used in models verification. The results showed that the model comprising of 18 input factors has better performance. The same model was also applied to typhoon-surge forecasting at Cheng-Kung Tidal Station in south eastern coast of Taiwan and at Tung-Shih Tidal station in the coast of south-western Taiwan. Results showed that the application of BPN model in typhoon-surge forecasting at Cheng-Kung Tidal Station has better performance than that at Tung-Shih Tidal Station.

Panizzo and Briganti (2007) developed ANN numerical model to forecast the wave transmission behind low-crested structures. Data used to train and test the network was gathered within the European research project DELOS. ANN results are compared with those from experimental formulations based on classical regression approach demonstrate a considerable improvement in the forecast accuracy.

Altunkaynak (2008) proposed Genetic algorithm and Kalman filters method also called Geno-Kalman filtering for station 46002 located in the Coos Bay at Oregon, USA, to determine the relation among wind speed previous and current wave parameters. A comparison has been made between Perceptron Kalman filtering and Geno-Kalman filtering techniques. The results showed that the Geno-Kalman filtering methodology has smaller absolute mean square and relative errors than Perceptron Kalman filtering. Also coefficient of efficiency value which was used to evaluate results between observed and estimated is higher at Geno-Kalman filtering than perceptron kalman filtering.

Zamani et al. (2008) developed ANN and Instance-Based Learning (IBL) models to forecast significant wave heights for several hours ahead using buoy measurements. Experiments show that the ANN's yield slightly better agreement with the measured data than IBL. According to them ANN's can also predict extreme wave conditions better than the other existing methods.

Gaur and Deo (2008) applied genetic programming (GP) to forecast ocean waves on real-time. They analyzed the wave rider buoy measurements available at two locations in the Gulf of Mexico. The forecasts of significant wave height are made over lead times of 3, 6, 12 and 24h. They used a sample size belong to a period of 15 years and a testing period of 5 years. The forecast made by the approach of GP can be regarded as a promising tool for future applications to ocean predictions.

Londhe (2008) presents ANN and GP approach for estimation of missing wave heights at a particular location on a real time basis using wave height at other locations. Both approaches perform well in terms of accuracy of estimation, whereas GP model work better in case of extreme events.

Gunaydin (2008) used ANN and regression method to predict monthly mean significant wave height from meteorological data. He used seven different ANN models comprising of various input combinations of monthly mean wind speeds, sea level pressures and air temperature ratios based on hourly observations. He found that ANN model having all parameters in the input layer, gave the best prediction performance.

According to Malekmohamadi et al. (2008) Numerical wave modeling (NWM) is not justified due to economical consideration whereas ANN model is inexpensive but needs a long time period of wave data for training, which is generally inconvenient to achieve. He solved this problem by combining NWM and ANN. Wave data was generated by a NWM by means of a short period of assumed winds at a concerned point. This data was used to train ANN. The method was applied for wave hindcasting

to two different sites; Lake Superior and the Pacific Ocean. Simulation results showed the superiority of the combined method.

Beltrami (2008) implemented an ANN algorithm in the software of bottom pressure recorders (BPRs) for the automatic, real time detection of a tsunami within recorded signals. The performance and efficiency of ANN algorithms was compared to the one developed under the Deep-ocean Assessment and Reporting of Tsunami (DART) program run by the U.S. National Oceanic and Atmospheric Administration (NOAA). Results indicated that ANN algorithm showed an improvement in tsunami detection.

The contribution of non-astronomical components to tidal level may be as significant as that of astronomical components under the weather, such as typhoon and storm surge. The traditional harmonic analysis method and other models based on the analysis of astronomical components do not work well in these situations. Liang et al. (2008) resolve this problem by developing three back-propagation neural networks (BPNN) models viz; difference neural network model (DNN) for the supplementing of tidal record; minus-mean-value neural network (MMVNN) for the corresponding prediction between tidal gauge station; weather-data based neural network model (WDNN) for set up and set down. They found that above models perform well in the prediction of tidal level or supplement of tidal record including strong meteorological effects

Verhaeghe et al. (2008) developed a 2-phase neural prediction method i.e. ‘classifier’ and ‘quantifier’. To train the network they used the overtopping database set up within the EC project CLASH (De Rouck, J; et al. 2005). The ‘classifier predicts whether overtopping occurs or not. If the classifier predicts overtopping, then the ‘quantifier’ is used to determine the mean overtopping discharge. The method has an overall predictive capacity.

Coastal structures like breakwater, groins and gabions are constructed to reduce the coastal erosion. The stability of individual stones on a sloping surface of breakwater is very important because many breakwaters fail due to a defective design. Mandal et al.

(2008) developed neural network technique in predicting the stability number. Parameters used in training the models are permeability of breakwater, number of attacking waves, significant wave height, mean wave period, damage level, slope angle, berm width and reduced armor weight ratio. Predicted stability number is compared with the estimated stability number by Hudson and Van der Meer. It is found that the network predicts lesser armor units compared to empirical formulae which makes the design more economical and safe. The coefficient correlation between the estimated stability number by empirical formulae and predicted stability number by neural networks are close to one.

To avoid property loss and reduce risk caused by typhoon surges, accurate prediction of surge deviation is essential. Many conventional numerical methods and experimental methods for typhoon surge forecasting have been investigated, but none of them gave the accurate predictions, still it is a complex ocean engineering problem. To overcome this problem Rajasekaran et al. (2008) develop a support vector regression model for forecasting storm surges. To verify the performance of model they used original data of Longdong station at Taiwan invaded directly by the *Aere* typhoon. Results obtained were compared with numerical methods and neural network indicate that storm surges and surge deviations can be efficiently predicted using support vector regression.

Sylaios et al. (2009) used Takagi- Sugeno rule based fuzzy inference system for forecasting wave parameters based on the wind speed, direction and the lagged wave characteristics. They used subtractive clustering method to identify the initial and final antecedent fuzzy membership functions. This model was applied on the wind and wave dataset recorded in years 2000 to 2006 (12,274 data points) by an oceanographic buoy deployed in the Aegean Sea. The model showed perfect fit for the training period and expanded its hindcasting ability during 2006 (1,044 data points) as the verification part of the series. Model results showed good agreement between the predicted and the observed significant wave height and zero up-crossing periods for a lead time of three hours.

According to Shahidi and Mahjoobi (2009) ANNs are not as transparent as semi-empirical regression based models. In addition, neural network approach needs to find network parameters such as number of hidden layers and neurons by trial and error, which is time consuming. They have invoked model tree as a new soft computing method for prediction of significant wave height. The main advantage of model trees is that, compared to neural networks, they represent understandable rules, which can be readily expressed so that humans can understand. Model trees were developed using wind and wave data obtained from 6 April to 10 November 2000 and 19 April to 6 November 2001. M5 algorithm was employed for building and evaluating model trees. Wind speed as the input variable and the significant wave height (H_s) as output variable was used for training and testing data. Results indicate that error statistics of model trees was marginally more accurate. In addition model trees show that for wind speed above 4.7m/s, the wave height increases nonlinearly by the wind speed.

Reikord (2009) used time varying parameter regression in logs. This time varying regression is estimated using kalman filter and a sliding window, with various window widths. He found that sliding window method is preferable. He also used hybrid model where they have combined neural networks with time-varying regression. This model was tested at an hourly frequency over a horizon of 1-4h, and at a daily frequency over 1-3 days. He found that all the models improve relative to a random walk. In the hourly data sets, forecasting the components separately achieves the best results, whereas in daily data sets, the hybrid and regression models yield similar outcomes.

Mahjoobi and Mosabbebi (2009) used support vector machine (SVM) for prediction of significant wave height. The data used in this study was gathered from deep water locations in Lake Michigan. They used current wind speed (u) and those belonging up to six previous hours are given as input variables and significant wave heights (H_s) as output parameter. The SVM results are compared with those of ANN's, multilayer perceptron (MLP) and radial basis function (RBF) models. After comparing they come to the conclusion that SVM can be successfully used for prediction of H_s , the

error statistics of SVM model marginally outperforms ANN with less computational time.

Lee et al. (2009) applied ANN combined with thermographic analysis for estimating the depth of eroded caves in a seawall. From experimental setup, the interior condition of a structure was detected by using thermographic device by measuring the temperature changes on the surface. They obtain the difference between the air temperature and the measured concrete surface point on a thermographic image for neural network. They used this data to obtain an optimum ANN model for the estimation of the depth of eroded caves in sea wall. The model was verified using data from a seawall in Tainan city, Taiwan, and it was found that the ANN model efficiently estimates the depth of eroded caves in a sea wall.

Genetic programming (GP) has nowadays attracted the attention of researchers in the predictions of hydraulic data. Guven et al. (2009) used field measurements to develop linear genetic programming (LGP) and Adaptive neuro fuzzy inference system (ANFIS) models for prediction of scour depth around a circular pile due to waves in medium dense silt and sand bed. The LGP model result was compared with ANFIS model. LGP model was observed to be in good agreement with measured data, and quite better than ANFIS and regression based equation of scour depth at circular piles.

Hashemi et al. (2010) used feed forward back propagation ANN to predict seasonal beach profile evolution at various locations along the Tremadoc Bay, eastern Irish Sea. The beach profile variations were studied at 19 stations for a period of 7 years using ANN. Since ANN is a data driven techniques, principal component analysis and correlation analysis were employed to detect the proper dataset. The geometric properties of the beach, wind data, local wave climate, and the corresponding beach level changes were fed to the network. The model results were compared with field data. The performance is calculated using mean square error which is less than 0.0007. ANN can predict seasonal beach profile changes effectively and are generally more accurate when compared with computationally expensive mathematical model.

Aydogan et al. (2010) developed feed forward back propagation artificial neural network model with different inputs and neuron numbers to predict vertical current profiles of a given point in a narrow strait, the Strait of Istanbul. The model was built on 7039 hours of concurrent measurements of current profiles, meteorological conditions, and surface elevations. The model predicted 12 outputs of East and North velocity components at different depths in a given location. The best model is accepted by trial and error in accordance with the observations with average root mean square error of 0.16 m/s. The same input parameters were then used to build models that predicted current velocities. Results of these predictions show good overall agreement with observations and can be used as a reliable tool for forecasting current profiles in straits.

Iglesias et al. (2010) developed an Artificial Intelligence (AI) model with the focus on the effective draft, or draft available for containment that a floating boom will provide in open waters. The dataset were obtained through an extensive laboratory campaign in which seven model booms are subjected to numerous wave and current combinations. This dataset is randomly divided into two subsets, one for training and the other for testing or validating the model. Input and output variables are selected based on dimensional analysis and laboratory results. The AI technique chosen for the model is multilayer feed forward artificial neural networks trained with the back-propagation algorithm, for their capability to apprehend higher-order patterns from the training examples and subsequently generalize them to other (validation) cases. In order to find efficient network architecture, a comparative study involving 640 neural networks is carried out. Having selected the best performing architecture, the model is successfully validated and becomes a virtual laboratory.

Yoon et al. (2011) developed a two nonlinear time-series models for predicting groundwater level (GWL) fluctuations at a coastal aquifer in Korea using artificial neural networks (ANNs) and support vector machines (SVMs). The performance of the models is verified based on root mean squared error (RMSE) values. ANN models showed lower values than those of SVM during model training and testing stages. However, the overall model performance criteria of the SVM are similar to or even

better than those of the ANN in prediction stage. The generalization ability of a SVM model is superior to ANN model for input structures and lead times. The uncertainty analysis for model parameters detects an equifinality of model parameter sets and higher uncertainty for ANN model than SVM in this case. These results mean that the model-building process should be carefully conducted, especially when using ANN models for GWL forecasting in a coastal aquifer.

From the review of literatures on applications of CI in coastal/ocean engineering it is observed that ANNs is commonly used by many researchers to evaluate or predict ocean wave parameters like wave height, wave period, wave direction, tidal levels and its timings, sea levels, water temperature, wind speeds, coastal currents sediment movement rate etc. Apart from this, damages of coastal structures, seabed liquefaction, storm surges and wave transmission have also been predicted using ANNs. For calibration and verification of the neural network model, many researchers used in-situ data, experimental data, and data generated by numerical or mathematical analysis. It is also found that in most of the applications a three layered feed forward back propagation neural network was used, apart from this some researchers trained the network with conjugate gradient and cascade correlation.

It is also noticed that apart from improving the performance of ANN, computational effort and time needed for training and testing the model is significantly reduced compared to traditional methods. It is also reported that ANN model can learn with much less data sets. Sometimes single network may not always fit the entire domain of the training sample and in such cases different networks are developed over different sub-domain of the training sample size

When the performance of ANN alone is poor in mapping input-output relation many researchers developed a hybrid model by combining ANN with fuzzy system, genetic algorithm, and ANN with numerical wave modeling. Apart from ANNs, many authors have used a new approach to solve coastal engineering problems like genetic programming, ANFIS, Model trees, Support vector machines or combinations of these techniques.

2.4 PROBLEM FORMULATION

The literature review work carried on theoretical and experimental analysis on floating breakwater revealed that the researchers have carried out number of studies by considering simple form of floating breakwater and adopting some common assumptions in hydrodynamics to derive mathematical model for predicting wave transmission, but these models showed very poor agreement with experimental or in-situ data. A physical wave system in nature is very complicated and physical model study like floating breakwaters is expensive and time consuming. This is due to complexity and vagueness associated with many of the governing variables and their effects on the performance of floating breakwater.

Similarly, for floating pipe breakwaters the energy dissipation process depends on various other factors like pipe interference effect, the spacing between the pipes and number of layers. As the effect of all these factors on transmission is not clearly understood, it will be extremely difficult to quantify them mathematically. Furthermore, it is a complex problem, and till now there has not been available a simple mathematical model to predict the wave transmission through HIMMFPB by considering all the boundary conditions, and hence one has to depend on physical model studies which are very much expensive and time consuming.

Literature review work carried on computational intelligence in coastal/ocean engineering reveals that CI techniques have been successfully used to solve complex problems associated with coastal/ocean engineering. However, it is observed that there are hardly any applications of CI on wave transmission of floating breakwaters and HIMMFPB.

In view of the above aspects, a detailed study was taken up on developing CI for the prediction of wave transmission through HIMMFPB, thereby providing a new approach to solve the problem of wave transmission prediction, which is highly complex and has huge non-linearity associated with its hydrodynamic performance.

2.5 OBJECTIVES OF THE PRESENT INVESTIGATIONS

The objectives of the present investigations involve the development of computational intelligence models to predict the transmission characteristics of Horizontal Interlaced Multi-layer Moored Floating Pipe Breakwater and are listed as follows:

- To investigate the ability of soft computing approaches like artificial neural networks (ANNs), adaptive neuro fuzzy inference systems (ANFIS), support vector machines (SVMs), genetic algorithm (GAs) to effectively address various hard-to-solve design tasks and issues associated with the HIMMFPB.
- To develop CI models in isolation for prediction of wave transmission of HIMMFPB.
- To integrate and hybridize the fuzzy logic, neural networks, GAs, and SVMs to improve the wave transmission predictions of HIMMFPB.
- To identify the most significant parameters as input to CI models by using principal component analysis (PCA).
- To verify the impact of most significant parameters obtained by PCA on the performance of CI models.
- To analyze and recommend the most reliable CI model in predicting wave transmission of HIMMFPB.

2.6 SUMMARY

Detailed literature review on the theoretical works on floating breakwaters including the latest available literature has been discussed in this chapter. The detailed literature review reveals that several researchers in the past have carried out theoretical investigations on different types of floating breakwaters, such as horizontal, sloping, A-type, Y-type, Cage, pontoon, tires etc. However, it is observed that these theoretical studies fail to give a simple mathematical model to predict wave transmission through floating breakwater and HIMMFPB by considering all the boundary conditions. This is because of complexity and non-linearity associated with wave-structure interaction. Also it is brought to the notice that physical model studies are time consuming. To overcome this problem, CI is successfully used to solve the issue of complexity and non-linearity. A detailed literature review on applications of CI in coastal/ocean engineering has been discussed including the latest available literature. However, it is observed that there are hardly any applications of CI on prediction of wave transmission through floating breakwater and HIMMFPB and it is observed that there is a great scope for developing CI models in prediction of wave transmission for HIMMFPB. The objectives of the present investigation are also discussed in this chapter.

CHAPTER 3

EXPERIMENTAL MODEL SETUP AND DATA USED

3.1 GENERAL

The prime factor in the construction of the floating breakwaters is to make the width of the breakwater (in the direction of wave propagation) greater than one-half the wavelengths and preferably as wide as the incident wavelength; else, the breakwater rides over the top of the wave without attenuating it. In addition to be effective, the floating breakwater must be moored in place with both leeward and windward ties otherwise, it would sag off and ride over the incident wave. Certain important features like large masses, large moment of inertia, and the combinations of two have influenced the development of floating breakwaters by various investigations. Most of the literature indicates that the parameter 'relative width' influences greatly the wave attenuation characteristics of the breakwater. A physical model study on wave transmission of HIMMFPB was carried out by (Magadum, 2005; Deepak, 2006; Jagadisha, 2007), using wave flume available in the Marine Structures Laboratory of Applied Mechanics and Hydraulics, Department of National Institute of Technology Karnataka, Surathkal, India. The data obtained by them has been used here in the present research work. For hydraulic model investigation, field conditions existing off Mangalore coast in Karnataka state of India were considered. The Laboratory conditions were decided through hydraulic modeling. The non-dimensional parameters influencing the phenomenon were obtained through dimensional analysis.

In the present work, experimental data obtained from physical model study on wave transmission of HIMMFPB was used in developing computational intelligence for predicting wave transmission through HIMMFPB. Experimental data was collected, categorized, compiled and organized in a systematic database. This database was divided into two sets for training and testing the computational intelligence models.

The input parameters that influence the wave transmission (K_t) of floating pipe breakwater, such as, relative spacing to pipes (S/D), relative breakwater width (W/L), ratio of incident wave height to water depth (H_i/d), incident wave steepness (H_i/L) were considered.

3.2 EXPERIMENTAL SETUP

3.2.1 Wave flume

Experiments were conducted by (Magadum, 2005; Deepak, 2006; Jagadisha, 2007) generating regular waves in two-dimensional wave flume available in the Marine Structures Laboratory of Applied Mechanics and Hydraulics Department, National Institute of Technology Surathkal, Karnataka State, India. The details of the wave flume facility are given below:

- Total Length : 50 m
- Channel length : 41.5 m
- Width : 0.71 m
- Maximum water depth : 0.70 m
- Wave flume type : Two dimensional
- Wave Generator : Bottom hinged flap type
- Waves generated : Monochromatic type
- Wave absorber : Rubble mound spending beach
- Range of wave height generation: 0.03 m to 0.24 m
- Range of wave period generation : 1.0 sec to 3.0 sec

The wave flume consists of glass panels on one side to facilitate observations and photography. The wave generating chamber has a length of 6.3 m. Gradual transition was ensured between the normal flume bed level and that of generating chamber by a

ramp. The wave filter consisted of a series of vertical asbestos cement sheets spaced at about 0.1 m centre-to-centre, parallel to the length of the flume. The purpose of the filter was to dampen the disturbance caused by successive reflections and to polarize the generated waves. Granite stones, which were laid to slope, acted as wave absorber behind the flap in the generating chamber. The flume had iron railings on top of the sidewalls to enable the movement of a trolley. Fig. 3.1 gives a schematic diagram of wave flume and Plate 3.1 shows the view of the experimental setup used (Jagadisha, 2007).

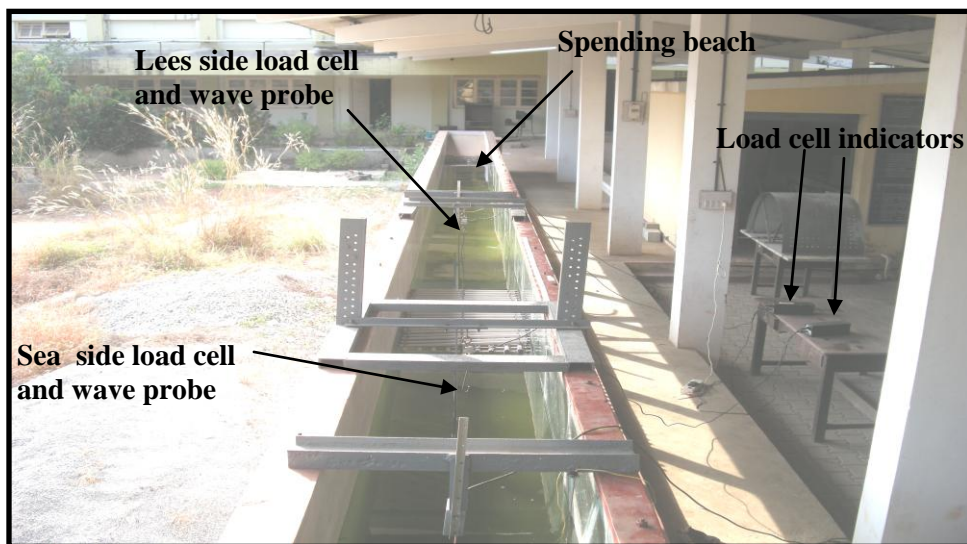
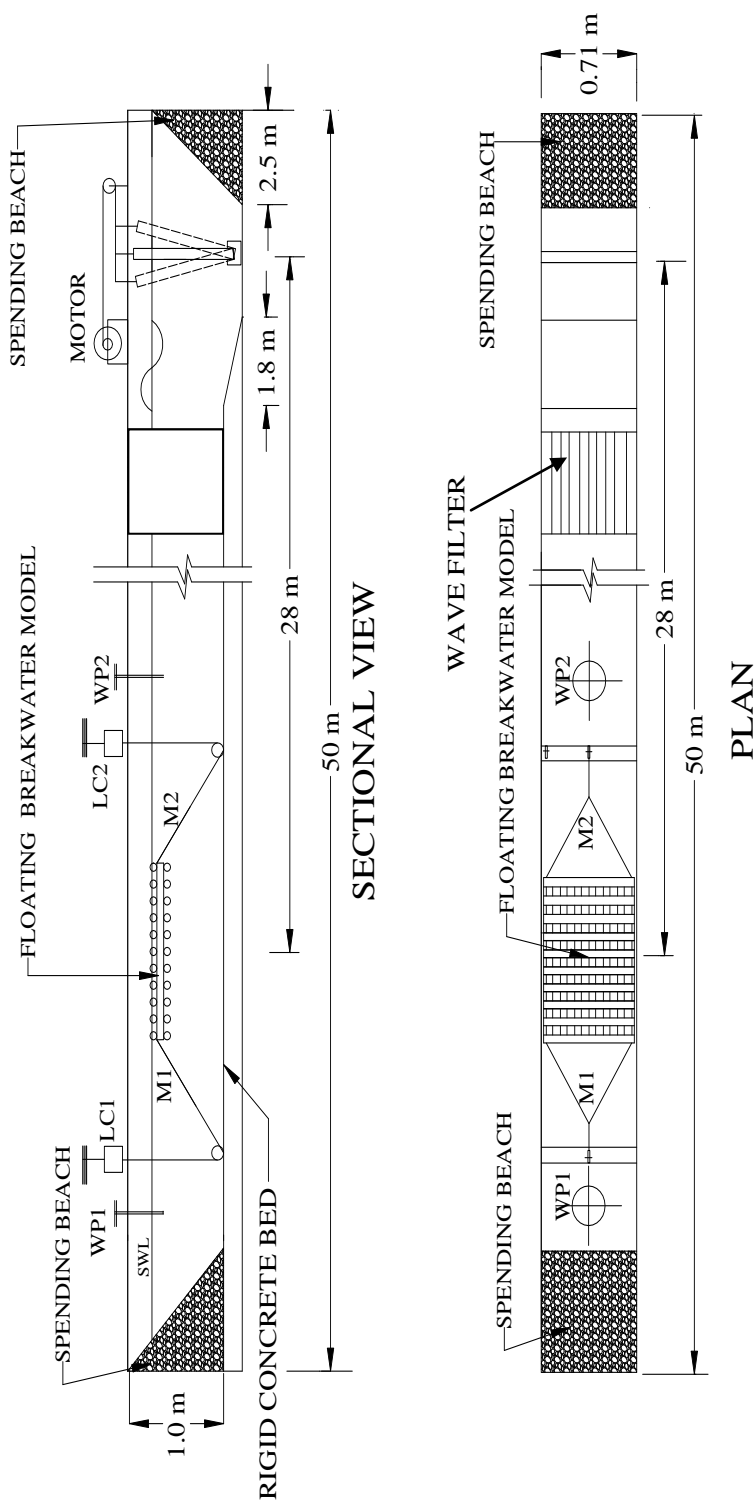


Plate 3.1 View of the experimental set up (Jagadisha, 2007)

The wave generator system consisted of a bottom-hinged flap, which is moved back and forth by induction motor of 11 kW, 1450 rpm. This motor was regulated by Kirloskar made inverter drive (0 to 50 Hz), to rotate with a speed range of 0 – 155 rpm. Desired wave period was obtained by changing the frequency through the inverter. A flywheel and bar-chain linked the motor with the flap. Wave height was varied for a particular wave period by changing the eccentricity of the bar-chain on the flywheel.



WP1 - WAVE PROBE ON LEESIDE M1 - MOORING LINE ON LEESIDE LC1- LOAD CELL ON LEESIDE
 WP2 - WAVE PROBE ON SEASIDE M2- MOORING LINE ON SEASIDE LC2- LOAD CELL ON SEASIDE

Fig. 3.1 Regular wave flume setup for HIMMFPB (Jagadisha, 2007)

3.2.2 About experimental HIMMFPB model

The experimental study carried out (Magadum, 2005; Deepak, 2006; Jagadisha, 2007), showed hydrodynamic characteristics of horizontally interlaced three and five layer floating breakwater systems, in which wave transmission is less for five layer systems. Spacings between the pipes of 2D, 3D, 4D and 5D were considered. In the flume, longitudinal pipes were placed along the direction of propagation of waves. The transverse pipes were placed perpendicular to longitudinal pipes and tied to them by binding wire of mild steel. The length of the longitudinal pipes defines the width W , of the floating breakwater. Both ends of the breakwater were tied with multi strand steel cables of nominal diameter 1.7 mm as moorings. One end of the cable was tied to the breakwater while other end was taken through a pulley (pulley was fixed to the bottom of the flume) and connected to the load cell, which was fixed to the frame as shown in Fig. 3.1. The model was kept in position by means of moorings with zero initial force (no tension) at a distance 28 m from the wave maker. All the experiments were conducted in water depths of 0.40 m, 0.45 m and 0.50 m.

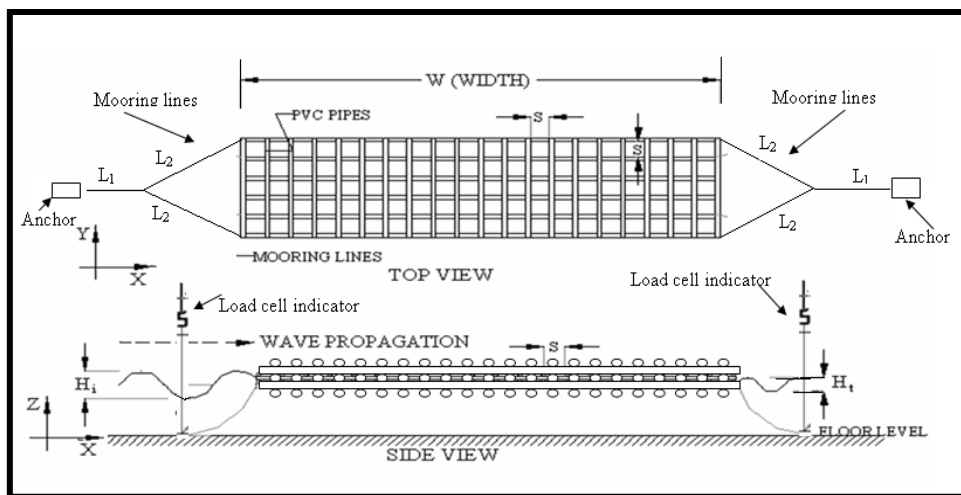


Fig. 3.2 Typical Experimental set up of HIMMFPB

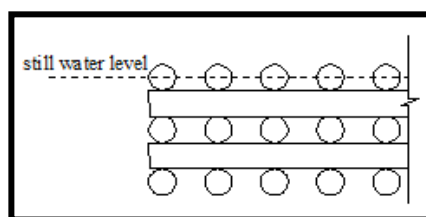


Fig. 3.3 Details of five layers of HIMMFPB

A pictorial representation of the model in plan and sectional view is shown in Fig. 3.2. The pipes of the breakwater model were ballasted with water to have only half the diameter of top layer of pipes above still water level as indicated in Fig. 3.3.

The breakwater consisted of PVC (polyvinyl chloride) circular pipes of 32 mm inner diameter and 0.75 mm thick wall. The pipes were placed parallel to each other with centre-to-centre spacing S between them in each layer. Plates 3.2 shows the view of HIMMFPB with five layers of pipes and $S/D = 5$.



Plate 3.2 View of the floating pipe breakwater model with five layers of pipes and $S/D = 5$ (Jagadisha, 2007)

3.2.3 Instrumentation used

Data acquisition system consisting of wave probes along with computational facility was used to acquire data on water surface elevations, incident wave heights and transmitted wave heights.

3.3 EXPERIMENTAL PROCEDURE

The Wave flume was filled with water to the required depth (0.40 m, 0.45 m or 0.5m). The wave probes were calibrated at the beginning of the work. For a given wave period, waves of different heights were generated by changing the eccentricity of the crank which controls the movement of the wave flap. Thus, the flume was run for different combinations of wave periods and wave heights. Before starting the experiments, the flume was calibrated without floating breakwater structure for 0.4 m, 0.45 m and 0.5 m water depths to find the incident wave heights for different combinations of frequency and eccentricity. The combinations producing the secondary waves in the flume were not considered in the experiments. The signals from the wave probe were recorded for transmitted wave height. Incident and transmitted wave heights were also cross-checked by measuring them manually. The waves were generated in bursts of five waves to avoid wave distortion due to reflection and re-reflection in the flume. The wave height on seaside and leeside of breakwater were recorded for each burst. Six such trials were conducted and the average of the six values was recorded. Similarly, the peak values of the mooring forces were recorded, for both seaside and leeside mooring lines. Plate 3.2 shows the view of experimental setup.

3.4 EXPERIMENTAL DETAILS OF HIMMFPB

The experiments conducted on Horizontal Interlaced Multi-layer Moored Floating Pipe Breakwater models with three layers of pipes and five layers of pipes with relative spacings of 2, 3, 4, and 5 (Magadum, 2005; Deepak, 2006; Jagadisha, 2007), are discussed in this section. The width of the breakwater model was varied from 1.65 m to 5.44 m for each case. These constitute 208 numbers of floating pipe breakwater model configurations. Each of these configurations was tested in 0.40 m, 0.45 m and 0.50 m depths of water, wave heights ranging from 0.030 m to 0.18m, and wave periods ranging from 1.2 sec to 2.2 sec. The widths of the breakwater were decided by varying the W/L values from 0.4 to 2.65. The transmitted wave heights on the leeside of the breakwater was measured using wave probes and the peak mooring forces in seaside and leeside has been measured using load cells. Table 3.1 shows details of wave-specific and structure-specific parameter considered.

Table 3.1 Details of the wave-specific and structure-specific parameters of HIMMFPB (Magadum, 2005; Deepak, 2006; Jagadisha, 2007)

Wave-specific parameters	Experimental range
Incident wave height, H_i (mm)	30, 60, 90,120,150 and180
Wave period, T (sec)	1.2, 1.4, 1.6, 1.8, 2.0 and 2.2
Angle of wave attack	90°
Depth of water, d (mm)	400, 450 and 500
Structure-specific parameters	Experimental range
Diameter of pipes, D	32 mm
Ratio of spacing to diameter of pipes, S/D	2, 3, 4 and 5
Relative breakwater width, W/L	0.4 to 2.65
Number of layers of pipes, n	5

3.5 EXPERIMENTAL DATA OF HIMMFPB

Experimental data obtained from physical model study on wave transmission of HIMMFPB was collected, categorized, compiled and organized in a systematic database. To develop computational intelligence models, non-dimensional input parameters that influence the wave transmission (K_t) of floating breakwater, such as, relative spacing of pipes (S/D), relative breakwater width (W/L), ratio of incident wave height to water depth (H_i/d), incident wave steepness (H_i/L) are used. These experimental data was divided into two sets, one for training and other for testing the computational intelligence models (Table 3. 2).

Table 3.2 Number of data points and input parameters used to train CI models

Input Parameters	S/D ratio	Number of data points for training	Number of data points for testing	Total data
$W/L, H_i/d, H_i/L$	2	609	203	812
$W/L, H_i/d, H_i/L$	3	576	233	809
$W/L, H_i/d, H_i/L$	4	366	143	509
$W/L, H_i/d, H_i/L$	5	580	234	814
$S/D, W/L, H_i/d, H_i/L$	Total	2131	813	2944

Experimental data on $W/L, H_i/d, H_i/L$ and K_t were used as a training data to train some of the CI models having S/D ratio as 2, 3, 4 and 5 respectively. To study over a range of S/D on K_t , an input parameter S/D is added. The numbers of data points used for training CI models are shown in Table 3.2.

3.6 SUMMARY

The chapter discusses in detail the physical model study on HIMMFPB carried out by (Magadam, 2005; Deepak, 2006; Jagadisha, 2007). It also discusses the wave flume, coastal area considered for prototype, experimental setup, experimental procedure and wave-specific and structure-specific parameters of HIMMFPB. Non-dimensional input parameters that influence the wave transmission (K_t) of floating breakwater, such as, relative spacing of pipes (S/D), relative breakwater width (W/L), ratio of incident wave height to water depth (H_i/d), incident wave steepness (H_i/L) are also discussed. Moreover, chapter also discusses the collection, categorization, compilation and organization of the data on wave transmission through HIMMFPB in a systematic database, which was consider developing the CI models.

CHAPTER 4

RESEARCH METHODOLOGY

4.1 GENERAL

To solve real-world problems, like hydrodynamic performance of HIMMFPB by considering all the boundary conditions and extracting knowledge from large amount of experimental or in-situ data is extremely difficult, since they are typically ill-defined systems, and complex to model. In these cases, precise models are impractical, too expensive, or non-existent. Furthermore, the relevant available information is usually in the form of empirical prior knowledge and input-output data representing instances of the system's behavior. Therefore, we need an approximate reasoning system capable of handling such imperfect information. Bezdek (1996) defines such approaches within a frame called computational intelligence; similarly, Zadeh (1998) explains the same using the soft computing paradigm. According to him “In contrast to traditional, hard computing, soft computing is tolerant of imprecision, uncertainty, and partial truth”. In this context ANN, Fuzzy Logic (FL), Probabilistic Reasoning (PR), SVMR, Evolutionary Algorithms (EAs) and combinations of these techniques are considered as main components of CI. Each of these technologies provides us with complementary reasoning and searching methods to solve complex, real-world problems like wave transmission through HIMMFPB. In this chapter, theoretical background of research methods used to developed CI models to predict wave transmission of HIMMFPB, such as, ANN, ANFIS, SVMR and GA are presented.

4.2 ARTIFICIAL NEURAL NETWORK

4.2.1 Introduction

An artificial neural network is an information processing system that has been developed as a generalization of the mathematical model of human cognition. A neural network is a network of interconnected neurons, inspired from the studies of the biological nervous system Fig. 4.1. In other words, neural network function in a way similar to the human brain. The function of a neural network is to produce an output pattern when presented with an input pattern. Neural network is the study of networks consisting of nodes connected by adaptable weights, which store experimental knowledge from task examples through a process of learning. The nodes of the brain are adaptable; they acquire knowledge through changes in the node weights by being exposed to samples. Neural network architecture are motivated by models of the human brain and nerve cells. A biological neuron has three types of components namely dendrites, soma and axon. The dendrites receive signals from other neurons. The soma sums the incoming signals. When sufficient input is received, the cell fires. The output area of the neuron is a long fiber called axon. The impulse signal triggered by the cell is transmitted over the axon to other cells. The connecting point between a neuron's axon and another neuron's dendrite is called a synapse. The impulse signals are then transmitted across a synaptic gap by means of a chemical process.

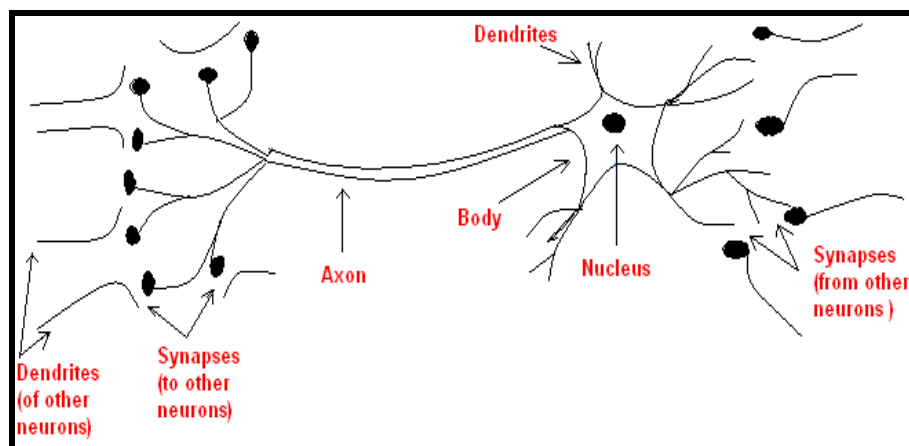


Fig. 4.1 A biological nerve cell

The artificial neuron mimics the characteristics of the biological neuron Fig. 4.2. A processing element possesses a local memory and carries out localized information processing operations. The artificial neuron has a set of inputs, each representing the output of another neuron. Each input is weighted before it reaches the main body of the processing element by the connecting strength or the weight factor analogous to the synaptic strength. The amount of information about the input that is required to solve a problem is stored in the form of weights. Each signal is multiplied with an associated weight before it is applied to the summing node.

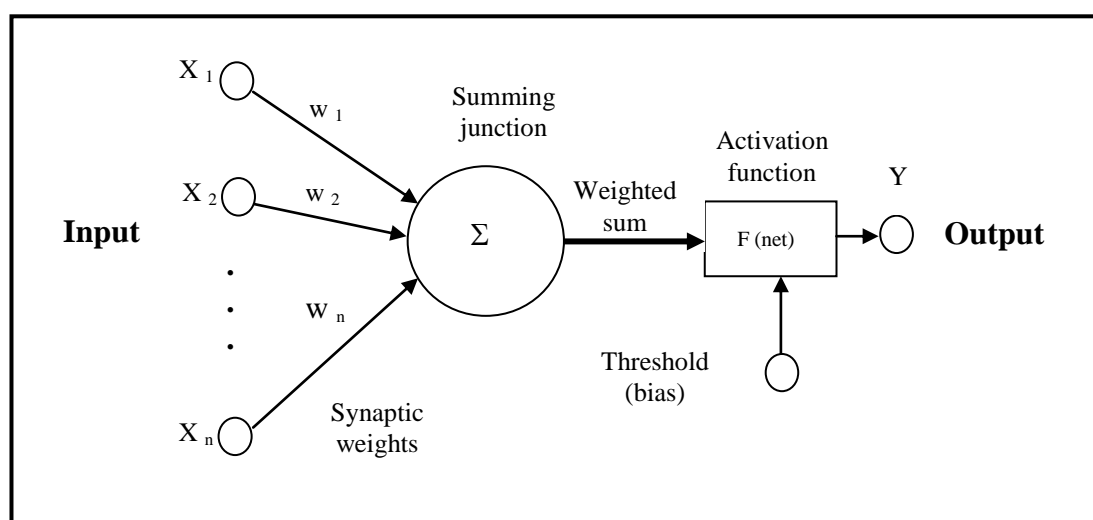


Fig. 4.2 Basic Neuron Model

In addition, the artificial neuron has a bias term, a threshold value that has to be reached or extended for the neuron to produce a signal, a nonlinear function (F) that acts on the produced signal net and output (Y) after the nonlinearity function.

In recent years, the research interest in Artificial Neural Networks (ANN) has increased and many efforts have been made on applications of neural networks to various coastal engineering problems. ANN in coastal/ocean engineering is commonly used by the researchers to predict ocean wave parameters like wave height, wave period, impact wave force etc. (Deo et al., 2001; Deo and Jagdale, 2003; Gunaydin, 2008; Londhe and Deo, 2003). Apart from this, it has provided promising results in prediction of tidal levels (Chang and Lin, 2006), damages to coastal

structures (Mandal et al., 2007), depth of eroded caves in a seawall (Lee et al., 2009), seabed liquefaction (Jeng et al., 2004), storm surges (Tseng et al., 2007) etc. The most significant features of neural networks are the extreme flexibility due to learning ability and the capability of nonlinear function approximations. This fact leads us to expect neural networks to be an excellent tool for solving the motion characteristics of the floating pipe breakwater while overcoming complexity and non-linearity associated with wave-structure interaction of HIMMFPB.

4.2.2 Architecture of a ANN

The neurons are assumed to be arranged in layers, and the neurons in the same layer behave in the same manner. All the neurons in a layer usually have the same activation function. Within each layer, the neurons are either fully interconnected or not connected at all. The neurons in one layer can be connected to neuron in other layer. The arrangement of neurons into layers and the connection pattern within and between layers is known as network architecture.

Input layer: the neurons in this layer receive the external input signals and perform no computation, but simply transfer the input signals to the neurons in another layer.

Output layer: the neuron in this layer receive signals from neurons either in the input layer or in the hidden layer

Hidden layer: the layer of neurons that are connected in-between the input layer and the output layer is known as hidden layer.

Neural nets are often classified as single layer networks or multilayer networks. The number of layers in a net can be defined as the number of layers of weighted interconnection links between various layers. While determining the number of layers, the input layer is not counted as a layer, because it does not perform any computation.

4.2.3 Feed forward back-propagation neural network

In the present research work, feed forward back-propagation neural network is used. The feed forward back-propagation architecture was developed in the early 1970s. Its greatest strength is in non-linear solutions to ill-defined problems. The typical back-propagation network has an input layer, an output layer, and at least one hidden layer. There is no theoretical limit on the number of hidden layers but typically, there is just one or two. Each layer is fully connected to the succeeding layer, as shown in Fig. 4.3.

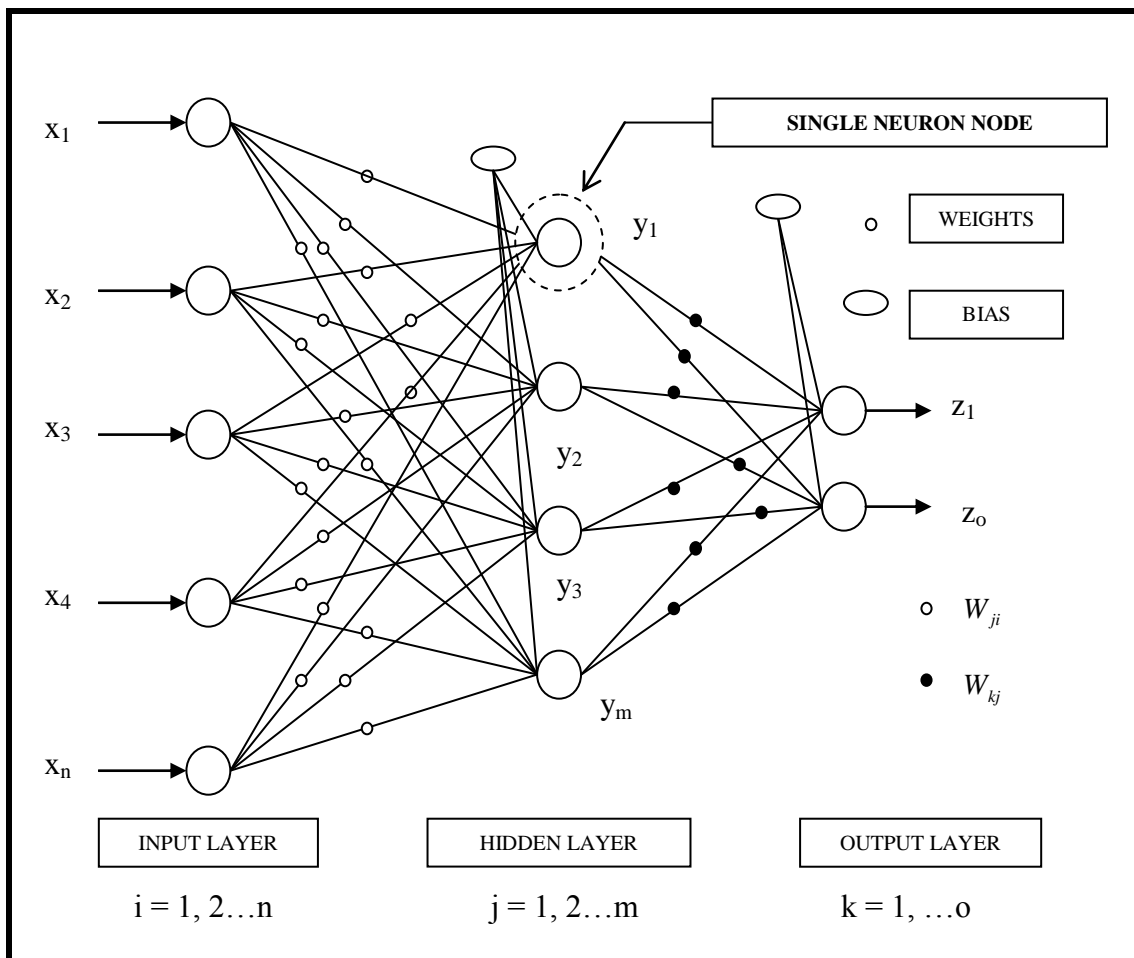


Fig. 4.3 Feed forward Back-propagation Network

According to Kosko (2003), learning of feed forward back-propagation neural network is based on some variant of the Delta Rule, which begins with the calculated difference between the actual outputs and the desired outputs. The complex part of this learning mechanism is for the system to determine which input contributed the most to an incorrect output and how is that element changed to correct the error. An inactive node would not contribute to the error and would have no need to change its weights. To solve this problem, training inputs are applied to the input layer of the network, and desired outputs are compared at the output layer. During the learning process, a forward sweep is made through the network, and the output of each element is computed layer by layer. The difference between the output of the final layer and the desired output is back propagated to the previous layer(s), usually modified by the derivative of the transfer function, and the connection weights are normally adjusted using the Delta Rule. This process proceeds for the previous layer(s) until the input layer is reached. There are many variations to the learning rules for back-propagation network. Different error functions, transfer functions, and even the modifying method of the derivative of the transfer function can be used.

Mathematically, the feed forward artificial neural network is expressed as:

$$Z_k(x) = \sum_{j=1}^m W_{kj} \times T_r(y) + b_{ko} \quad (4.1)$$

$$Y_j = \sum_{i=1}^n W_{ji} \times x_i + b_{ji} \quad (4.2)$$

Where x is input value from 1 to n , W_{ji} are the weights between input layer and hidden layer nodes and W_{kj} are the weights between hidden layer and output layer nodes. b_{ji} and b_{ko} are bias values at hidden and output layer respectively. m is the number of hidden layer nodes and $T_r(y)$ is transfer function. This transfer function allows a non-linear conversion of summed inputs.

A non-linear transfer function is applied between input nodes and hidden nodes. In the present research work, *Tansig* is used as transfer function, which is expressed as:

$$T_r(y) = \left[\frac{2}{1 + \exp(-2 \times y)} - 1 \right] \quad (4.3)$$

y is the summation of input values with weights and biases. The transfer function improves the network generalization capabilities and speeds up the convergence of the learning process. The bias values for both hidden layer and output layer get adjusted at each time of iterations. The weights between hidden and output layers are calculated using updated Levenberg-Marquardt algorithm.

In the present research work, the linear transfer function *purelin* is applied between hidden layer and output layer, and it is expressed as:

$$purelin(n) = n \quad (4.4)$$

The overall objective of training algorithm is to reduce the global error, E , defined as:

$$E = \frac{1}{p} \sum_{p=1}^p \left[\sum_{k=1}^k (d_{kp} - o_{kp})^2 \right] \quad (4.5)$$

Where; p is the total number of training patterns, d_{kp} is the desired value of the k^{th} output and the p^{th} pattern, o_{kp} is the actual value of the k^{th} output and p^{th} pattern. Here, Levenberg-Marquardt (LM) updated algorithm (Wilamoski et al, 2001) is used to train the network.

4.2.4 Levenberg-Marquardt method

In the present research work, Levenberg-Marquardt method is used to train the feed forward back-propagation neural network. The Levenberg-Marquardt method is a second-order method (Hagan and Menhaj; 1994, Masters; 1995). Rather than finding the error minimum directly, it aims to locate the zero of the error gradient. The zero α of a univariate function f may be found using the Newton-Raphson method according to the iterative formula of equation 4.6

$$\alpha_{n+1} = \alpha_n - \frac{f(\alpha_n)}{f'(\alpha_n)} \quad (4.6)$$

When extended to a multivariate function, α becomes a vector and the derivative of the function is now a vector derivative, as in equation 4.7.

$$\alpha_{n+1} = \alpha_n - \frac{f(\alpha_n)}{\nabla f(\alpha_n)} \quad (4.7)$$

In the case of neural network optimization, we wish to find the zero of the error gradient \mathbf{g} with respect to the network weights. Since \mathbf{g} is a vector quantity and is itself a derivative, we have to work with the Hessian matrix \mathbf{H} (equation 4.8).

$$\mathbf{w}_{n+1} = \mathbf{w}_n - [\mathbf{g}(\mathbf{w}_n) / \mathbf{H}(\mathbf{w}_n)] \quad (4.8)$$

Each element in the Hessian contains second derivatives of the error function, summed over all training patterns. However, the error measure E is related to the outputs and target outputs. The elements within the Hessian therefore contain values like that in equation 4.9, summed across all training patterns.

$$\frac{\partial^2 E}{\partial w_i \partial w_j} = 2 \left(\frac{\partial y}{\partial w_i} \frac{\partial y}{\partial w_j} + (y - t) \frac{\partial^2 y}{\partial w_i \partial w_j} \right) \quad (4.9)$$

One can calculate local values of the first derivatives. These are the ∂ values used in the gradient descent method. The second derivatives in the above equation are disregarded when estimating the Hessian. This is a reasonable estimate since the error $(y-t)$ is expected to be small. Further, we expect the values of $(y - t)$ to have an approximately Gaussian distribution with mean zero. When summed over a large number of training patterns the second terms are therefore likely to cancel out to a large extent. Having obtained an approximation of the Hessian, the Newton-Raphson method may be used to find the nearest zero of the error gradient. Two problems may arise. Firstly, the local Hessian estimation may not be an adequate representation of the underlying function. Secondly, the second-order algorithm by itself may approach a maximum or saddle point on the error surface, rather than a minimum. In order to avoid these problems, the Levenberg-Marquardt method includes an additional gradient descent term. The weight adjustment vector is then given by equation 4.10.

$$\Delta w = (H + \lambda \text{diag} (H))^{-1} g \quad (4.10)$$

The parameter λ adjusts the relative weighting given to Newton's method and to gradient descent. If the error falls after applying the weight adjustment, λ is decreased. If, on the other hand, the error increases, the weight changes are reversed λ is increased and the weight changes are re-calculated.

In the present study, three-layered feed forward, back-propagation with Levenberg-Marquardt updated algorithm is used to predict the wave transmission of HIMMFPB.

4.2.5 Feed forward back-propagation neural network model for wave transmission prediction of HIMMFPB

In order to allow the network to learn both non-linear and linear relationships between input nodes and output nodes, multiple-layer neural networks are often used. In the present work, the three layers feed forward back -propagation neural network is used

representing the input nodes as first layer, hidden nodes as second layer and output nodes as third layer.

The back-propagation is a supervised learning technique used for training the neural network. The back propagation needs to know the correct output for any input parameters. The number of input nodes depends upon the complexity of the problem and the parameters, which influence the output parameters.

In the present research work, the input parameters that influence the wave transmission (K_t) of HIMMFPB, such as, relative spacing of pipes (S/D), relative breakwater width (W/L), ratio of incident wave height to water depth (H_i/d), incident wave steepness (H_i/L) are considered. Based on above input parameters, two ANN models are constructed to predict the transmission coefficient of HIMMFPB as shown in Table 4.1.

Table 4.1 ANN models with input parameters

Model	Input Parameters
ANN1	$W/L, H_i/d, H_i/L$
ANN2	$S/D, W/L, H_i/d, H_i/L$

The main objective of back propagation neural network technique is to train the model such that the result outputs are nearer to the desired values. Therefore, the error between network output and desired value is minimum.

Mathematically, the feed forward artificial neural network is expressed as:

$$Z_k(x) = \sum_{j=1}^m W_{kj} \times T_r(y) + b_{ko} \tag{4.11}$$

$$Y_j = \sum_{i=1}^n W_{ji} \times x_i + b_{ji} \quad (4.12)$$

Where x is input value from 1 to n , W_{ji} are the weights between input layer and hidden layer nodes and W_{kj} are the weights between hidden layer and output layer nodes. b_{ji} and b_{ko} are bias values at hidden and output layer respectively. m is the number of hidden layer nodes and $T_r(y)$ is transfer function. This transfer function allows a non-linear conversion of summed inputs.

A non-linear transfer function is applied between input nodes and hidden nodes. In the present research work, *Tansig* is used as transfer function, which is expressed as:

$$T_r(y) = \left[\frac{2}{1 + \exp(-2 \times y)} - 1 \right] \quad (4.13)$$

y is the summation of input values with weights and biases. The transfer function improves the network generalization capabilities and speeds up the convergence of the learning process. The bias values for both hidden layer and output layer get adjusted at each time of iterations. The weights between hidden and output layers are calculated using updated Levenberg-Marquardt algorithm.

In the present research work, the linear transfer function *purelin* is applied between hidden layer and output layer, and it is expressed as

$$purelin(n) = n \quad (4.14)$$

The overall objective of training algorithm is to reduce the global error, E , defined as:

$$E = \frac{1}{P} \sum_{p=1}^P \left[\sum_{k=1}^k (d_{kp} - o_{kp})^2 \right] \quad (4.15)$$

Where; p is the total number of training patterns, d_{kp} is the desired value of the k^{th} output and the p^{th} pattern, o_{kp} is the actual value of the k^{th} output and p^{th} pattern. Here, Levenberg-Marquardt (LM) updated algorithm (Wilamoski et al, 2001) is used to train the network. The codes are written in MATLAB 7 Release 14 (Appendix A-1 to A-3).

The correlation coefficient is calculated to know the how best the network predicted K_t values are matches with the measured K_t values. The straight line is drawn at an angle of 45° between the two axes to fit the data points. A high correlation is obtained when all the points lies exactly on this straight line.

4.3 ADAPTIVE NEURO FUZZY INFERENCE SYSTEM

4.3.1 Introduction

Fuzzy inference systems are the most popular constituent of the soft computing area since they are able to represent the human expertise in the form of IF antecedent THEN consequent statements. In this domain, the system behavior is modeled using linguistic descriptions. Although the earliest work by Zadeh (1965) on fuzzy systems has not been paid the attention, which it deserved in early 1960s, since then the methodology has become a well-developed framework. The typical architecture of fuzzy inference systems (FIS) are introduced by Wang (1994, 1997), Takagi and Sugeno (1985), and Jang et al. (1997). A fuzzy system having generalized bell membership function, product inference rule and weighted average defuzzifier has become the standard method in most applications. Takagi and Sugeno (1985) change the defuzzification procedure where dynamic systems are introduced as defuzzification subsystems.

4.3.2 ANFIS architecture

Inspired by the idea of basing the fuzzy logic inference procedure on a feed forward network structure, Jang (1993) proposed a fuzzy neural network model – the Adaptive

Neural Fuzzy Inference System or semantically equivalent, Adaptive Network-based Fuzzy Inference System (ANFIS), whose architecture is shown in Fig. 4.4. Jang (1993) reported that the ANFIS architecture can be employed to model nonlinear functions, identify nonlinear components on-line in a control system, and predict a chaotic time series. It is a hybrid neuro-fuzzy technique that brings learning capabilities of neural networks to fuzzy inference systems. The learning algorithm tunes the membership functions of a Sugeno-type Fuzzy Inference System using the training set of input-output data. A detailed coverage of ANFIS can be found in Jang (1993), Jang et al. (1997). The ANFIS, from the topology point of view, is an implementation of a representative fuzzy inference system using a back propagation neural network-like structure. It consists of five layers. The role of each layer is

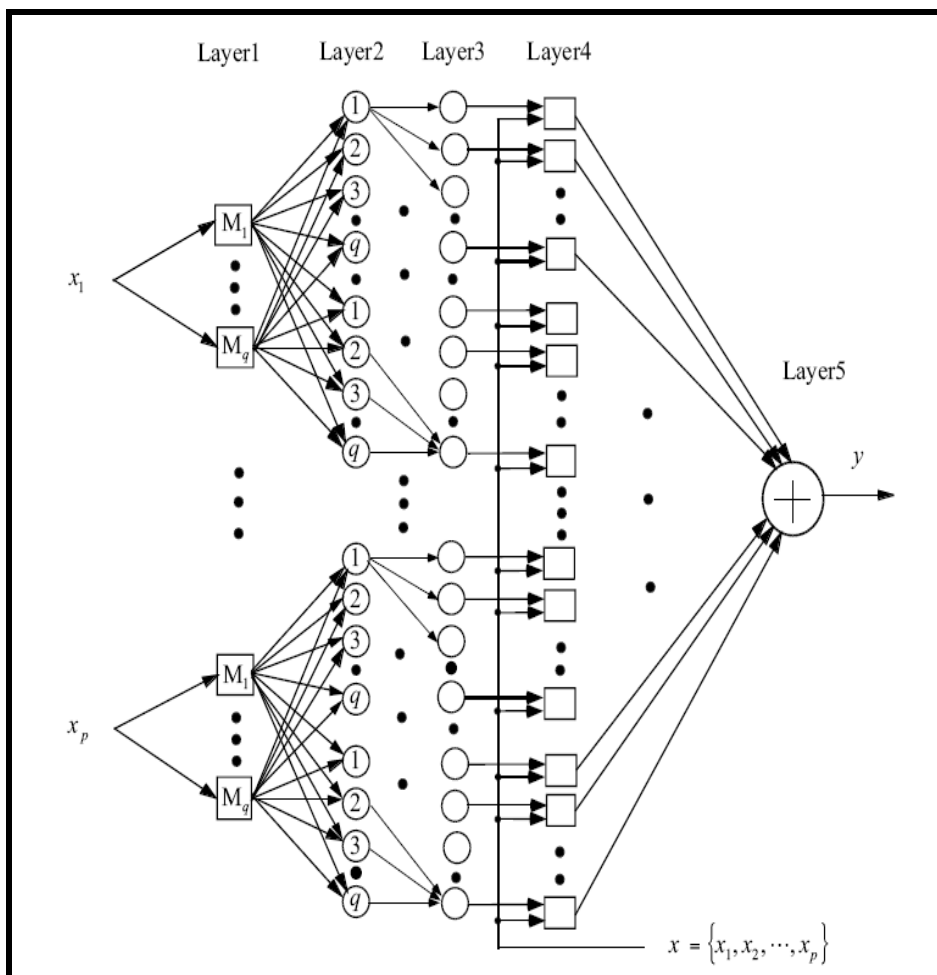


Fig. 4.4 ANFIS Structure

briefly presented as follows: let O_i^l denote the output of node i in layer l , and x_i is the i^{th} input of the ANFIS, $i = 1, 2, \dots, p$. In layer 1, there is a node function M associated with every node:

$$O_i^l = M_i(x_i) \quad (4.16)$$

The role of the node functions M_1, M_2, \dots, M_q here, is same as the membership functions $\mu(x)$ used in the regular fuzzy systems, and q is the number of nodes for each input. Generalized bell membership function is the typical choice. The adjustable parameters that determine the positions and shapes of these node functions are referred to as the premise parameters. The output of every node in layer 2 is the product of all the incoming signals:

$$O_i^2 = M_l(x_l) \text{ AND } M_j(x_j) \quad (4.17)$$

Each node output represents the firing strength of the reasoning rule. In layer 3, each of these firing strengths of the rule is compared with the sum of all the firing strengths. Therefore, the normalized firing strengths are compared in this layer as:

$$O_i^3 = \frac{O_i^2}{\sum_i O_i^2} \quad (4.18)$$

Layer 4 implements the Sugeno-type inference system, i.e. a linear combination of the input variables of ANFIS x_1, x_2, \dots, x_p plus a constant term c_1, c_2, \dots, c_p , from the output of each *IF-THEN* rule. The output of the node is a weighted sum of these intermediate outputs:

$$O_i^4 = O_i^3 \sum_{j=1}^p (P_j x_j + c_j) \quad (4.19)$$

where, parameters P_1, P_2, \dots, P_p and c_1, c_2, \dots, c_p , in this layer are referred to as the consequent parameters. The node in layer 5 produces the sum of its inputs, i.e., defuzzification process of fuzzy system (using weighted average method) and is obtained as:

$$O_i^5 = \sum_i O_i^4 \quad (4.20)$$

ANFIS distinguishes itself from normal fuzzy logic systems by the adaptive parameters, i.e., both the premise and consequent parameters are adjustable. The most remarkable feature of the ANFIS is its hybrid-learning algorithm. The adaptation process of the parameters of the ANFIS is divided into two steps. For the first step of the consequent parameters training, the Least Squares method (LS) is used, because the output of the ANFIS is a linear combination of the consequent parameters. The premise parameters are fixed at this step. After the consequent parameters have been adjusted, the approximation error is back propagated through every layer to update the premise parameters as the second step. This part of the adaptation procedure is based on the gradient descent principle, which is the same as in the training of the feed forward back propagation neural network. The consequence parameters identified by the LS method are optimal in the sense of least squares under the condition that the premise parameters are fixed. Therefore, this hybrid-learning algorithm is more effective than the pure gradient decent approach, because it reduces the search space dimensions of the original back propagation method. The pure back propagation learning process could easily be trapped into local minima. When compared with employing either one of the above two methods individually, the ANFIS converges with a smaller number of iteration steps with this hybrid learning algorithm.

The present research work considers the ANFIS structure with first order Sugeno model containing generalized bell membership functions. At fuzzification level, all ANFIS models use product inference rule and hybrid learning algorithm that

combines least square method with gradient descent method to adjust the parameter of membership functions, whereas weighted average is used as defuzzifier.

4.3.3 Fuzzy logic approach for wave transmission prediction of HIMMFPB

In the present investigation, the input parameters that influence the wave transmission (K_t) of HIMMFPB, such as, relative spacing of pipes (S/D), relative breakwater width (W/L), ratio of incident wave height to water depth (H_i/d), incident wave steepness (H_i/L) are considered to develop ANFIS. Based on above input parameters, Six ANFIS models are constructed to predict the transmission coefficient of HIMMFPB as shown in Table 4.2.

Table 4.2 ANFIS models with input

Model	S/D ratio	Input Parameters
ANFIS1	2	$W/L, H_i/d, H_i/L$
ANFIS2	3	$W/L, H_i/d, H_i/L$
ANFIS3	4	$W/L, H_i/d, H_i/L$
ANFIS4	5	$W/L, H_i/d, H_i/L$
ANFIS5	Total	$S/D, W/L, H_i/d, H_i/L$
ANFIS6	Total	$S/D, W/L, H_i/d$

$W/L, H_i/d, H_i/L$ and K_t are used as a training data to train ANFIS1, ANFIS2, ANFIS3 and ANFIS4 network having S/D ratio as 2, 3, 4 and 5 respectively. Experimental analysis shows that K_t is better with increase in S/D ratio, in this regard to study over a range of S/D on K_t , an input parameter, S/D is added to form ANFIS5 model. ANFIS6 model is the same as ANFIS5 model without H_i/L parameter. The codes are written in MATLAB 7 Release 14 (Appendix A-4 and A-5).

The flowchart of ANFIS procedure used in the present research work, is shown in Fig. 4.5. In the first step, initialization of the fuzzy system is done using *genfis1* command, which specifies the structure and initial parameters of the fuzzy inference system (FIS) with training data matrix, number of membership functions and membership function type associated with each input. In the above, the number of membership functions is determined by trial and error. In the second step, parameters for learning are set with the number of iterations and tolerance. Once the learning parameters are set, *anfis* command is used for learning; *anfis* uses a hybrid learning algorithm to identify parameters of sugeno-type fuzzy inference systems.

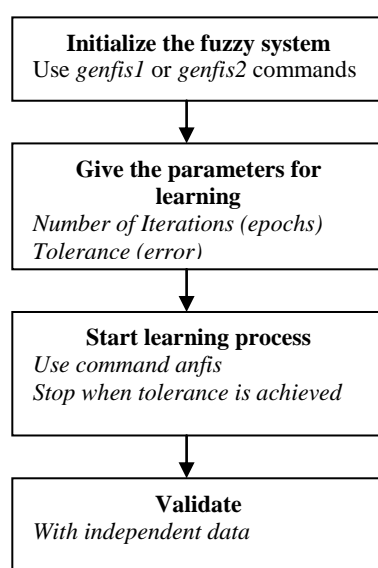


Fig. 4.5 ANFIS procedure

An ANFIS distinguishes itself from normal fuzzy logic systems by the adaptive parameters, i.e. both the premise and consequent parameters are adjustable. The most remarkable feature of the ANFIS is its hybrid-learning algorithm. The adaptation process of the parameters of the ANFIS is divided into two steps. For the first step of consequent parameters training, Least Squares method (LS) is used because the output of ANFIS is a linear combination of the consequent parameters. The premise parameters are fixed at this step. After the consequent parameters have been adjusted, the approximation error is back propagated through every layer to update the premise parameters as the second step. This part of the adaptation procedure is based on the

gradient descent principle, which is the same as in the training of the back-propagation neural network. The consequent parameters identified by the LS method are optimal in the sense of least squares under the condition that the premise parameters are fixed. Therefore, this hybrid-learning algorithm is more effective than the pure gradient decent approach, as it reduces the search space dimensions of the original back propagation method. The pure back propagation learning process could easily be trapped into local minima. When compared with employing either one of the above two methods individually, the ANFIS converges with a smaller number of iteration steps with this hybrid learning algorithm. Once the tolerance is achieved, the learning process is stopped and the validation is carried out by testing data set to compare the efficiency of the ANFIS model with actual system. In the present work, three generalized bell membership functions have been assigned to each input variables as the initial membership function and is obtained by:

$$\mu_{A_i}(X) = \frac{1}{1 + \left[\left(\frac{X - c_i}{a_i} \right)^2 \right]^{b_i}} \quad (4.21)$$

where $\{a_i, b_i, c_i\}$ is the premise parameters set that changes the shape of the membership function with maximum equal to 1 and minimum equal to 0 and X is the input variable. The physical meaning of the parameters in bell membership function is given in Fig. 4.6, where a = half width of bell function, b = slope at crossover point (where degree of membership = 0.5) and c = center of corresponding membership function. Each input variable is classified into three fuzzy categories with linguistic attributes as Low_{*i*}, Medium_{*i*}, and High_{*i*} ($i = 1 - 3$ for ANFIS1, ANFIS2, ANFIS3, and ANFIS4 models, whereas for ANFIS5 model, $i = 1 - 4$). Initial values of premise parameters before learning are set in such a way that the centers of the membership functions are equally spaced along the range of each input variable. Fig. 4.7 shows the initial membership function before learning for an ANFIS5 model associated with 4 inputs S/D , W/L , H_i/d and H_i/L . As the training process, takes place values

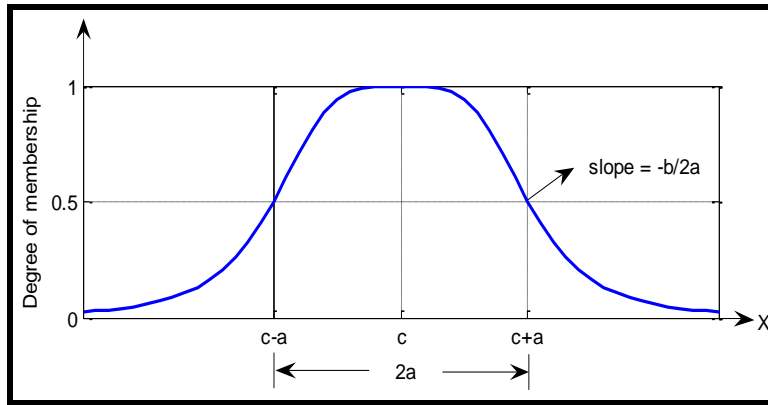
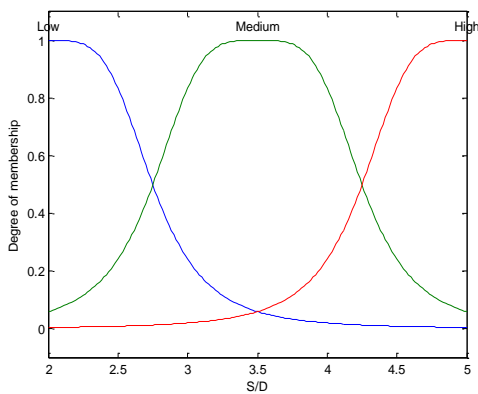
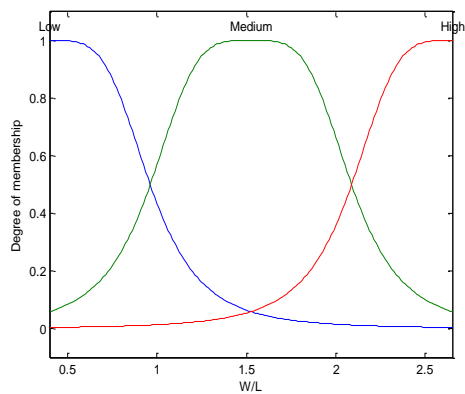


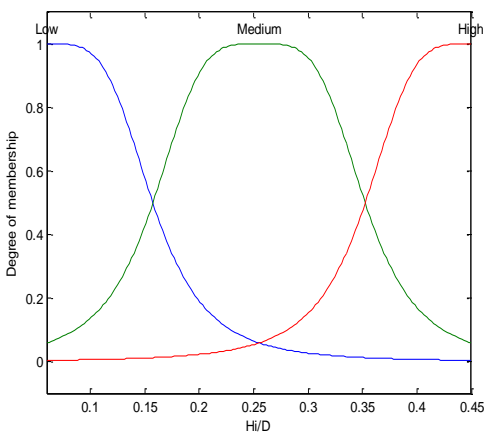
Fig. 4.6 Physical meaning of the parameters in the bell membership function



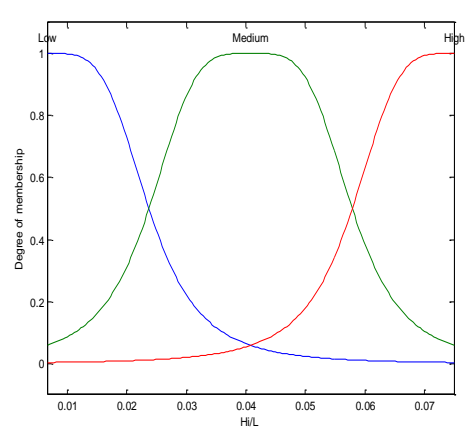
(a) S/D



(b) W/L



(c) H_i/d



(d) H_i/L

Fig. 4.7 Initial membership functions of input parameters (x-axis) for ANFIS5 model

of a , b and c change, the bell shaped function vary accordingly, thus exhibiting various forms of membership functions on linguistic attributes A_i . The hybrid-learning algorithm that combines least square method with gradient descent method is used to adjust the parameters of membership function. In present investigation, product inference rules are used at the fuzzification level and weighted average is used as defuzzifier for all ANFIS models.

4.3.4 Principal component analysis

In order to assess the influence of input parameters, principal component analysis (PCA) is carried out. The code is written in MATLAB 7 Release 14 (Appendix A-8). PCA is simple, non-parametric method for extracting relevant information from confusing data sets (Shlens, 2009). It transfers the data set on to different axes orthogonal to each other in the data space. The projections of the data on those vectors are the principal components and are found by calculating the eigenvectors of the data correlation matrix. The corresponding eigen values give an indication of the amount of information that the respective principal components represents. Thus by discarding those components, which explains a negligible part of the data variance, a high rate of data compression can be obtained.

PCA estimates eigen values and variances of four non-dimensional parameters for each component, as shown in Table 4.3. The first component alone accounts for 84.914 % of the total variance, the second component alone accounts for 14.431%, the 3rd and 4th components together account less than 1% respectively. According to PCA, the first two components together account more than 99%. The factorial weights of the four components are shown in Table 4.4. This shows the first principal component has strong relation to the S/D , and the second principal component has strong relation to W/L . In fact first principal component reflect the porosity parameter accounts for 84.914% of the total variance and the second principal component reflects the relative breakwater width, which accounts for 14.431%.

Table 4.3 Principal component analysis

Principal Components Numbers	PC1	PC2	PC3	PC4
Eigen Value	1.35350	0.23002	0.01038	0.00005
% Variance	84.914	14.431	0.652	0.003
Cumulative % variance	84.914	99.345	99.997	100.000

Table 4.4 Factor loading of principal components

Input Parameters	PC1	PC2	PC3	PC4
S/D	-0.99991	0.01327	0.00107	0.00025
W/L	0.01328	0.99966	-0.02056	-0.00944
H_i/d	0.00074	-0.02164	-0.99089	-0.13293
H_i/L	0.00048	0.00661	-0.13310	0.99108

From this study, it is observed that H_i/L is the least influential parameter. Based on the PCA study considering the first three input parameters, ANFIS6 model was developed.

4.4 SUPPORT VECTOR MACHINE REGRESSION

4.4.1 Introduction

SVMs are the recently developed learning techniques that have gained enormous popularity in the field of classification, pattern recognition and regression. SVM works on structural risk minimization principle that has greater generalization ability and is superior to the empirical risk minimization principle as adopted in conventional neural network models. Han et al. (2007) applied SVM for flood forecasting, Msiza, et al. (2008) used ANN and SVR for water demand prediction, Rajasekaran et al. (2008) developed a support vector machine regression (SVMR) model for forecasting

storm surges. They compared these results with numerical methods and ANN, which indicated that storm surges and surge deviations are efficiently, predicted using SVMR. Radhika and Shashi (2009) used SVM for prediction of atmospheric temperature. Mahjoobi and Mosabbebi (2009) presented that the SVM creates a more reliable model with better generalization error, in comparison to ANN, they also reveal that SVMs do not over-fit, while ANNs may face such problem and need to deal with it. However, it is observed that there are hardly any applications of SVMs on wave transmission of floating breakwater. This fact leads us to use SVM models in this work.

4.4.2 Theoretical background of SVMR

Vapnik (1998) proposed the support vector machines (SVMs), which is based on statistical learning theory. The basic idea of support vector machines is to map the original data x into a feature space with high dimensionality through a non-linear mapping function and construct an optimal hyper-plane in new space. Hence, given a set of data $S = \{(x_i, d_i)\}_{i=1}^N$, where x_i is the input data set, d_i is the desired result, and N corresponds to the size of the data set. Then, according to Smola and Scholkopf (1998), the SVM regression function is expressed as

$$y = f(x) = w_i \phi_i(x) + b \quad (4.22)$$

Where $\phi_i(x)$ is the non-linear function in feature of input x , and both w_i and b are coefficients, which are estimated by minimizing the regularized risk function as expressed below:

$$\text{Minimize : } R(C) = \frac{1}{2} \|w\|^2 + C \frac{1}{N} \sum_{i=1}^N L_\varepsilon(d_i, y_i) \quad (4.23)$$

where;

$$L_\varepsilon(d_i, y_i) = \begin{cases} |d_i - y_i| - \varepsilon, & |d_i - y_i| \geq \varepsilon, \\ 0, & \text{others,} \end{cases} \quad (4.24)$$

The first term in equation 4.23 is called regularized term, measures the flatness of the function. The second term is the empirical error measured by the ε -insensitive loss function, which is defined as equation 4.24. C and ε are user determined parameters, d_i is the actual value at period i , y_i is the forecasted value at period i , and C is a weighing parameter considered to specify the trade-off between the empirical risk and model flatness. Equation 4.24 defines a range where the loss will be zero if the forecasted value is within the ε -tube (Equation 4.24 and Fig. (4.8)). However, if the value is out of the ε -tube then the loss is the absolute value, which is the difference between forecasted value and ε . Introducing two positive slack variables ζ_i and ζ_i^* in Equation 4.24, it is possible to transform it into a primal objective function given by:

$$\text{Minimize : } R(w, \zeta_i, \zeta_i^*) = \frac{1}{2} \|w\|^2 + C \sum_{i=1}^N (\zeta_i + \zeta_i^*) \quad (4.25)$$

subject to the constraints;

$$\begin{aligned} d_i - w_i \phi(x_i) - b &\leq \varepsilon + \zeta_i, \\ w_i \phi(x_i) + b - d_i &\leq \varepsilon + \zeta_i^*, \\ \text{where, } \zeta_i, \zeta_i^* &\geq 0, \quad i = 1, 2, \dots, N. \end{aligned}$$

ζ_i and ζ_i^* represents the distance from the actual values to the corresponding boundary values of ε -tube.

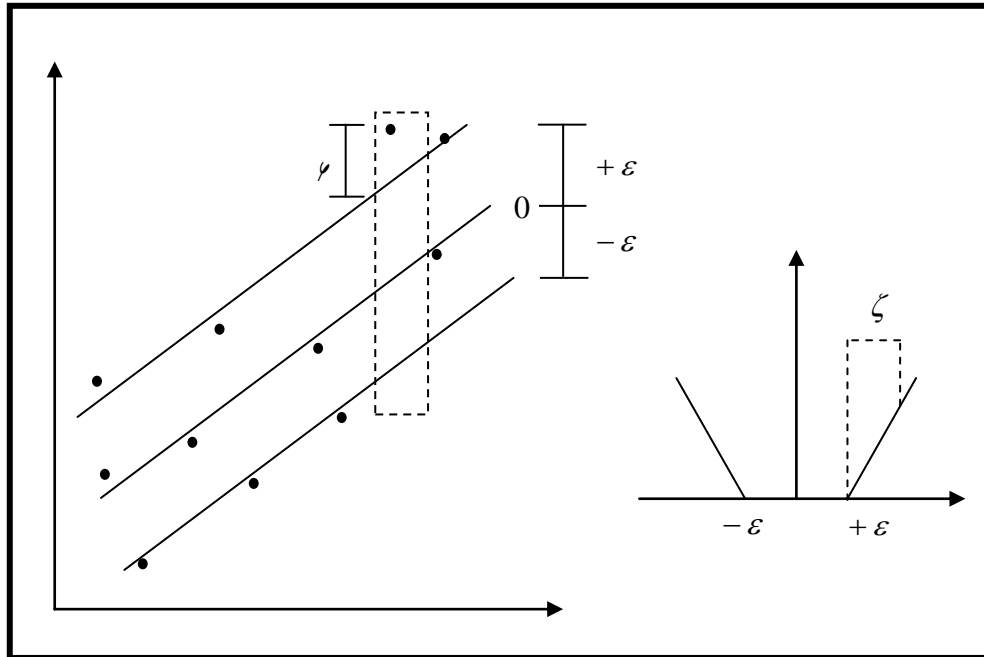


Fig. 4.8 The loss margin setting corresponds to one-dimensional linear SV machine

The key idea is to construct the Lagrange function from the primal objective function and corresponding constraints by introducing the dual set of variables,

$$L(w_i, \zeta_i, \zeta_i^*, \alpha_i, \alpha_i^*, \beta_i, \beta_i^*) = \frac{1}{2} \|w\|^2 + C \sum_{i=1}^N (\zeta_i + \zeta_i^*) - \sum_{i=1}^N \alpha_i [w_i \phi(x_i) + b - d_i + \varepsilon + \zeta_i] - \sum_{i=1}^N \alpha_i^* [d_i - w_i \phi(x_i) - b + \varepsilon + \zeta_i^*] - \sum_{i=1}^N (\beta_i \zeta_i + \beta_i^* \zeta_i^*) \quad (4.26)$$

Equation 4.26 is minimized with respect to primal variables w_i, b, ζ, ζ^* , and maximized with respect to non-negative Lagrangian multipliers $\alpha_i, \alpha_i^*, \beta_i$ and β_i^* . Finally, Karush-Kuhn-Tucker conditions are applied to the regression, and Equation 4.26 thus yields the dual Lagrangian,

$$J(\alpha_i, \alpha_i^*) = \sum_{i=1}^N d_i (\alpha_i - \alpha_i^*) - \varepsilon \sum_{i=1}^N (\alpha_i + \alpha_i^*) - \frac{1}{2} \sum_{i=1}^N \sum_{j=1}^N (\alpha_i - \alpha_i^*) (\alpha_j - \alpha_j^*) K(x_i, x_j) \quad (4.27)$$

subject to the constraints;

$$\sum_{i=1}^N (\alpha_i - \alpha_i^*) = 0, \quad 0 \leq \alpha_i, \alpha_i^* \leq C, \quad i = 1, 2, \dots, N.$$

In Equation 4.27, α_i and α_i^* are called Lagrangian multipliers that satisfy equalities, $\alpha_i \times \alpha_i^* = 0$. After calculating α_i and α_i^* , an optimal desired weights vector of the regression hyper-plane is represented as:

$$w^* = \sum_{i=1}^N (\alpha_i - \alpha_i^*) K(x_i, x_j) \quad (4.28)$$

Therefore, the regression function is expressed as:

$$f(x, \alpha, \alpha^*) = \sum_{i=1}^N (\alpha_i - \alpha_i^*) K(x_i, x_j) + b \quad (4.29)$$

Here, $K(x_i, x_j)$ is called the kernel function. The value of the kernel equals the inner product of two vectors x_i and x_j in the feature space $\phi(x_i)$ and $\phi(x_j)$, i.e., $K(x_i, x_j) = \phi(x_i) \times \phi(x_j)$. The role of the kernel function simplifies the learning process by changing the representation of the data in the input space to a linear representation in a higher-dimensional space called a feature space. A suitable choice of kernel allows the data to become separable in the feature space despite being non-separable in the original input space. This allows us to obtain non-linear algorithm from algorithms previously restricted in handling linearly separable datasets. The function that satisfies Mercer's condition by Vapnik (1995) can be used as the kernel function.

4.4.3 Support vector machine regression for wave transmission prediction of HIMMFPB

In the present study, the input parameters that influence the wave transmission (K_t) of floating breakwater, such as, relative spacing of pipes (S/D), relative breakwater width (W/L), ratio of incident wave height to water depth (H_i/d), incident wave steepness (H_i/L) are used to train SVMR models are shown in Table 4.5.

Table 4.5 Data used for training and testing the SVMR models with input parameters

Model	Input Parameters	Number of data points for training	Number of data points for testing
SVMR(linear)	$(S/D), (W/L), (H_i/d), (H_i/L)$	2131	813
SVMR(polynomial)			
SVMR(rbf)			
SVMR(erbf)			
SVMR(spline)			
SVMR(b-spline)			

In the present work, we have experimented with the six kernels as shown in Table 4.6. The linear kernel function is used for linear SVMR model, whereas the polynomial, radial basis function (rbf), exponential radial basis function (erbf), spline and b-spline kernels are used for non-linear SVMR models. According to Karatzoglou and Meyer (2006), Gaussian radial basis function kernel is the general purpose kernel used when there is no prior knowledge about the data. The linear kernel is useful, when dealing with large sparse data vectors, as usually the case in text categorization. The polynomial kernel is popular in image processing, whereas, the spline kernels typically perform well in regression. Selection of two kernel parameters (d, γ) and

support vector machine parameters (C, ε) of a SVMR model is significant in accuracy of the forecasting, where, the parameter d represents the degree of polynomial and b-spline kernel functions, whereas, γ is the width of rbf and erbf kernel functions. The

Table 4.6 Kernel Functions

Kernels	Functions
linear	$K(x_i, x_j) = a_1 x_i x_j + a_2$
polynomial	$K(x_i, x_j) = ((x_i, x_j) + 1)^d$
rbf	$K(x_i, x_j) = \exp\left(-\frac{\ x_i - x_j\ ^2}{2\gamma^2}\right)$
erbf	$K(x_i, x_j) = \exp\left(-\frac{\ x_i - x_j\ }{2\gamma^2}\right)$
spline	$K(x_i, x_j) = 1 + (x_i, x_j) + \frac{1}{2}(x_i, x_j)\min(x_i, x_j) - \frac{1}{6}\min(x_i, x_j)^3$
b-spline	$K(x_i, x_j) = B_{2d+1}(x_i - x_j)$

generalization performance of SVMR depends on a good setting of C, ε and kernel parameters d and γ . Parameter C determines the trade-off between the model complexity (flatness) and the degree to which deviations larger than ε tube (Smola 1996 and Gunn, 1998). If C is too large (infinity), then the objective is to minimize the empirical risk only, without regard to the model complexity (Cherkassky and Ma, 2004). In the present study, quadratic loss function is used. The main idea of using this loss function is to ignore the errors, which are situated within the certain distance of the true value. Parameter ε controls the width of the ε -insensitive zone, which is used to fit the training data. The number of support vectors (nsv) used to construct regression function depends on ε , the big ε , the fewer support vectors are selected and results in data compression (Kecman, 2001). The performance of SVMR depends on the good setting of SVM and kernel parameters. As there are no general rules to

determine the free parameters, the optimum values are set by two-stage grid search method. Initially a coarse grain search (i.e. for $C=100,500,1000$; $\varepsilon =1,2$; d and $\gamma = 1,2,3$) is performed to identify the near optimal values, and then a fine grain search (i.e. for $C = 10, 20, 30$; $\varepsilon = 0.001, 0.01, 0.1, 1$; d and $\gamma = 0.001, 0.01, 0.1, 1$) is done to identify the optimal values.

To optimize these parameters for better generalization of SVMR model, SVMR model is hybridized with GAs. Section 4.5 details the genetic algorithm in parameter selection, whereas section 4.6. details interface of genetic algorithm with support vector machine regression to obtain the best GA-SVMR model.

4.5 GENETIC ALGORITHM FOR SELECTING PARAMETERS IN THE SVMR MODEL

Genetic algorithms are search methods based on principles of natural selection and genetics (Holland, 1975). The algorithm is based on the principle of the survival of the fittest, which tries to retain genetic information from generation to generation. In the present work, GAs is used to search for better combination of C , ε and kernel parameters (d and γ) to maximize the generalization performance of SVMR model. The procedure of genetic algorithms in parameter selection is shown in Fig. 4.9, whereas Fig. 4.10 shows the proposed GA-SVMR model. The codes are written in MATLAB 7 Release 14 (Appendix A-6 and A-7). The steps involved in GA for selecting SVMs and kernel parameters are as follows:

Step 1. (Initialization): In the present paper initial population of chromosomes is generated randomly. Population size is set to 50. The chromosomes are real coded string, consist of SVMs parameters C , ε and kernel parameters (d and γ).

Step 2. (Evaluating fitness): In this step fitness of each chromosome is evaluated. In the present paper, a negative normalized mean square error is used as the fitness

function, which is defined as:

$$\text{Fitness Function} = \frac{1}{-\sigma^2 N} \sum_{i=1}^N (d_i - y_i)^2 \quad (4.30)$$

$$\text{Where, } \sigma^2 = \frac{1}{N} \sum_{i=1}^N (d_i - \bar{d}_i)^2 \quad (4.31)$$

N is the total number of data in the test set, \bar{d}_i is the mean of the actual value, d_i is the actual value, and y_i is the predicted value.

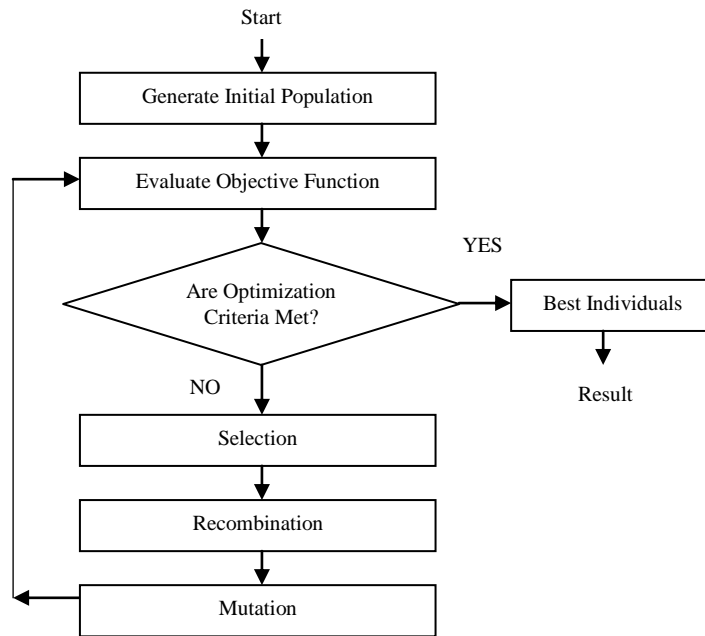


Fig. 4.9 Genetic Algorithm Procedure

Step 3. (New population): In this step new population is created by repeating following steps until the new population is complete

i) [Selection]: In the present study, two parent chromosomes from a population are

selected according to fitness function (Equation 4.30). The roulette wheel selection principle (Holland, 1975) is used to select chromosomes for reproduction

ii) [Crossover]: Here with crossover probability crossover of the parents is done to form new offspring's (children). In cross over, chromosomes are paired randomly. The intermediate crossover principle is used and offspring's are produced according to the following rule:

$$\text{Offspring} = \text{parent1} \pm \alpha (\text{parent2} - \text{parent1}) \quad (4.32)$$

Where α is the scaling factor chosen uniformly at random over an interval $[-d, 1+d]$. In the present study, d is chosen as 0.25.

iii) [Mutation]: After cross over operation is performed the string is subjected to mutation operation, this is to prevent falling all solutions of the population into local optimum of solved problem. The variable in the string to be mutated is selected randomly, where incremental operator is used. The rate of crossover and mutation is determined by probabilities. In the present paper, the probabilities of crossover and mutation are set to 0.8 and 0.05 respectively.

iv) [Accepting]: Accept and place new offspring in the new population.

Step 4. (Replace): Here new generated population is used for a further run of the algorithm.

Step 5. (Stop condition): If the end condition is satisfied, stop, and return the best solution in current population. Otherwise,

Step 6. (Loop): Go to *step 2*.

4.6 THE PROPOSED GA-SVMR MODEL

In the present study, MATLAB support vector machine toolbox (Gunn, 1998) is interfaced with genetic algorithm to optimize the SVMs and kernel parameters simultaneously for better generalization of the proposed GA-SVMR model. Six GA-SVMR models were developed by using six kernel functions (Table 4.6). In order to study, the performance of each kernel in predicting wave transmission of HIMMFPB, GA-SVMR is trained by applying these kernel functions. For training, experimental data set is used and is divided in to two groups one for training and other for testing (Table 4.7).

Table 4.7 Data used for training and testing the GA-SVMR models with input parameters

Model	Input Parameters	Number of data points for training	Number of data points for testing
GA-SVMR (linear)	$(S/D), (W/L), (H_i/d), (H_i/L)$	2131	813
GA-SVMR (polynomial)			
GA-SVMR (rbf)			
GA-SVMR (erbf)			
GA-SVMR (spline)			
GA-SVMR (b-spline)			

Fig. 4.13 illustrates the proposed GA-SVMR model. In the first stage training input, training target, kernel function, and range of kernel and SVM parameters are fed to the system. GA generates the initial population that would be used to find optimum factors of kernel functions and SVMs. In the second stage, the system performs typical SVM process using assigned value of the factors in the chromosomes, and calculates the performance of each chromosome. The performance of each

chromosome is calculated using fitness function for GAs given in Equation 4.30. In the present study, the main goal is to find the best parameters that produce the most accurate prediction. If the calculated fitness value satisfies the terminal condition in GAs, then the optimal parameters are selected, otherwise, the new generation of the population is produced by applying genetic operators, such as, selection, crossover, and mutation. After the production of new generation, the training process with calculation of the fitness value is performed again. From this point, stage two and stage three are iterated again and again until the stopping conditions are satisfied.

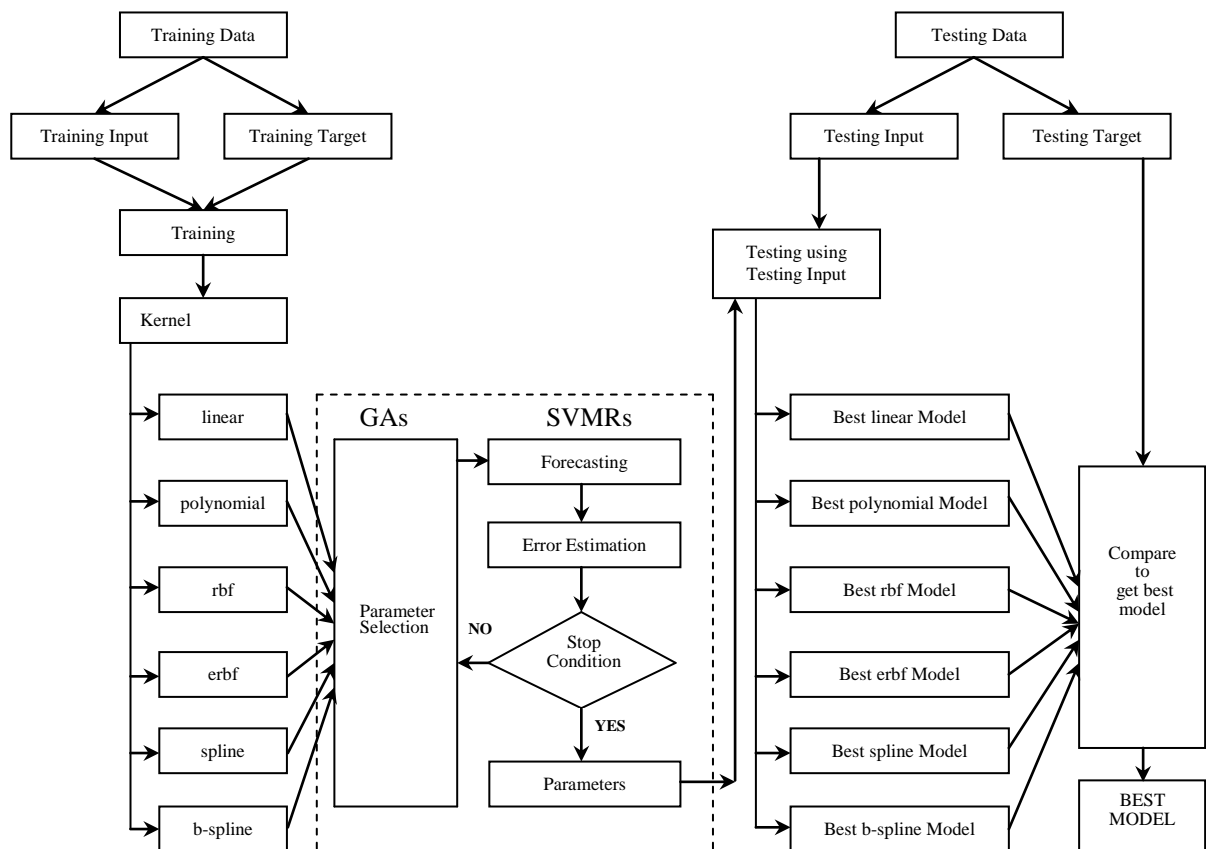


Fig. 4.10 Flow chart of GA-SVMR

Once the stopping condition is satisfied, the genetic search finishes and the chromosomes that shows the best performance in the last population is selected as the

result. In the forth and final stage optimized parameters obtained by GA are tested with the test data. The final decision about the optimum models is not based on the training data, but on the testing data, as illustrated in Fig. 4.10. Once the testing is over, the six models with linear, polynomial, rbf, erbf, spline and b-spline kernels are compared based on statistical measures to get the best model.

4.7 SUMMARY

This chapter describes in detail the research methods used to develop CI models, such as, ANN, ANFIS, SVMR and GA-SVMR to predict the wave transmission of HIMMFPB. Feed forward back propagation neural network model used in the present research work is explained in detail. Mathematical background of Levenberg-Marquardt algorithm used to train feed forward back propagation neural network is also presented. This chapter also describes the ANFIS architecture along with PCA procedure to identify the most influential parameters. A basic of SVMR and kernel techniques used in present research work is also presented. GAs procedure used to optimize the parameters of SVMR and kernels are described. Details of proposed GA based SVMR model is explained in detail.

CHAPTER 5

RESULTS AND DISCUSSION

5.1 GENERAL

The chapter details the performance of ANN, SVMR, ANFIS and GA-SVMR models in prediction of wave transmission through HIMMFPB. Data used to train and test these models are detailed in chapter 3, whereas, methodology used in developing these models are detailed in Chapter 4. Performance of these CI models are based on statistical measures, such as, *CC*, *RMSE* and *SI*.

5.2 PERFORMANCE OF FEED FORWARD BACK-PROPAGATED NEURAL NETWORK MODEL

In neural network technique, training of the network plays a very important role and it mainly depends upon the updated algorithms to be chosen to train the network. The ANN modeling of wave transmission of floating breakwater is carried out for five layer pipes with S/D of 2, 3, 4 and 5. The input parameters of ANN1 model are W/L , H_i/d , and H_i/L . To study over a range of spacing of pipes S/D on K_t , an input parameter S/D is added to form ANN2 model. After training and testing of both network models, *CCs* are calculated between desired output and network output using Equation 5.1.

$$CC = \frac{\sum_{i=1}^N (K_{mi} - \overline{K_m}) (K_{tpi} - \overline{K_{tp}})}{\sqrt{\sum_{i=1}^N (K_{mi} - \overline{K_m})^2} \times \sqrt{\sum_{i=1}^N (K_{tpi} - \overline{K_{tp}})^2}} \quad (5.1)$$

Where K_{mi} and K_{pi} represents the measured and predicted wave transmission coefficient, respectively, $\overline{K_m}$ and $\overline{K_p}$ are the mean value of measured and predicted observations, N is the number of observations.

In the present research work, updated algorithm, such as Levenberg-Marquardt algorithm (Wilamoski, et al, 2001) is used to train the two network models ANN1 and ANN2 with 100 and 200 epochs. The trained and tested ANN1 model's correlation coefficients (CC) and mean square error (MSE) of K_t for different S/D values are shown in Tables 5.1 to 5.4. This shows that the CC increases with S/D . The trained and tested ANN2 model's correlation coefficients of K_t are shown in Table 5.5. The final trained and tested results (CCs) of two network models are shown in Table 5.6 and Figures 5.1 to 5.5. It is observed that the correlation coefficients obtained are above 0.90. A high correlation coefficient is obtained at epoch equal to 200 with hidden nodes equal to 4 for ANN1 model (CCtrain=0.9672, CCtest=0.9649) and hidden nodes equal to 5 for ANN2 model (CCtrain=0.9537, CCtest=0.9488). Since all S/D values are considered in ANN2 model, CCs are in general less than that for ANN1 model with spacing ratio (S/D) of 5. The highest CC is obtained for ANN1 model (N-3-4-200) with spacing ratio of 5.

Table 5.1 Correlation coefficient of K_t for ANN1 model with $S/D=2$

Hidden Nodes	CCtrain	CCtest	MSEtrain	Epochs
2	0.9377	0.9312	0.00342	100
3	0.9449	0.9400	0.00303	100
4	0.9495	0.9426	0.00279	100
2	0.9376	0.9302	0.00342	200
3	0.9488	0.9430	0.00282	200
4	0.9552	0.9504	0.00248	200

Table 5.2 Correlation coefficient of K_t for ANN1 model with $S/D=3$

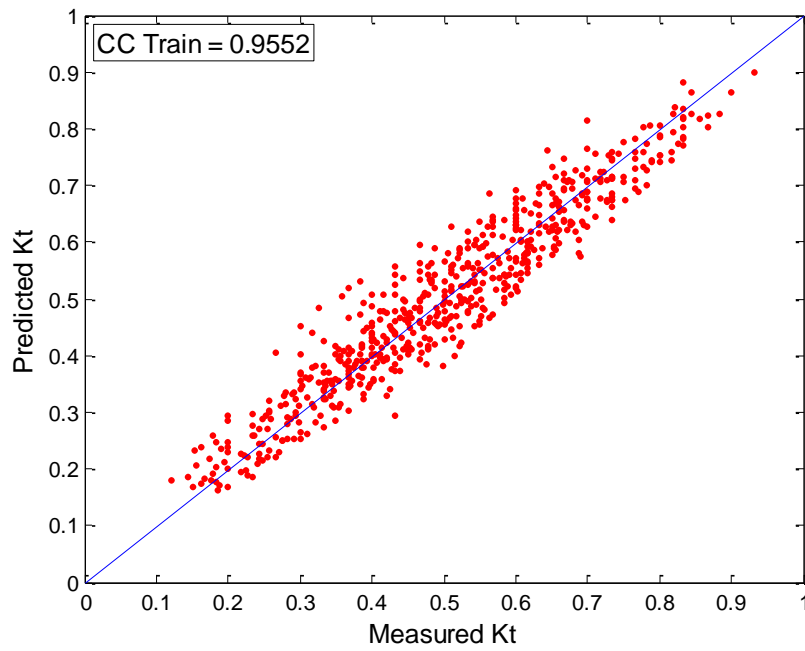
Hidden Nodes	CCtrain	CCtest	MSEtrain	Epochs
2	0.9310	0.9205	0.00230703	100
3	0.9382	0.9260	0.00207239	100
4	0.9419	0.9328	0.0019508	100
2	0.9263	0.9126	0.0024562	200
3	0.9469	0.9368	0.00178878	200
4	0.9506	0.9404	0.00166577	200

Table 5.3 Correlation coefficient of K_t for ANN1 model with $S/D=4$

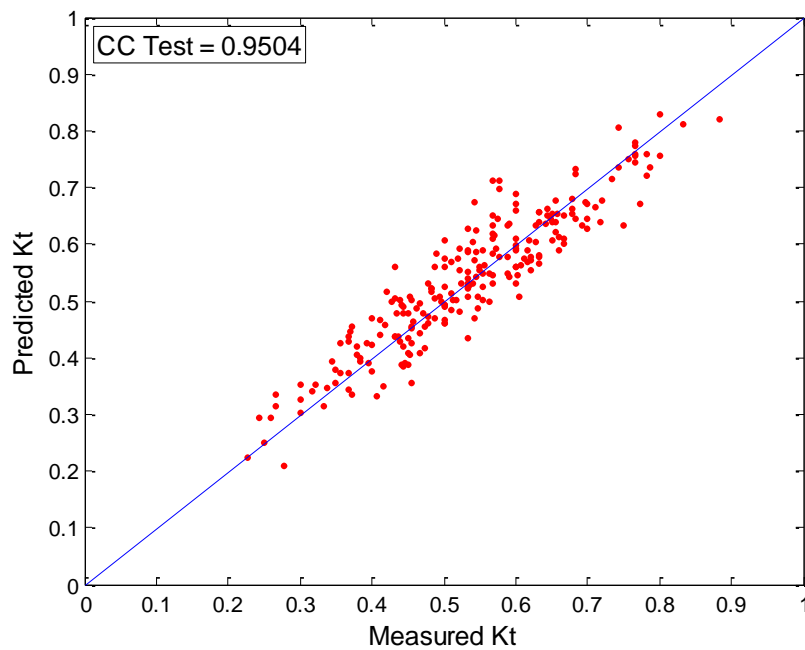
Hidden Nodes	CCtrain	CCtest	MSEtrain	Epochs
2	0.9490	0.9447	0.00164663	100
3	0.9620	0.9562	0.00122984	100
4	0.9647	0.9563	0.00114397	100
2	0.9551	0.9534	0.00144801	200
3	0.9619	0.9569	0.00123356	200
4	0.9642	0.9601	0.0011579	200

Table 5.4 Correlation coefficient of K_t for ANN1 model with $S/D=5$

Hidden Nodes	CCtrain	CCtest	MSEtrain	Epochs
2	0.939	0.937	0.00286544	100
3	0.9508	0.9488	0.00232692	100
4	0.9654	0.9642	0.00164658	100
2	0.9401	0.9369	0.00281679	200
3	0.9586	0.9567	0.00196222	200
4	0.9672	0.9649	0.00156346	200

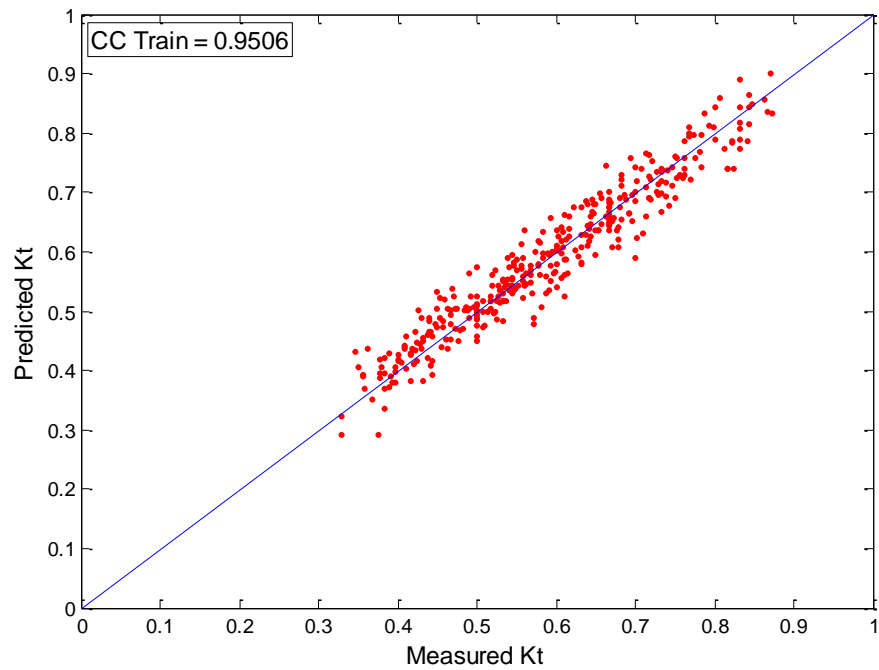


(a) Train Data

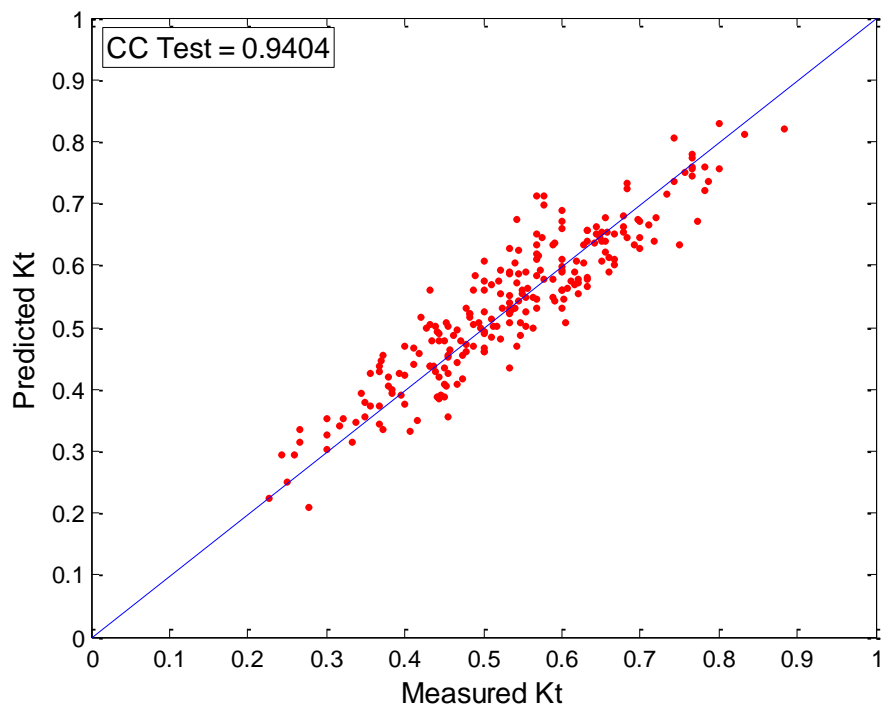


(b) Test Data

Fig. 5.1 Comparison of predicted and measured K_t for ANN1 model with $S/D = 2$

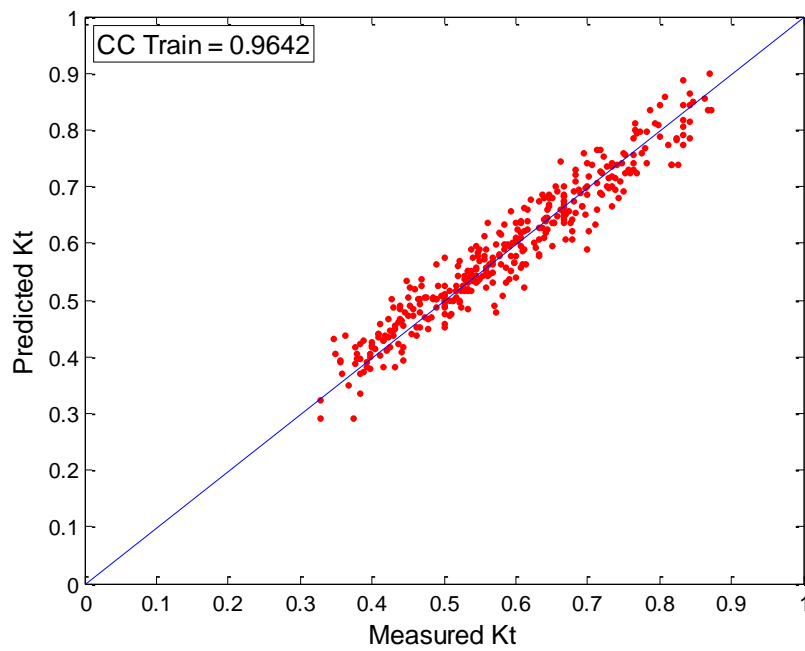


(a) Train Data

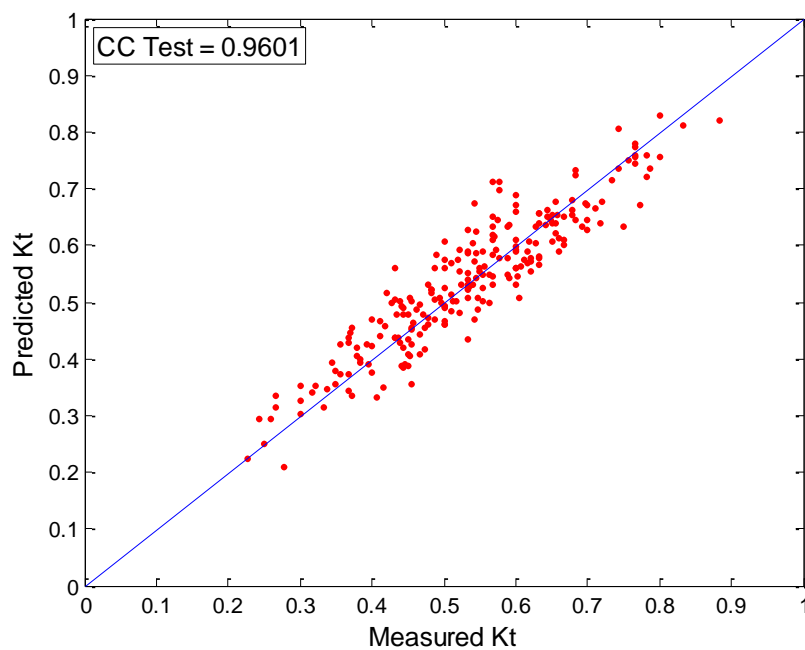


(b) Test Data

Fig 5.2 Comparison of predicted and measured K_t for ANN1 model with $S/D = 3$

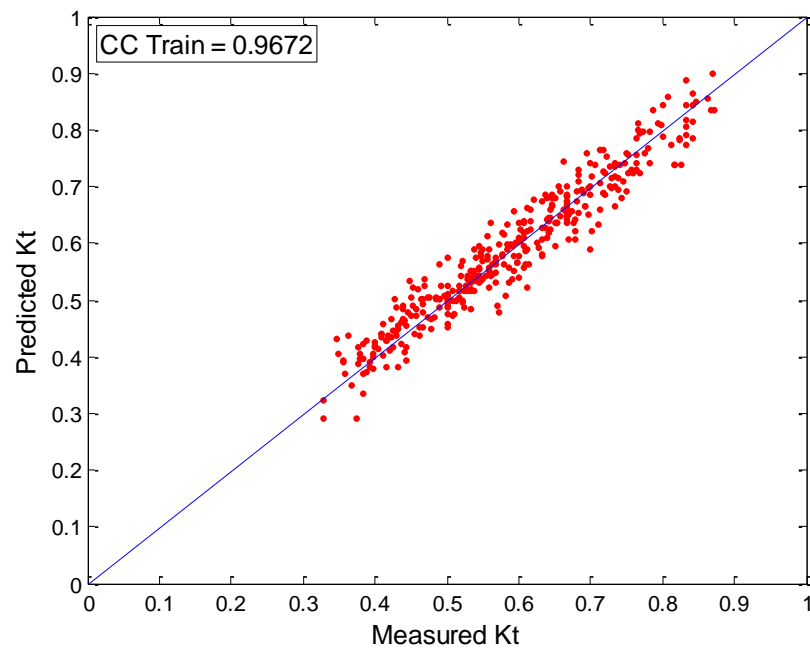


(a) Train Data

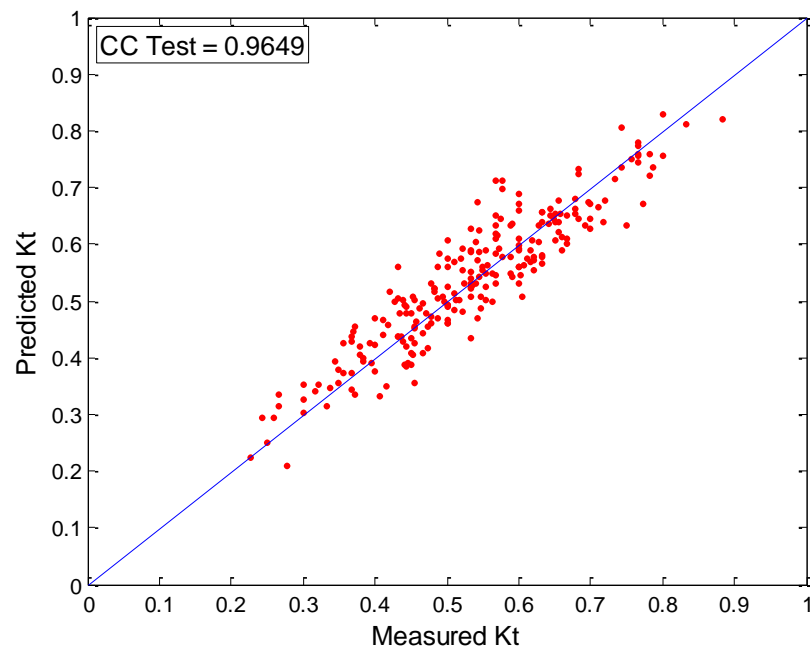


(b) Test Data

Fig 5.3 Comparison of predicted and measured K_t for ANN1 model with $S/D = 4$

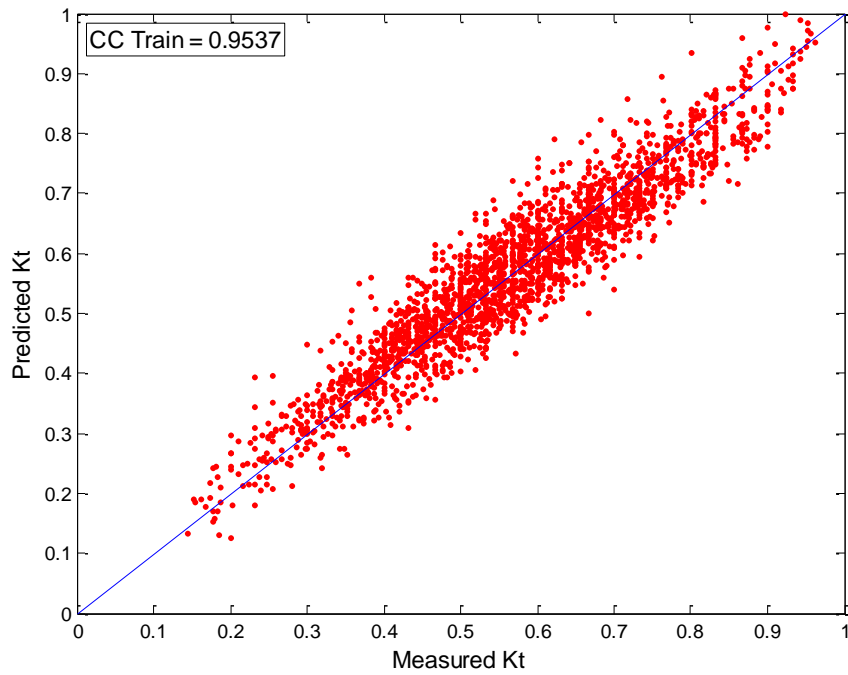


(a) Train Data

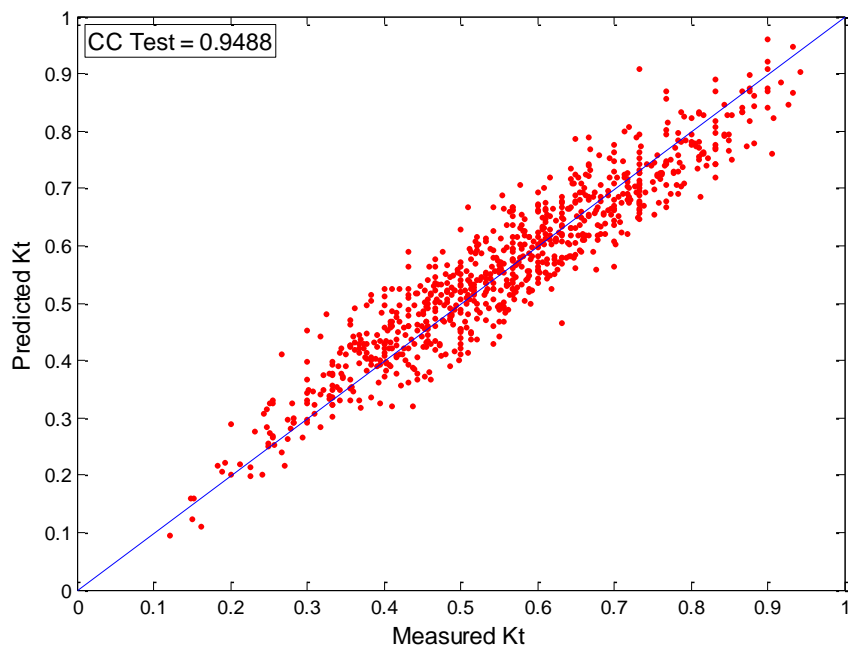


(b) Test Data

Fig 5.4 Comparison of predicted and measured K_t for ANN1 model with $S/D = 5$



(a) Train Data



(b) Test Data

Fig 5.5 Comparison of predicted and measured K_t for ANN2 model

Table 5.5 Correlation coefficient of K_t for ANN2 model

Hidden Nodes	CCtrain	CCtest	MSEtrain	Epochs
2	0.9102	0.9003	0.00444906	100
3	0.9353	0.9286	0.00325118	100
4	0.9467	0.9414	0.00269082	100
5	0.9508	0.9473	0.00248828	100
2	0.9294	0.9237	0.00353477	200
3	0.9372	0.9345	0.00315484	200
4	0.9453	0.9421	0.00276019	200
5	0.9537	0.9488	0.00234973	200

Table 5.6 Correlation coefficients of K_t for two network models

Model	Network (Input nodes - Hidden nodes - Epochs)	CCtrain	CCtest
ANN1	3-4-200	0.9672	0.9649
ANN2	4-5-200	0.9537	0.9488

5.2.1 Estimation of K_t by ANN2 Model

The ANN2 structure constructed for estimating K_t of HIMMFPB is shown in Fig. 5.6. The structure consists of four input nodes, five hidden nodes, and one output node. After training the network model, weights and biases of the network are fixed. These fixed weight and bias values are shown in Fig. 5.6. Here each input value is multiplied with the weight and adds with bias value, total sum is then the input at each hidden node, which is pass through a transfer function as defined in equation 5.2. Further the output from hidden node get multiplied with the weight and adds with the bias value, and then the total sum is passed through *purelin* as shown in equation 5.2. The wave transmission (K_t) is estimated using following formulations:

$$\text{Transfer function } F_i = \left[\frac{2}{1 + \exp(-2 \times N_i)} - 1 \right] \quad (5.2)$$

where $i = 1$ to 5 , N_i are values of hidden nodes and F_i are the transfer functions of hidden node i .

For ANN model, the trained hidden nodes and its transfer functions are

$$N_1 = S/D(0.061688) + W/L(0.6525) + H_i/d(-2.2203) + H_i/L(-16.4858) - 1.7113$$

$$N_2 = S/D(-0.023903) + W/L(0.21875) + H_i/d(0.36001) + H_i/L(-0.64689) + 0.28667$$

$$N_3 = S/D(1.4946) + W/L(-0.39512) + H_i/d(-0.34849) + H_i/L(-7.5453) - 3.9858$$

$$N_4 = S/D(0.032214) + W/L(0.63925) + H_i/d(2.4551) + H_i/L(-16.1498) - 1.4167$$

$$N_5 = S/D(-0.0085584) + W/L(-0.71574) + H_i/d(-2.8797) + H_i/L(-21.1578) + 1.5445$$

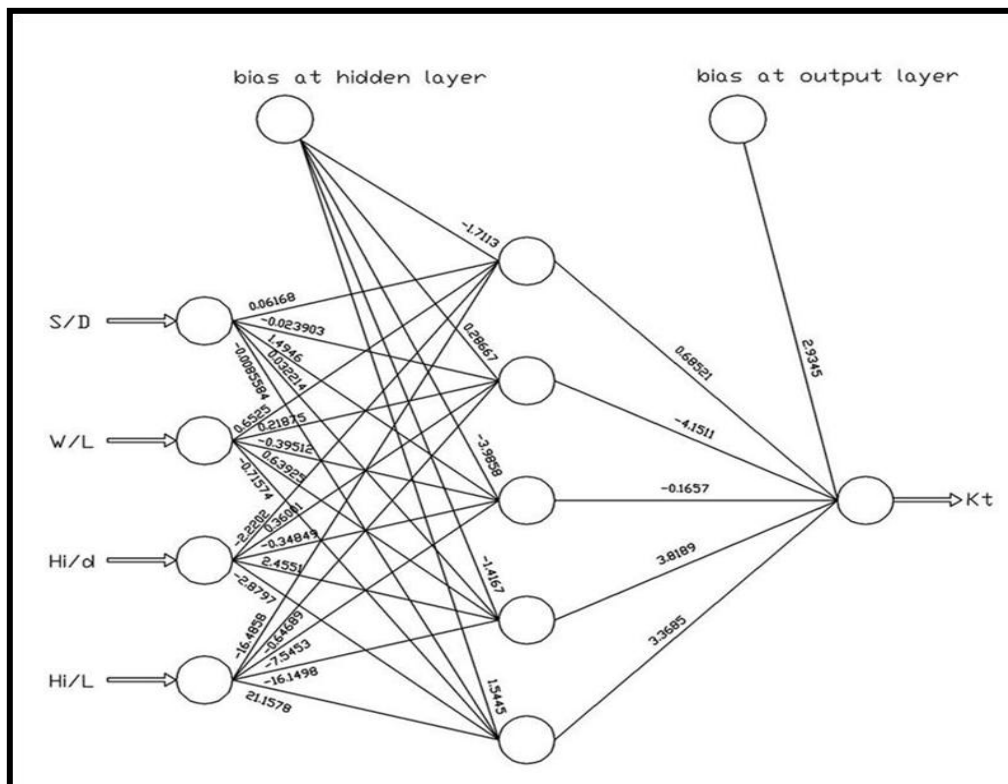


Fig. 5.6 ANN2 structure with weights and biases

$$F_1 = [2/1 + \exp(-2 \times N_1)] - 1$$

$$F_2 = [2/1 + \exp(-2 \times N_2)] - 1$$

$$F_3 = [2/1 + \exp(-2 \times N_3)] - 1$$

$$F_4 = [2/1 + \exp(-2 \times N_4)] - 1$$

$$F_5 = [2/1 + \exp(-2 \times N_5)] - 1$$

N_1 to N_5 and F_1 to F_5 , represents summation function and transfer function at each hidden node respectively.

The K_t is computed as:

$$K_t = F_1(0.68521) + F_2(-4.1511) + F_3(-0.1657) + F_4(3.8189) + F_5(3.3685) + 2.9345 \quad (5.3)$$

Equation 5.3 provides trained ANN2 model for estimating wave transmission (K_t) of HIMMFPB.

5.3 PERFORMANCE OF SUPPORT VECTOR MACHINE REGRESSION MODEL (SVMR)

To study the effectiveness of the approach, statistical comparison of measured and predicted values of K_t , CC is used. Apart from this, other statistical measures computed are root-mean-square error ($RMSE$), and scatter index (SI). These are defined as:

$$RMSE = \sqrt{\frac{1}{N} \sum_{i=1}^N (K_{mi} - K_{tpi})^2} \quad (5.4)$$

$$SI = \frac{RMSE}{\overline{K_m}} \quad (5.5)$$

Statistical measures computed using train and test data for SVMR are shown in Table 5.7. Train and test data are used to compare the models results. The trained and test results (CCs) of six models are shown in Table 5.7 and Fig. 5.7-5.12.

Table 5.7 SVMR models with statistical measures

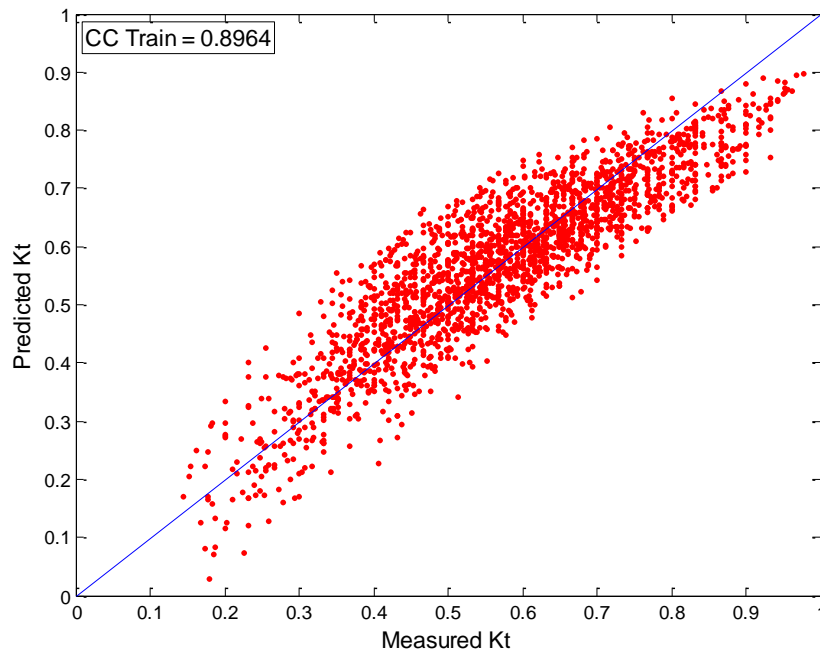
Model	CC Train	CC Test	Train Data		Test Data	
			<i>RMSE</i>	<i>SI</i>	<i>RMSE</i>	<i>SI</i>
SVMR (linear)	0.8964	0.8924	0.07072	0.12375	0.07245	0.12925
SVMR (polynomial)	0.9474	0.9437	0.05105	0.08933	0.05312	0.09477
SVMR (rbf)	0.9557	0.9475	0.04694	0.08214	0.05138	0.09166
SVMR (erbf)	0.9431	0.9383	0.05307	0.09287	0.05556	0.09923
SVMR (spline)	0.9596	0.9523	0.04490	0.07857	0.04905	0.08751
SVMR (b-spline)	0.9779	0.9685	0.03335	0.05837	0.03993	0.07125

Performance of SVMR depends on the good setting of SVM and kernel parameters. In developing SVMR models these parameters are randomly selected initially by a coarse grain search (i.e. for $C=100, 500, 1000$; $\varepsilon =1, 2$; d and $\gamma = 1, 2, 3$) to identify the near optimal values, and then a fine grain search (i.e. for $C = 10, 20, 30$; $\varepsilon = 0.001, 0.01, 0.1, 1$; d and $\gamma = 0.001, 0.01, 0.1, 1$) is done to identify the final optimal values. Final optimal values obtained are presented in Table 5.8. Number of support vectors for all SVMR models are 100%, which indicates that there is no noise in the data set. Compared to all SVMR models linear kernel function shows poor generalization performance in predicting wave transmission through HIMMFPB (CC

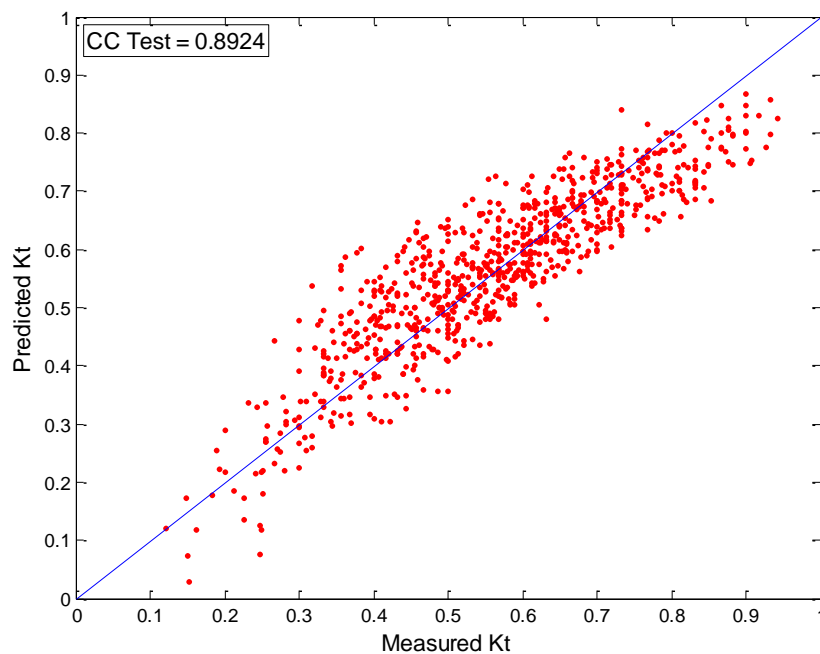
Train = 0.8964 and CC test = 0.8924). *RMSE* and *SI* is very high in case of SVMR model with linear kernel function, whereas SVMR with bspline kernel function has low *RMSE* and *SI* (Table 5.7). A b-spline kernel function has better generalization performance with CC Train = 0.9779 and CC Test = 0.9685. In case of SVMR with b-spline kernel, optimal *C* is 20 and $\varepsilon = 0.001$.

Table 5.8 Optimal parameters for SVMR models with different kernels

Kernel	<i>nsv</i>	<i>C</i>	ε	γ	<i>d</i>
linear	2131	100	0.001	-	-
polynomial	2131	100	0.001	-	4
rbf	2131	100	0.001	0.3	-
erbf	2131	100	0.001	0.3	-
spline	2131	100	0.001	-	-
b-spline	2131	20	0.001	-	2

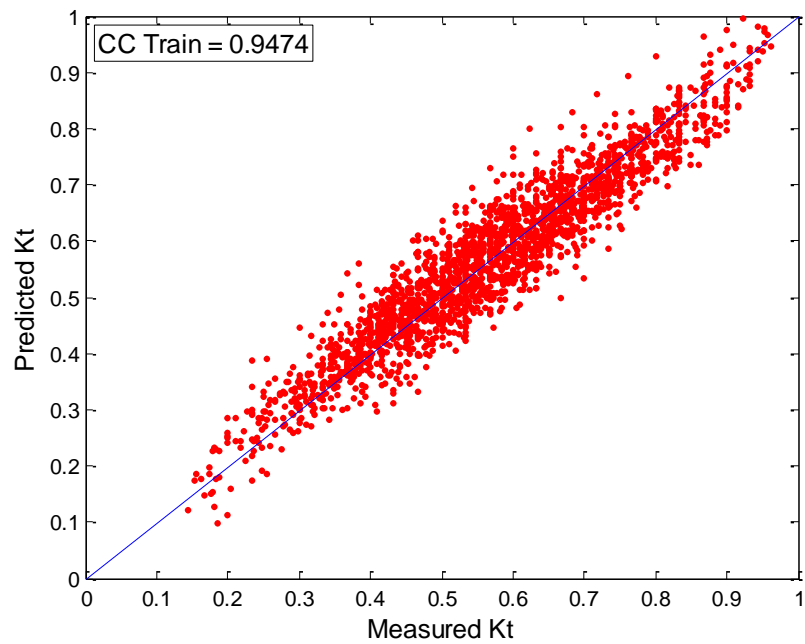


(a) Train Data

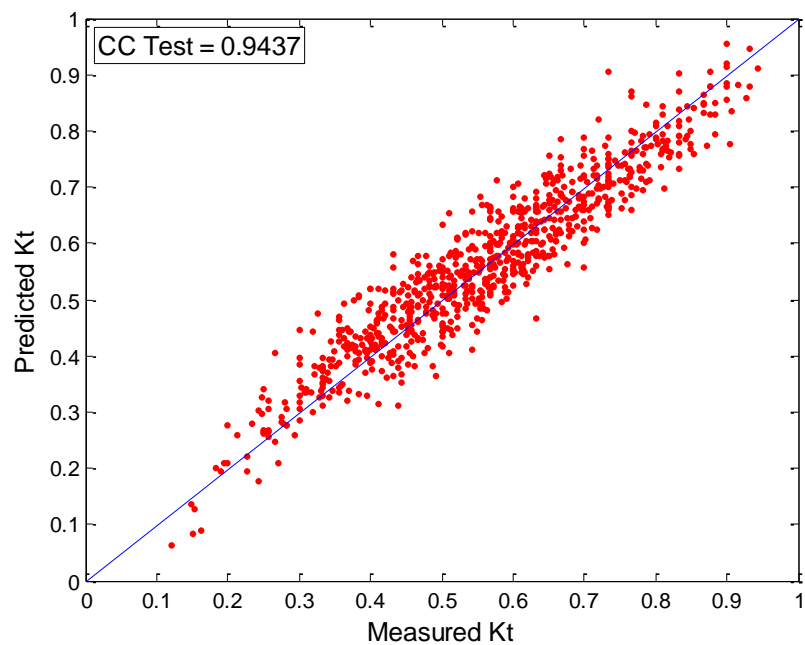


(b) Test Data

Fig. 5.7 Comparison of predicted and measured K_t for SVMR (linear) model

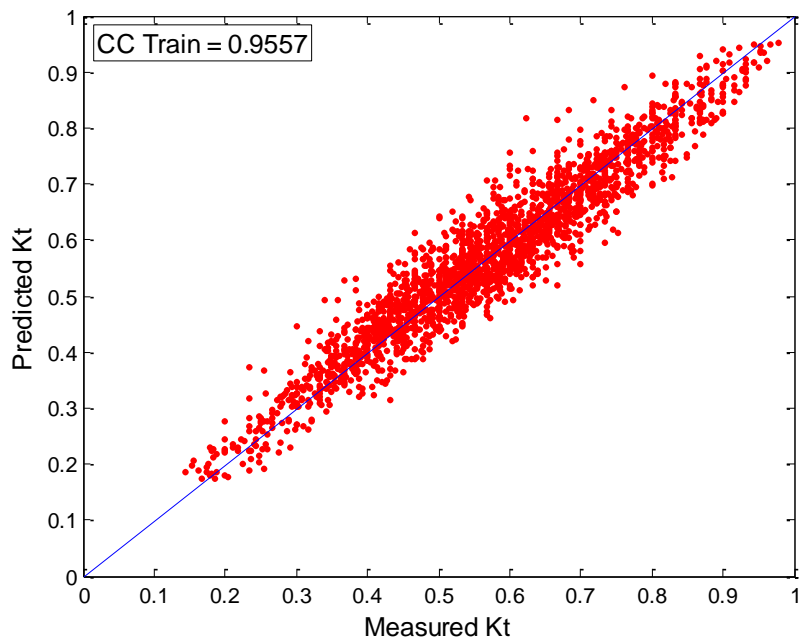


(a) Train Data

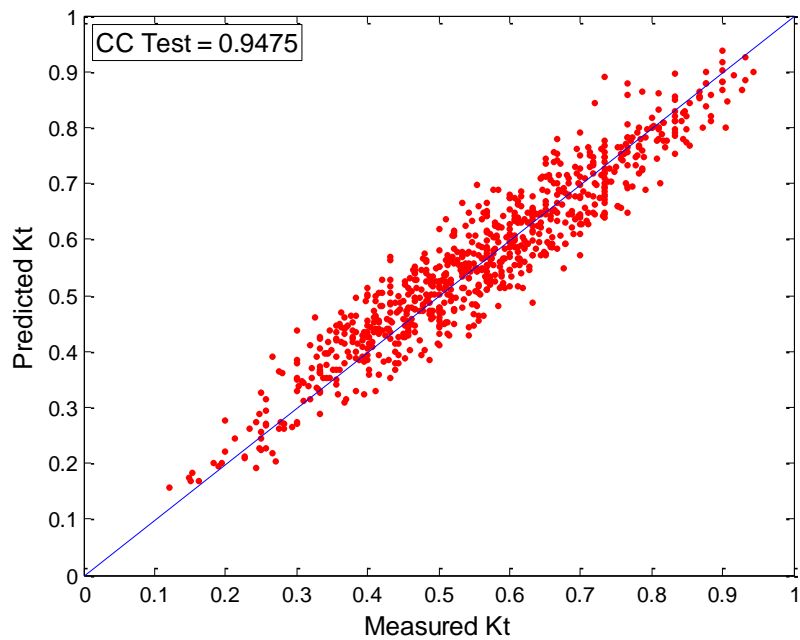


(b) Test Data

Fig. 5.8 Comparison of predicted and measured K_t for SVMR (polynomial) model

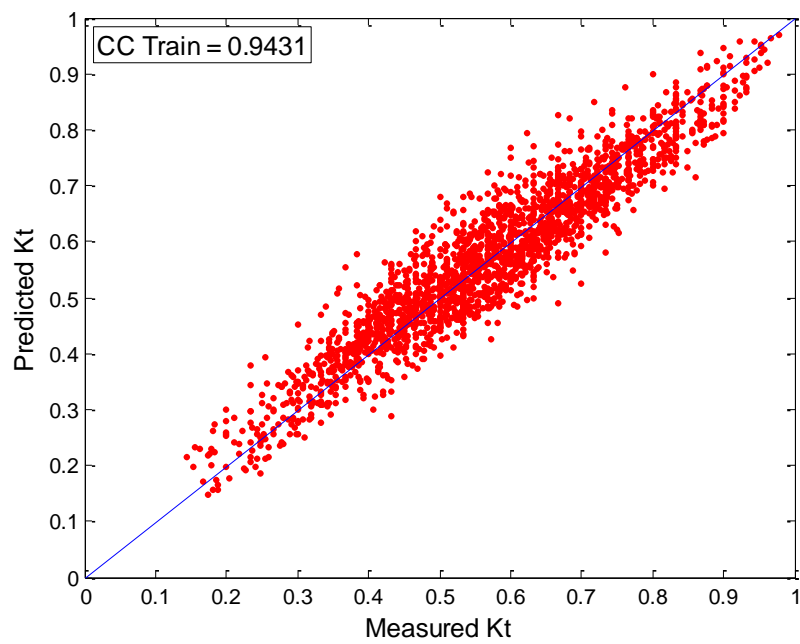


(a) Train Data

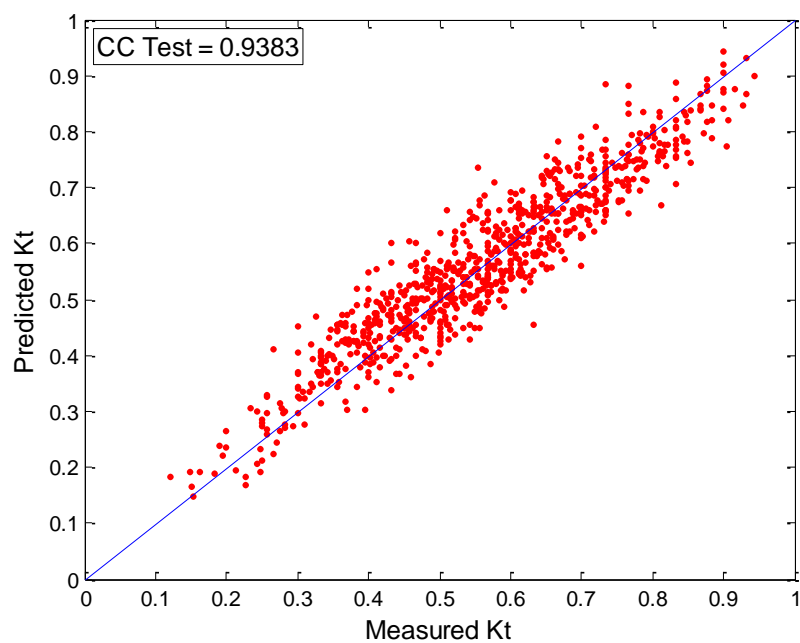


(b) Test Data

Fig. 5.9 Comparison of predicted and measured K_t for SVMR (rbf) model

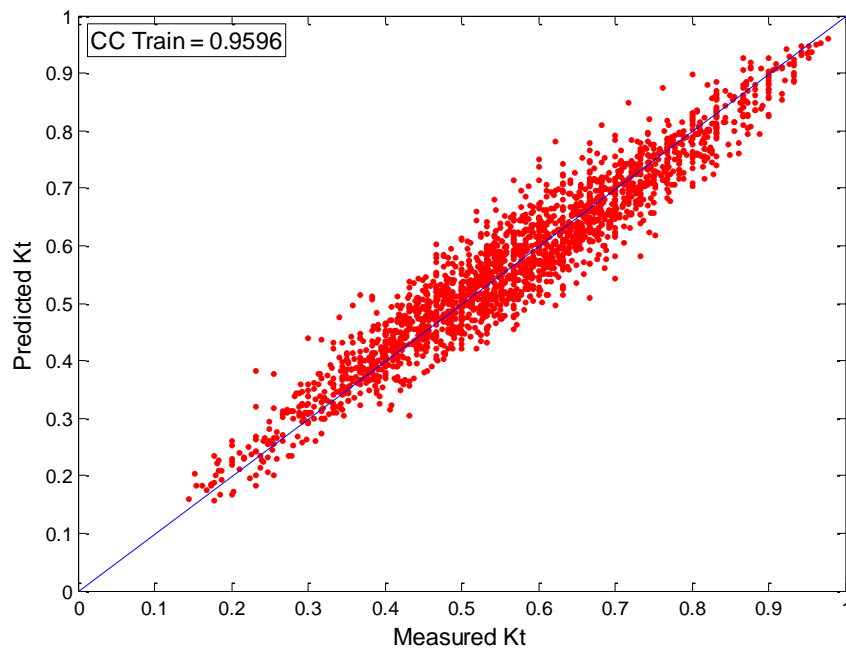


(a) Train Data

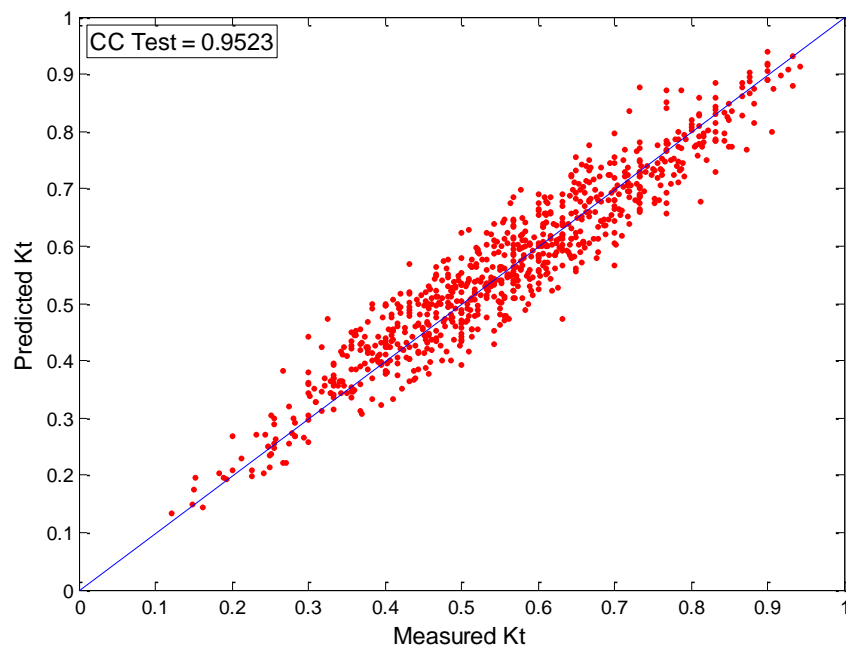


(b) Test Data

Fig. 5.10 Comparison of predicted and measured K_t for SVMR (erbf) model

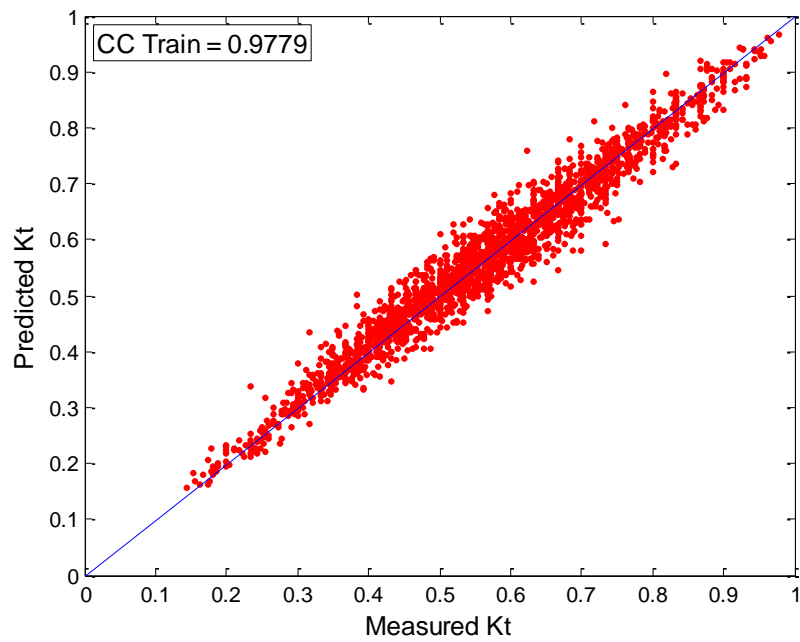


(a) Train Data

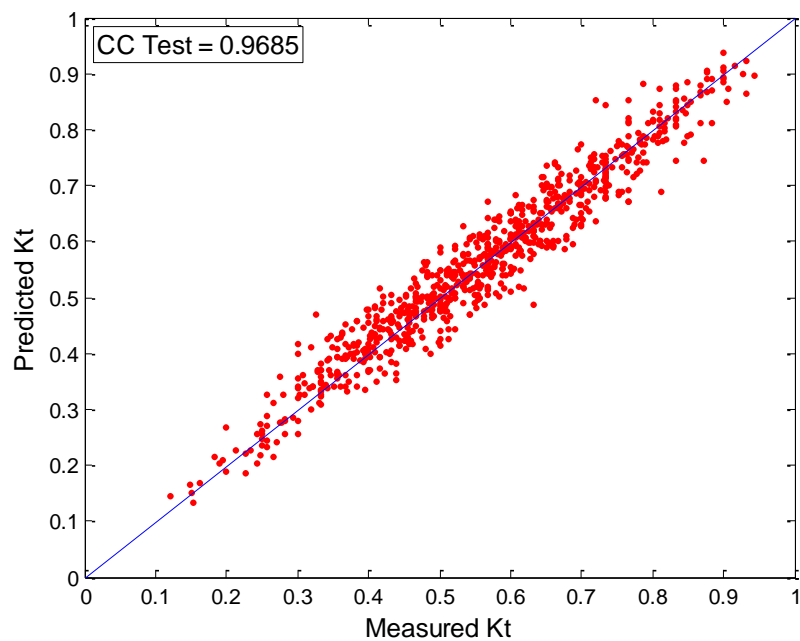


(b) Test Data

Fig. 5.11 Comparison of predicted and measured K_t for SVMR (spline) model



(a) Train Data



(b) Test Data

Fig. 5.12 Comparison of predicted and measured K_t for SVMR (b-spline) model

5.4 PERFORMANCE OF ADAPTIVE NEURO FUZZY INFERENCE SYSTEM MODEL (ANFIS)

As the training process takes place values of a, b and c change, the bell shaped function vary accordingly, thus exhibiting various forms of membership functions on linguistic attributes A_i . Fig. 5.13 shows the final membership function after training for ANFIS5 model. Table 5.9 lists the linguistic attributes A_i and the corresponding premise parameters for ANFIS5 model. The hybrid learning algorithm that combines

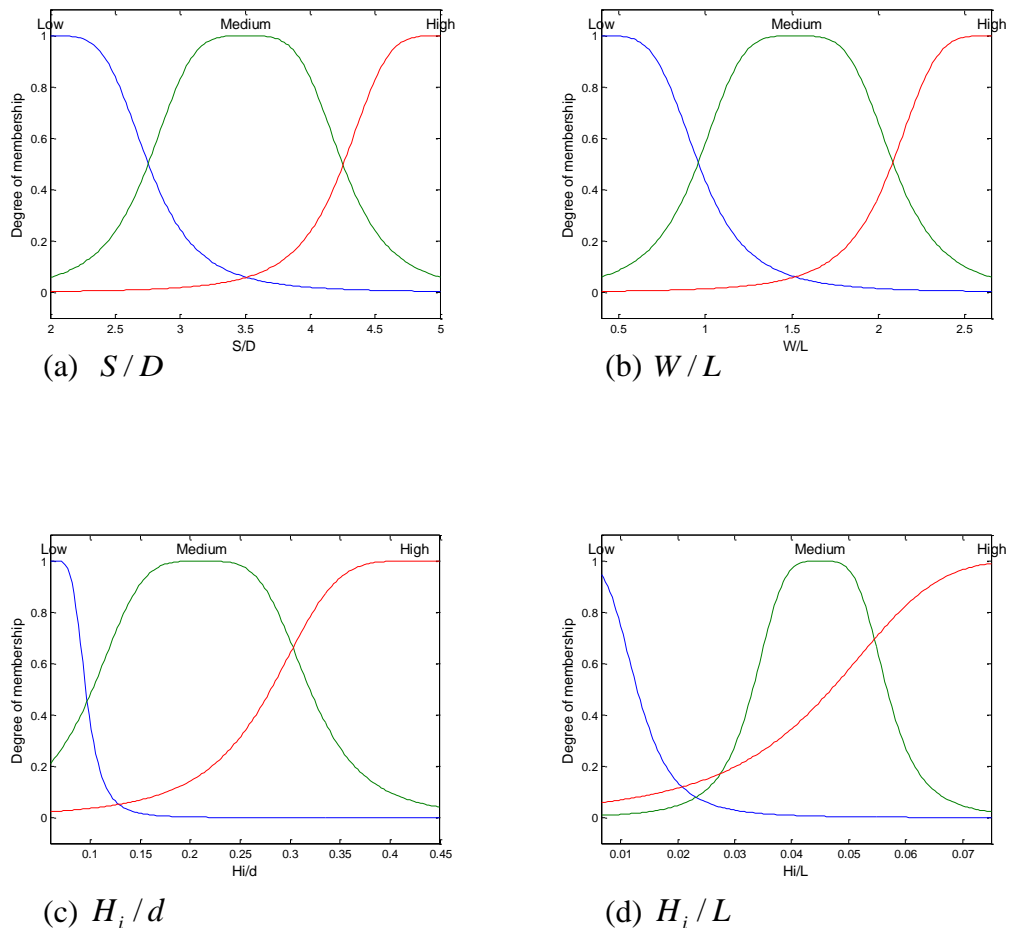


Fig. 5.13 Final membership functions of input parameters (x-axis) for ANFIS5 model

least square method with gradient descent method is used to adjust the parameters of membership function. Trained ANFIS1, ANFIS2, ANFIS3 and ANFIS4 model consists of 27 rules and 3 generalized bell membership function. These membership functions are associated with 3 inputs W/L , H_i/d and H_i/L . Whereas, the trained ANFIS5 model consists of 81 fuzzy rules and 3 generalized bell membership function. These are associated with 4 inputs S/D , W/L , H_i/d and H_i/L . Fig. 5.14 shows the fuzzy rule architecture for ANFIS5 model.

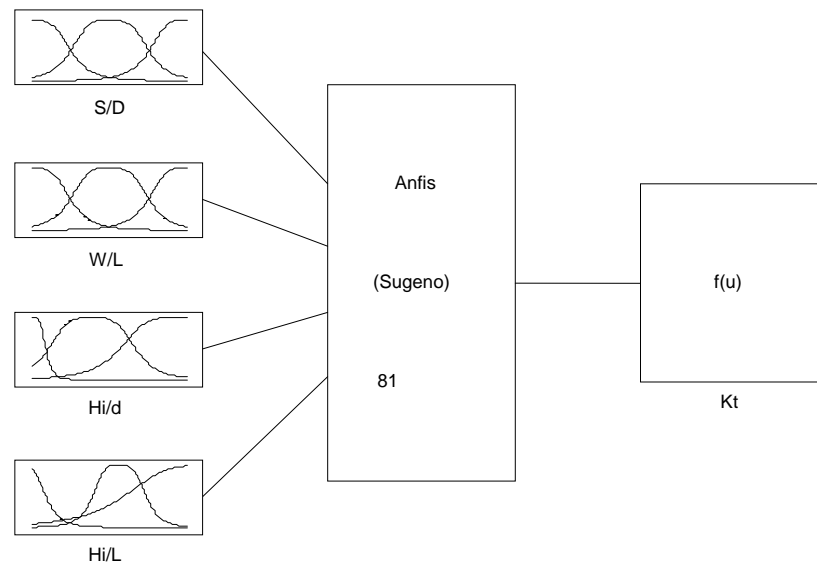


Fig. 5.14 Fuzzy rule architecture of the generalized bell membership function for ANFIS5 model

The fuzzy *IF – THEN* rules for ANFIS4 model after training are shown in Table 5.10

Rule1: If W/L is Low and H_i/d is Low and H_i/L is Low then,

$$K_t = \bar{c}_1 \cdot \bar{X} \tag{5.6}$$

Where, $\bar{X} = [W/L, H_i/d, H_i/L, 1]$ and \bar{c}_i is the i^{th} row of the consequent parameter matrix C (equation 5.7).

Table 5.9 Premise parameters for ANFIS5 model

A_i	a_i	b_i	c_i
Low ₁	0.7534	1.9998	2.0027
Medium ₁	0.7492	2.0001	3.5021
High ₁	0.7465	2.0003	5.0025
Low ₂	0.5635	1.9998	0.3999
Medium ₂	0.5655	1.9998	1.5219
High ₂	0.5680	1.9997	2.6477
Low ₃	0.0311	2.0016	0.0645
Medium ₃	0.1087	2.0017	0.2110
High ₃	0.1425	1.9989	0.4232
Low ₄	0.0122	0.0007	0.0000
Medium ₄	0.0118	1.9994	0.0449
High ₄	0.0405	1.9992	0.0874

To study effectiveness of the approach, statistical comparison of measured and predicted values of K_t , CC , $RMSE$ and SI is used. Statistical measures computed using trained and test data are shown in Table 5.11, trained and test data are used to compare the models results, all ANFIS models have shown CCs higher than 0.9600 for trained data, whereas in case of test data it is more than 0.9500. $RMSE$ is less than or equal to 0.044187 for training data and 0.051074 for test data, whereas the SI is less than or equal to 0.087728 for train data and 0.102296 for test data. The trained and test results (CCs) of all ANFIS models are shown in Table 5.11 and Figs. 5.15 to 5.20. K_t is better with increase in S/D values, but it is noticed that the CCs between

$$C = \begin{bmatrix} -0.2681 & -9.6906 & 29.4654 & 1.9173 \\ -0.0301 & 30.4673 & -66.7380 & -1.1623 \\ 6.9865 & -4.5467 & 0.7491 & 0.6122 \\ 0.3117 & 0.8894 & -0.0868 & 1.1323 \\ -0.7276 & 2.0967 & -14.4043 & 1.2034 \\ 0.8873 & -2.5686 & 29.4500 & -1.3169 \\ -2.8564 & 47.1644 & -12.1817 & -12.9159 \\ -0.0590 & -4.8697 & 24.0908 & 1.4401 \\ -0.5679 & 2.2597 & 2.4840 & -0.0311 \\ -0.6248 & 2.6189 & 26.7273 & 1.5391 \\ 0.6096 & -2.5181 & 9.3327 & -0.9857 \\ 4.0613 & -17.5433 & -0.4962 & 8.6854 \\ -0.0706 & -15.0819 & 82.7353 & 2.0097 \\ -0.2997 & 4.0968 & -20.6645 & 0.7287 \\ 0.0506 & -0.1335 & 12.2483 & -0.5003 \\ -7.2845 & 10.6947 & 24.3701 & 5.7094 \\ 0.3424 & -2.0854 & 17.9905 & 0.0653 \\ -0.1456 & 0.8293 & -2.4469 & 0.4715 \\ -0.3445 & -18.8356 & -16.1056 & 3.1411 \\ -0.0299 & 14.9003 & -12.4531 & -1.1065 \\ 6.8129 & 1.2283 & 0.0817 & 4.6369 \\ -2.1517 & -1.2561 & 2.1870 & 4.0987 \\ -0.5506 & 6.3736 & -2.4610 & 0.7510 \\ 0.0532 & 6.4288 & -4.1597 & -1.3002 \\ 7.1512 & -0.9702 & 0.1986 & -5.5973 \\ -0.9720 & 2.0068 & 2.6307 & -0.4460 \\ -0.1326 & 3.6693 & -6.2225 & -0.1971 \end{bmatrix} \quad (5.7)$$

Table 5.10 Fuzzy IF – THEN rules after training for ANFIS4 model

Rule	W/L	H _i /d	H _i /L	K_t
1	Low	Low	Low	$\bar{c}_1 \cdot \bar{X}$
2	Low	Low	Medium	$\bar{c}_2 \cdot \bar{X}$
3	Low	Low	High	$\bar{c}_3 \cdot \bar{X}$
4	Low	Medium	Low	$\bar{c}_4 \cdot \bar{X}$
5	Low	Medium	Medium	$\bar{c}_5 \cdot \bar{X}$
6	Low	Medium	High	$\bar{c}_6 \cdot \bar{X}$
7	Low	High	Low	$\bar{c}_7 \cdot \bar{X}$
8	Low	High	Medium	$\bar{c}_8 \cdot \bar{X}$
9	Low	High	High	$\bar{c}_9 \cdot \bar{X}$
10	Medium	Low	Low	$\bar{c}_{10} \cdot \bar{X}$
11	Medium	Low	Medium	$\bar{c}_{11} \cdot \bar{X}$
12	Medium	Low	High	$\bar{c}_{12} \cdot \bar{X}$
13	Medium	Medium	Low	$\bar{c}_{13} \cdot \bar{X}$
14	Medium	Medium	Medium	$\bar{c}_{14} \cdot \bar{X}$
15	Medium	Medium	High	$\bar{c}_{15} \cdot \bar{X}$
16	Medium	High	Low	$\bar{c}_{16} \cdot \bar{X}$
17	Medium	High	Medium	$\bar{c}_{17} \cdot \bar{X}$
18	Medium	High	High	$\bar{c}_{18} \cdot \bar{X}$
19	High	Low	Low	$\bar{c}_{19} \cdot \bar{X}$
20	High	Low	Medium	$\bar{c}_{20} \cdot \bar{X}$
21	High	Low	High	$\bar{c}_{21} \cdot \bar{X}$
22	High	Medium	Low	$\bar{c}_{22} \cdot \bar{X}$
23	High	Medium	Medium	$\bar{c}_{23} \cdot \bar{X}$
24	High	Medium	High	$\bar{c}_{24} \cdot \bar{X}$
25	High	High	Low	$\bar{c}_{25} \cdot \bar{X}$
26	High	High	Medium	$\bar{c}_{26} \cdot \bar{X}$
27	High	High	High	$\bar{c}_{27} \cdot \bar{X}$

measured and predicted K_t increases with S/D for ANFIS1, ANFIS2 and ANFIS3 models, whereas it is not true in case of ANFIS4 model. Even though there is an improve relation with increase of S/D as seen from ANFIS1, ANFIS2, and ANFIS3 (Table 5.11). An ANFIS4 shows marginally lower values of CCs. This also indicates that ANFIS3 model shows optimal K_t prediction in the present study. The highest Correlation Coefficient (CC Train = 0.9786, CC Test = 0.9698) is obtained for ANFIS3 model. Increase or decrease in S/D ratio does not show a clear relation in an increase or decrease of CCs, $RMSE$ and SI estimated for train and test data. To study over a range of S/D on K_t , an input parameter S/D is added to form ANFIS5 model.

After conducting computer simulation on trained and test data of ANFIS5 model, CCs are calculated between measured and predicted K_t are shown in Table 5.11 and Fig. 5.19. An ANFIS5 model predictions are very realistic when compared with the measured values (CC Train = 0.9723, CC Test = 0.9635), whereas the $RMSE$ and SI are 0.037269 and 0.065217 for train data, and 0.043068 and 0.076833 for test data, respectively. An ANFIS5 model performed better than ANFIS1 and ANFIS2 models, whereas the performance is almost same when compared with ANFIS3 and ANFIS4 models. Performance of an ANFIS model depends upon the input parameters chosen to train the model. Considering an S/D as an input parameter, there is a better CC between measured and predicted K_t when compared with ANFIS1 and ANFIS2. This clearly proves that an S/D plays an important role to train ANFIS5 model to map an input-output relation.

From ANFIS5 and ANFIS6, CCs of K_t show very little variation, as H_i/L is the least influential parameter. The same data set has been used for estimating K_t using ANN and SVMR model. CCs of K_t are shown in Table 5.12. From Tables 5.11 and 5.12, it is observed that the ANFIS models yield higher CCs as compared to that of ANN models, whereas the performance is poor when compared with SVMR (b-

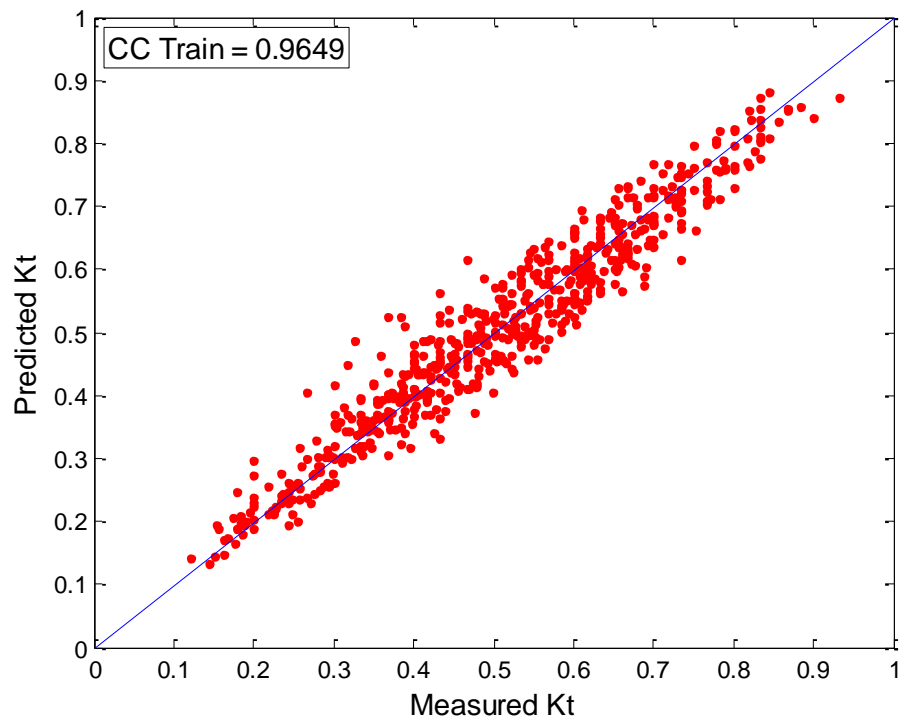
spline). SVMR with linear kernel function has shown poor generalization performance in predicting wave transmission through HIMMFPB when compared with ANN and ANFIS models.

Table 5.11 ANFIS models with statistical measures for train and test data

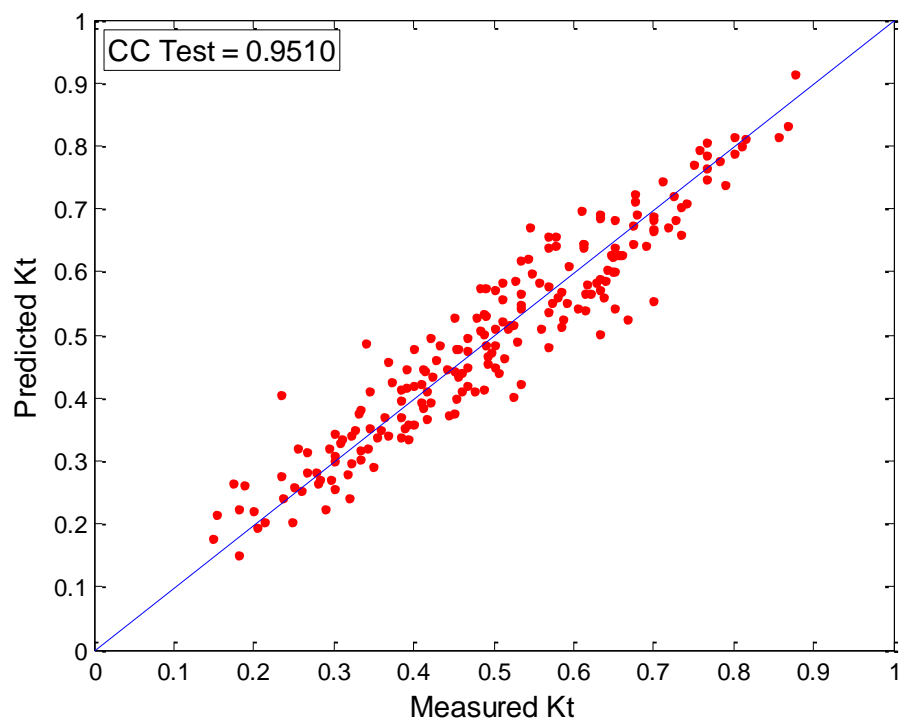
Model	CC Train	CC Test	Train Data		Test Data	
			RMSE	SI	RMSE	SI
ANFIS1	0.9649	0.9510	0.044187	0.087728	0.051074	0.102296
ANFIS2	0.9706	0.9528	0.031676	0.059149	0.038682	0.072278
ANFIS3	0.9786	0.9698	0.026438	0.044892	0.030780	0.053178
ANFIS4	0.9776	0.9674	0.032783	0.049827	0.039505	0.060767
ANFIS5	0.9723	0.9635	0.037269	0.065217	0.043068	0.076833
ANFIS6	0.9469	0.9378	0.05127	0.089716	0.055775	0.099503

Table 5.12 ANN and SVMR models with correlation coefficients of K_t

Model	S/D Ratio	CC Train	CC Test
ANN1	2	0.9552	0.9504
ANN2	3	0.9506	0.9404
ANN3	4	0.9642	0.9601
ANN4	5	0.9672	0.9649
ANN5	Total	0.9537	0.9488
SVMR (linear)		0.8964	0.8924
SVMR (polynomial)		0.9474	0.9437
SVMR (rbf)		0.9557	0.9475
SVMR (erbf)		0.9431	0.9383
SVMR (spline)		0.9596	0.9523
SVMR (b-spline)		0.9779	0.9685

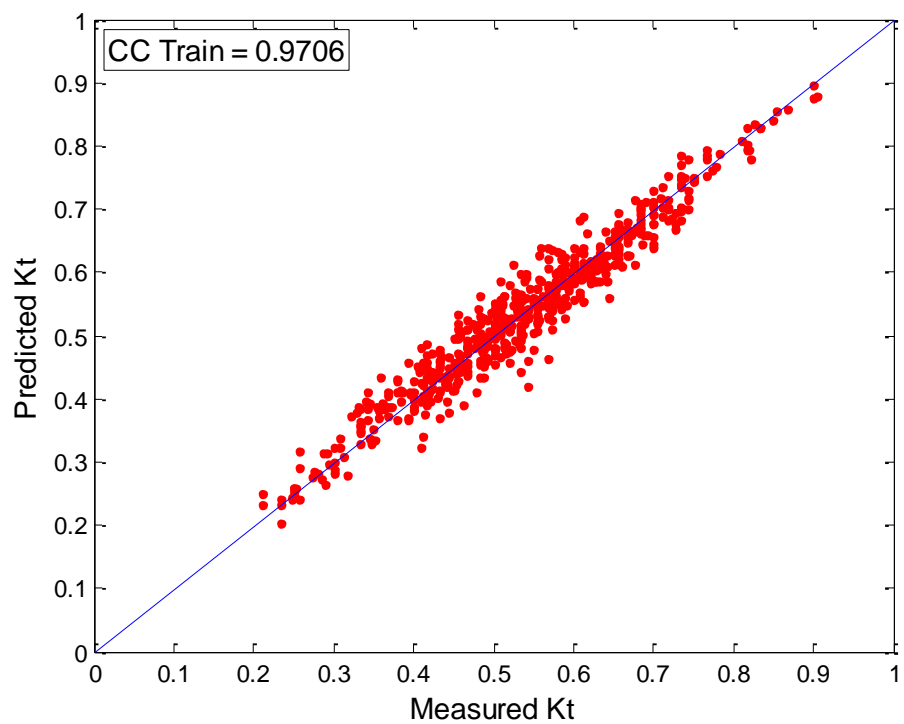


(a) Train Data

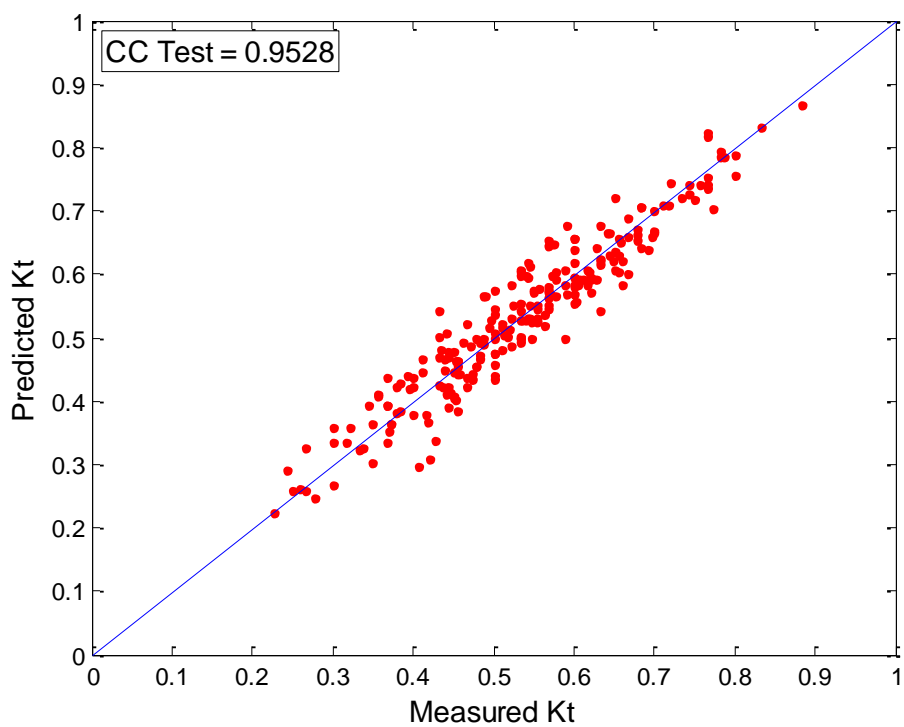


(b) Test Data

Fig. 5.15 Comparison of predicted and measured K_t for ANFIS1 model

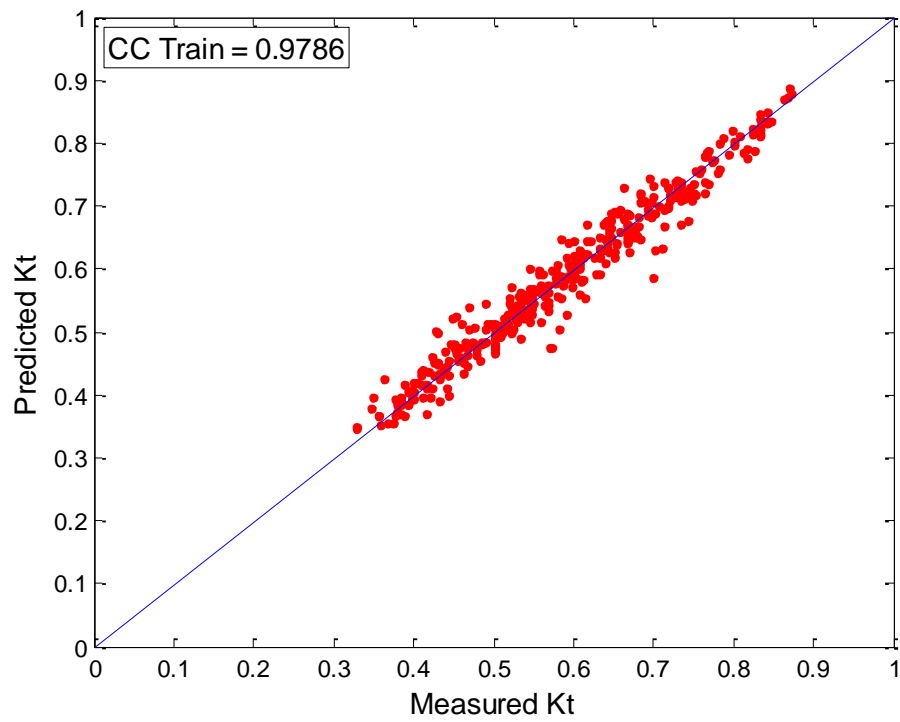


(a) Train Data

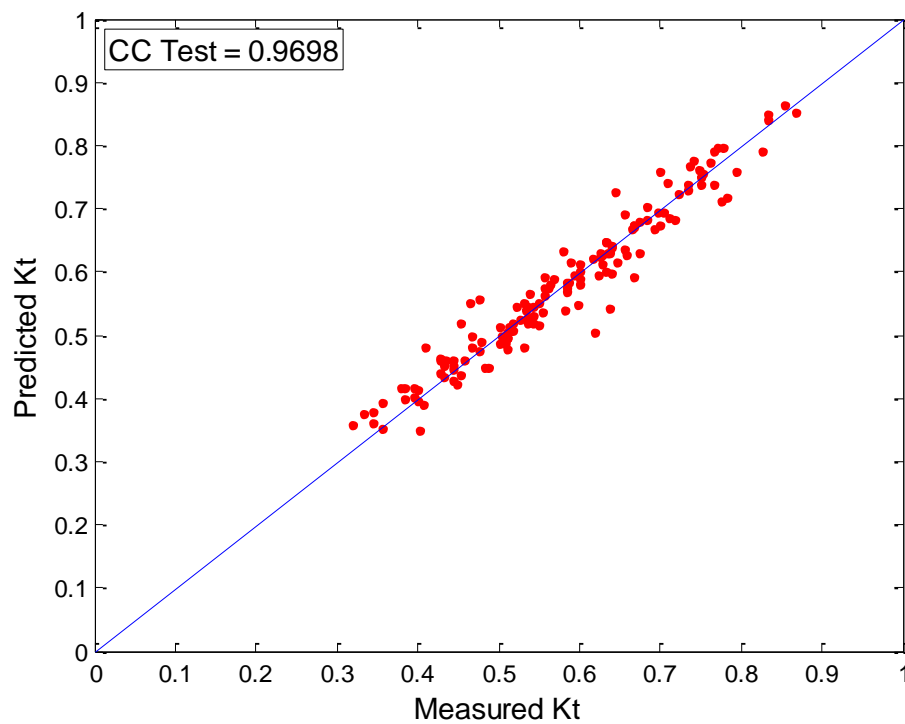


(b) Test Data

Fig. 5.16 Comparison of predicted and measured K_t for ANFIS2 model

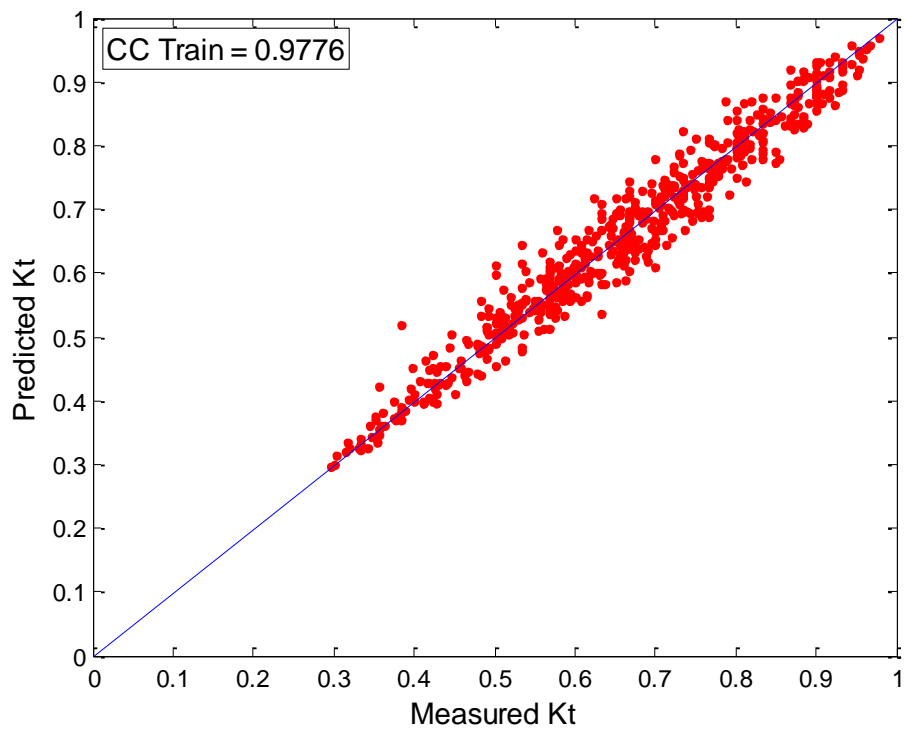


(a) Train Data

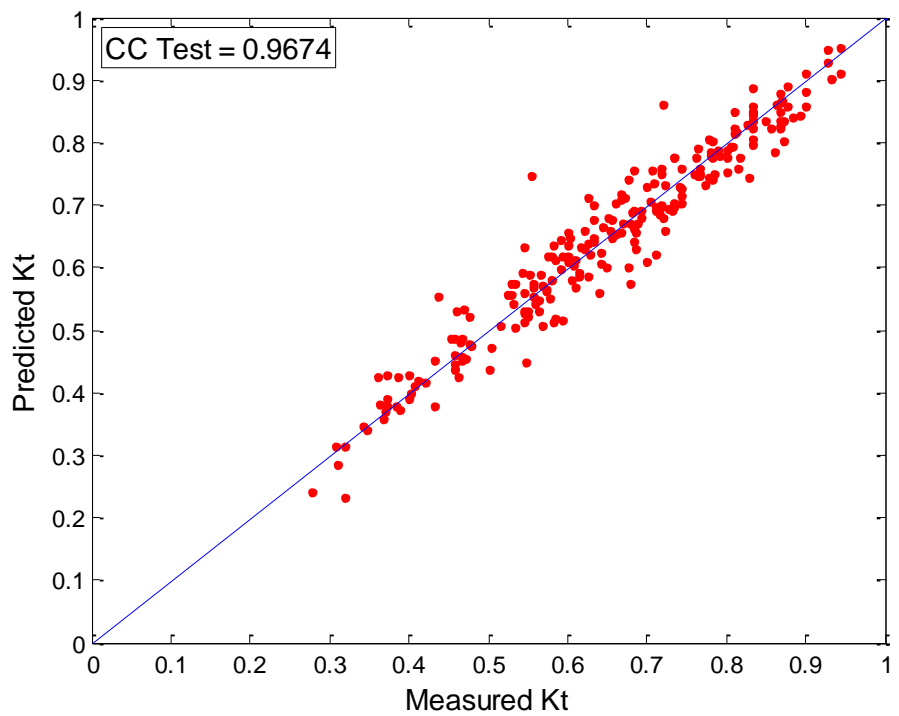


(b) Test Data

Fig. 5.17 Comparison of predicted and measured K_t for ANFIS3 model

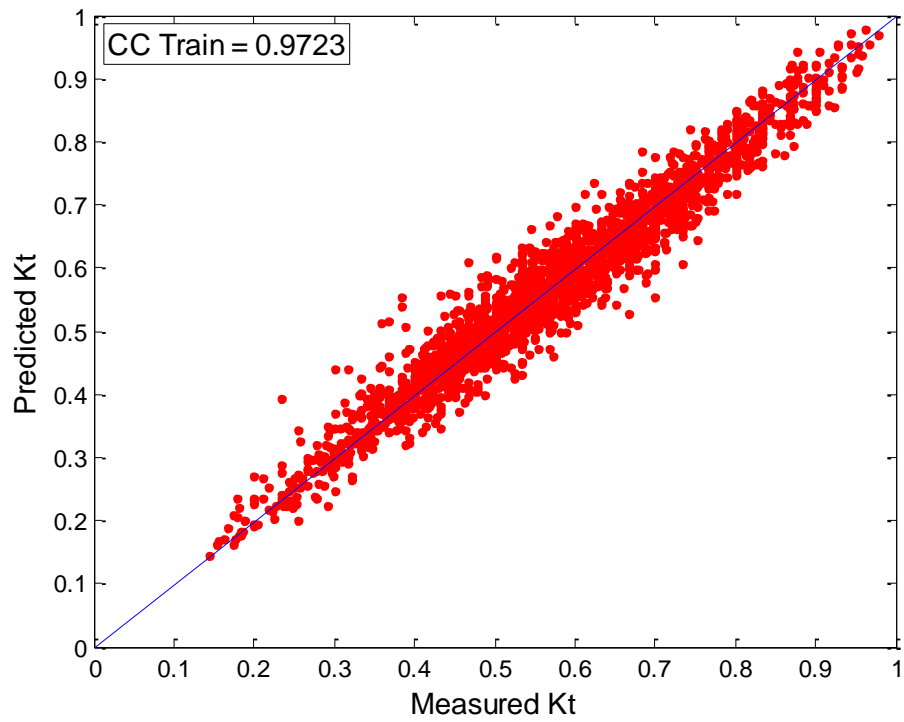


(a) Train Data

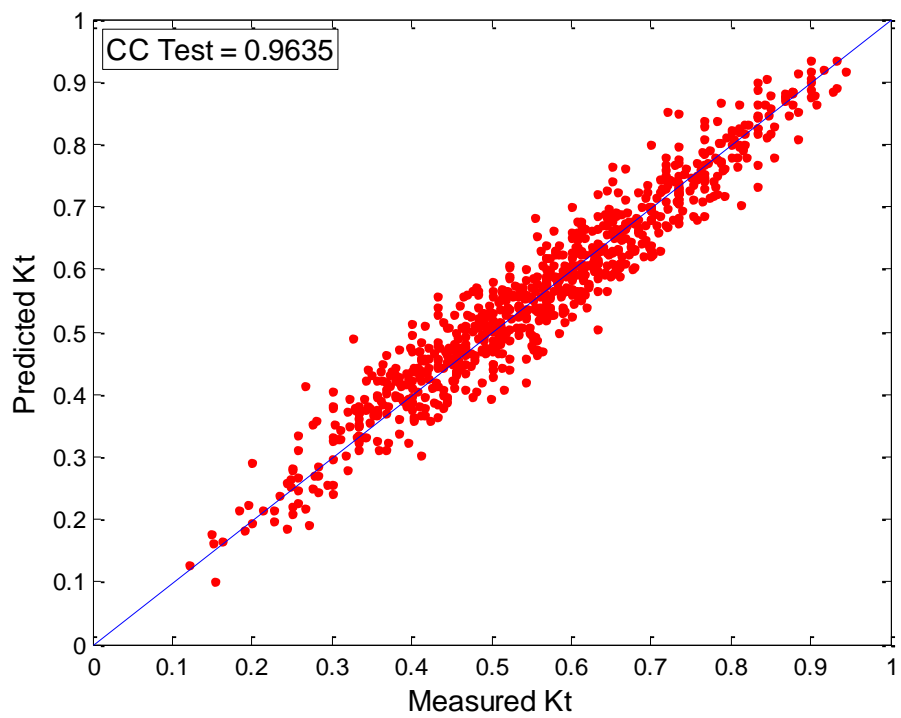


(b) Test Data

Fig. 5.18 Comparison of predicted and measured K_t for ANFIS4 model

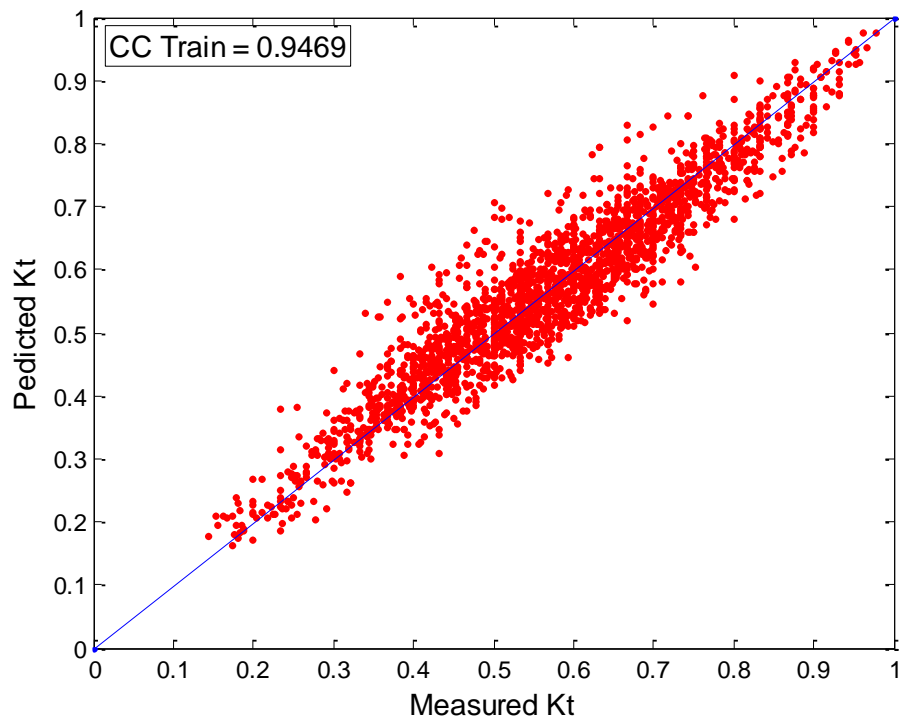


(a) Train Data

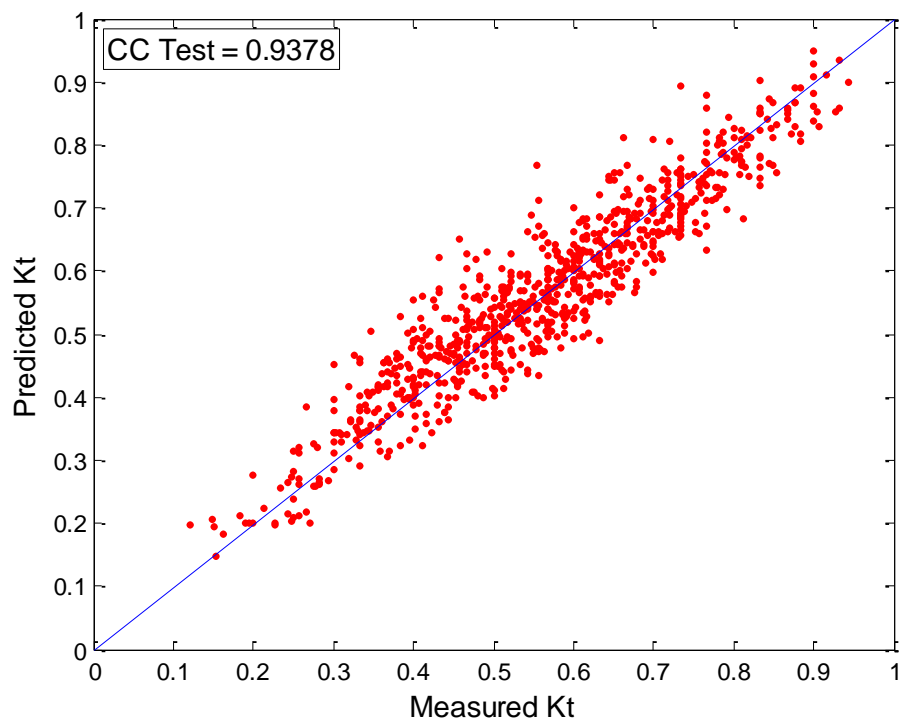


(b) Test Data

Fig. 5.19 Comparison of predicted and measured K_t for ANFIS5 model



(a) Train Data



(b) Test Data

Fig. 5.20 Comparison of predicted and measured K_t for ANFIS6 Model

5.5 PERFORMANCE OF GENETIC ALGORITHM BASED SUPPORT VECTOR MACHINE REGRESSION (GA-SVMR)

To study the effectiveness of the approach, statistical comparison of measured and predicted values of K_t , CC , $RMSE$ and SI is used. Train and test data are used to compare the models results. The trained and test results (CC s) of six models are shown in Table 5.13 and Fig. 5.21 -5.26.

Table 5.13 GA-SVMR models with statistical measures

Model	CC Train	CC Test	Train Data		Test Data	
			$RMSE$	SI	$RMSE$	SI
GA-SVMR (linear)	0.8964	0.8924	0.07072	0.12375	0.07245	0.12925
GA-SVMR (polynomial)	0.9568	0.9513	0.04638	0.08116	0.04946	0.08824
HGASVMR (rbf)	0.9563	0.9478	0.04662	0.08157	0.05119	0.09133
HGASVMR (erbf)	0.9640	0.9416	0.04253	0.07443	0.05412	0.09655
HGASVMR (spline)	0.9834	0.9735	0.02896	0.05068	0.03671	0.06549
GA-SVMR (b-spline)	0.9897	0.9741	0.02286	0.03900	0.03629	0.06474

Table 5.14 Optimal parameters for GA-SVMR models with different kernels

Kernel	nsv	C	ε	γ	d
linear	2131	100	0.001	-	-
polynomial	2131	96	0.001	-	6
rbf	2131	150	0.001	0.3	-
erbf	2131	6	0.001	1	-
spline	2131	40000	0.05	-	-
b-spline	2131	15	0.05	-	2

In comparison to all models, linear kernel function shows poor generalization performance (CC Train = 0.8964 and CC Test = 0.8924) in prediction of K_t for HIMMFPB with SI , 0.12375 and 0.12925 for train and test data respectively. SVMR models with linear kernel function also shows similar trend. Number of support vectors used in GA-SVMR with linear kernel function is 2131, which is 100%. Similarly, GA-SVMR with non-linear kernel functions also used 100% of support vectors, which indicates that every training input is utilized as support vector. This clearly proves that, there is no noise in the training data set, but there is non-linearity and complexity associated in mapping input and output parameters of HIMMFPB. Increasing the C will disturb the solution, but it can be helpful for other kernels like spline kernel, where C is 40000 as shown in Table 5.14. In case of b-spline kernel C is 15, whereas for erbf it is 6. For polynomial and linear kernel it is 96 and 100 respectively. A b-spline kernel function has better generalization performance with $RMSE$ 0.02286 and 0.03629 for train and test data respectively. Whereas, similar trend is shown by spline kernel function with slightly higher $RMSE$ 0.02896 and 0.03671 for train and test data respectively.

Correlation coefficient of GA-SVMR (b-spline) model (CC Train = 0.9897 and CC Test = 0.9741) is slightly better than GA-SVMR (spline) model, but considerably better than GA-SVMR (linear) model, whereas the performance of GA-SVMR (polynomial) model is better than GA-SVMR (rbf) and GA-SVMR (erbf) models with SI 0.08824 for test data, whereas, for rbf and erbf kernels it is 0.09133 and 0.09655 respectively. In comparison to GA-SVMR model with b-spline and spline kernel functions, SI and $RMSE$ is very high for GA-SVMR models with linear and erbf kernel function for test data (Table 5.13). It is noticed that the performance of these models depends on the better selection of SVM and kernel parameters. In case of polynomial kernel, the degree of the function d , when low; the function estimation is very bad, however, for higher d , performance is good. The optimal value of d in case of polynomial kernel function obtained by GAs is 6 and for b-spline kernel function it is 2. The optimal width (γ) obtained by GAs in case of rbf and erbf kernel functions

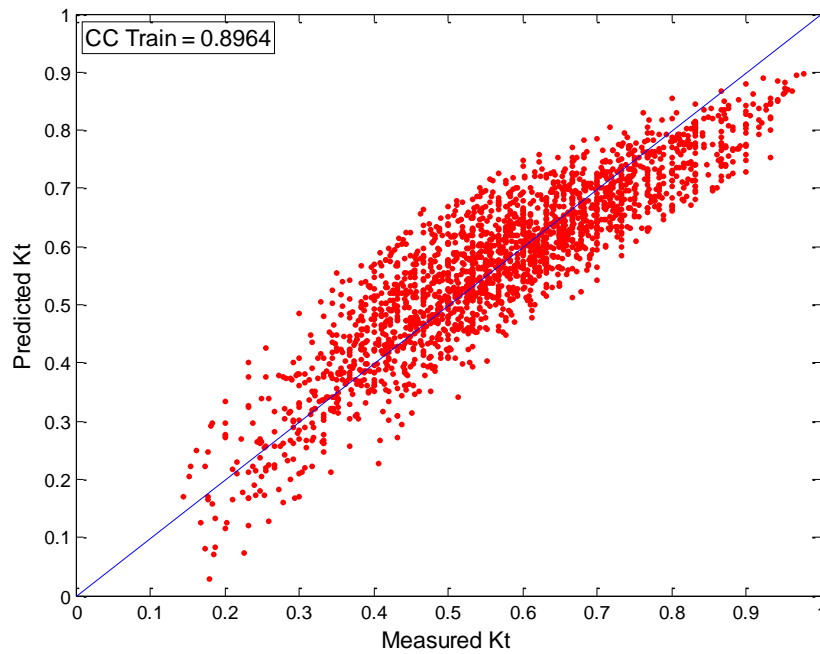
are 0.3 and 1 respectively. Kernel and SVM parameters obtained by GA (Table 5.14) is tested by using test data sets, which show better generalization performance with highest CC Test = 0.9741 for GA-SVMR (b-spline) model. By hybridizing GA with SVMR generalization performance of GA-SVMR shows improvement in terms of CC, *SI* and *RMSE* over SVMR models (Table 5.7 and 5.13).

The same data set has been used for estimating K_t using ANN2, ANFIS5 and SVMR (b-spline). CCs, *SI* and *RMSE* of K_t are shown in Table 5.15. From Tables 5.13 and 5.15, it is observed that the GA-SVMR (b-spline) model yields higher CCs as compared to that of ANN, SVMR and ANFIS models, whereas *RMSE* and *SI* values are higher in ANN and ANFIS models as compared to GA-SVMR (b-spline) model. However, the GA-SVMR model with linear kernel function has shown poor generalization, whereas, ANFIS model perform better than GA-SVMR models with polynomial, rbf and erbf kernel functions.

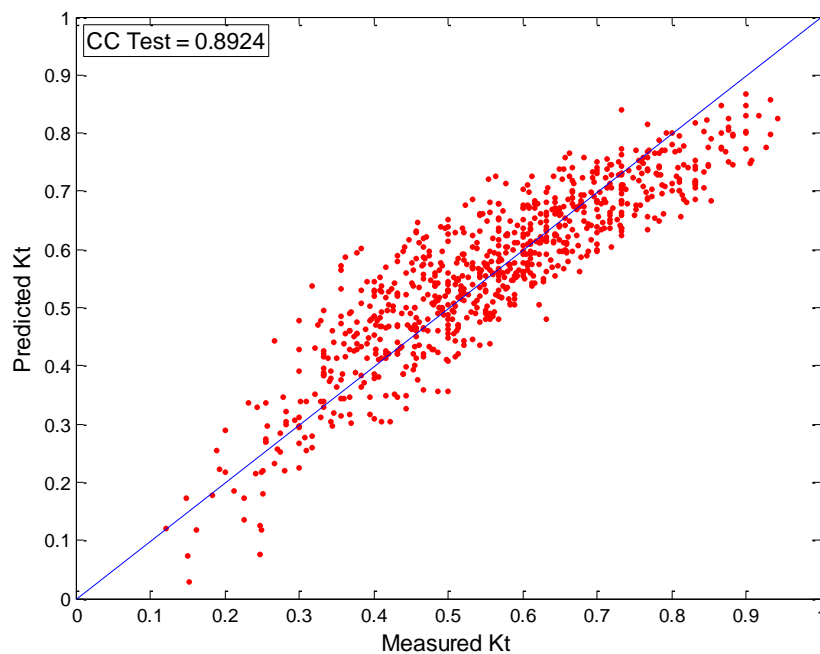
Table 5.15 ANN and ANFIS models with statistical measures

Model	CC Train	CC Test	Train Data		Test Data	
			<i>RMSE</i>	<i>SI</i>	<i>RMSE</i>	<i>SI</i>
ANN2	0.9537	0.9488	0.05176	0.09058	0.05395	0.09625
SVMR (b-spline)	0.9779	0.9685	0.03335	0.05837	0.03993	0.07125
ANFIS5	0.9723	0.9635	0.03727	0.06522	0.04307	0.07683

In SVM regression, the solution is unique for specific loss function, kernel type, and SVM and kernel parameters. If we run the same program, the results will be exactly the same. The model is much more complex and cannot be used in other implementations, whereas the results will not be same in case of ANN and ANFIS models.

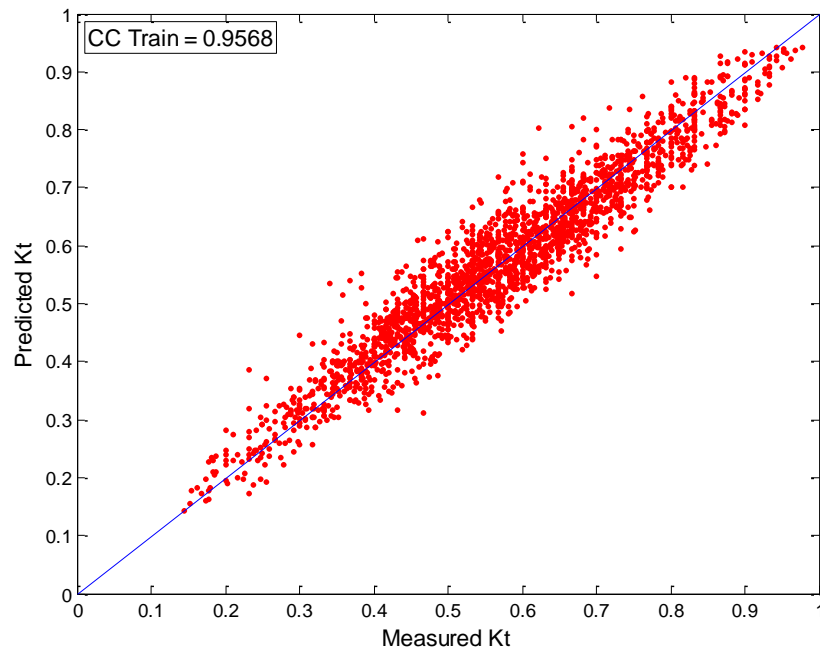


(a) Train Data

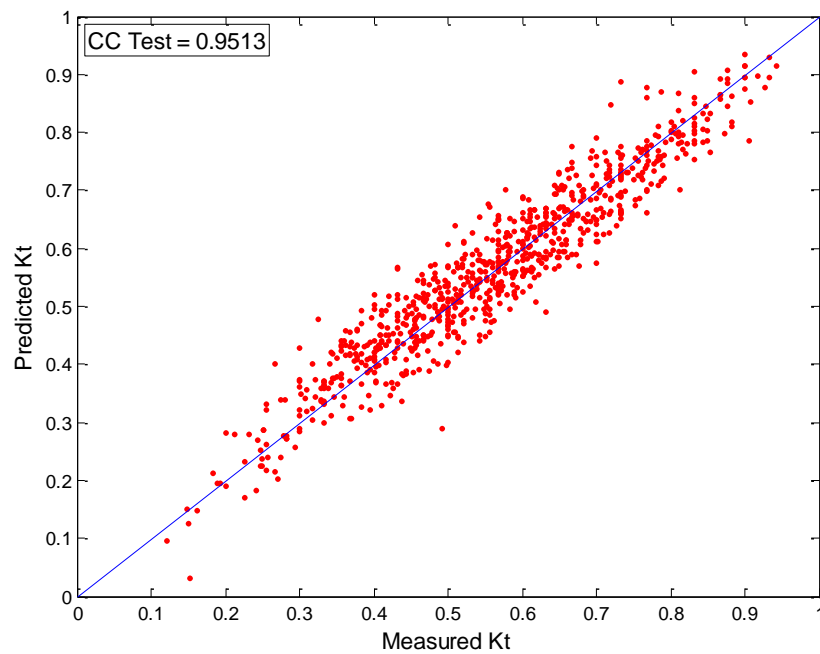


(b) Test Data

Fig. 5.21 Comparison of predicted and measured K_t for GA-SVMR (linear) model

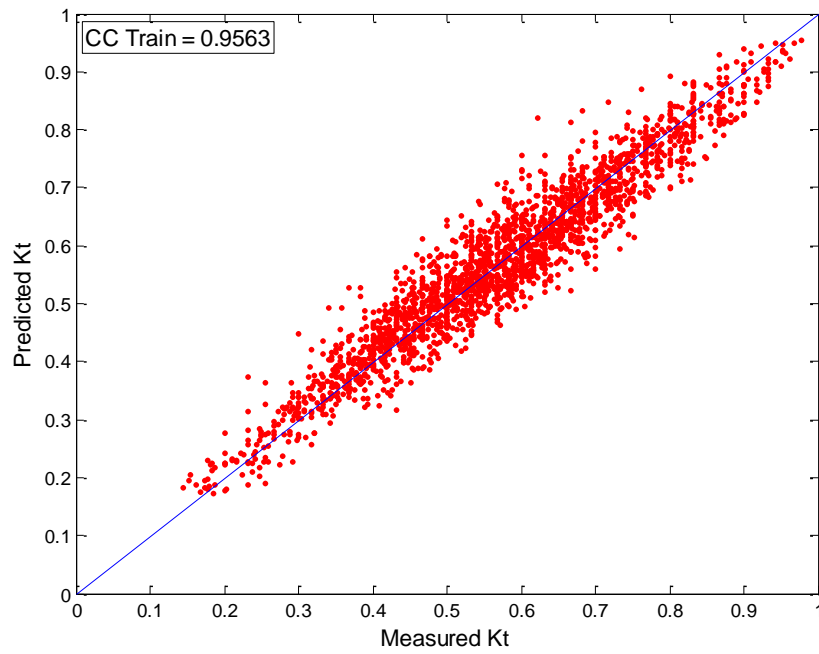


(a) Train Data

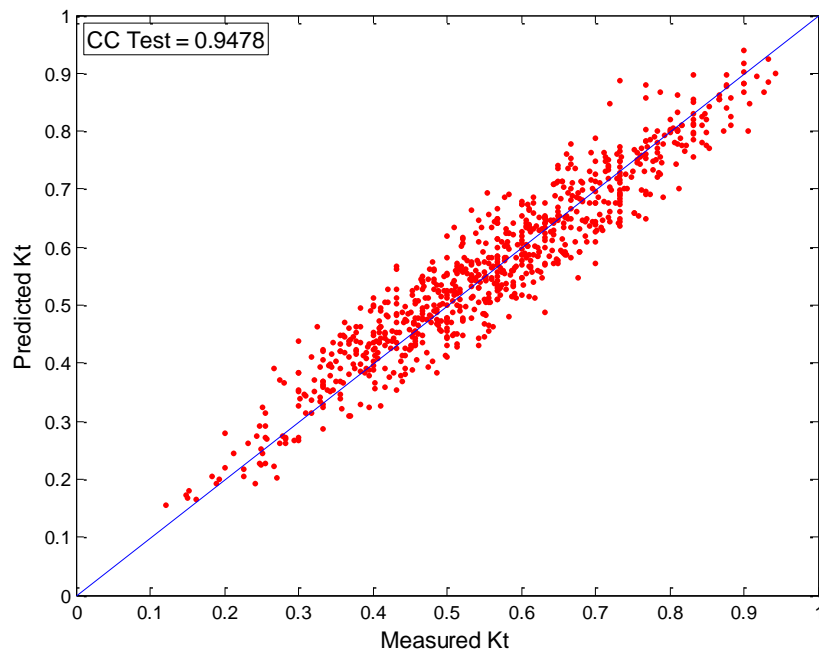


(b) Test Data

Fig. 5.22 Comparison of predicted and measured K_t for GA-SVMR (polynomial) model

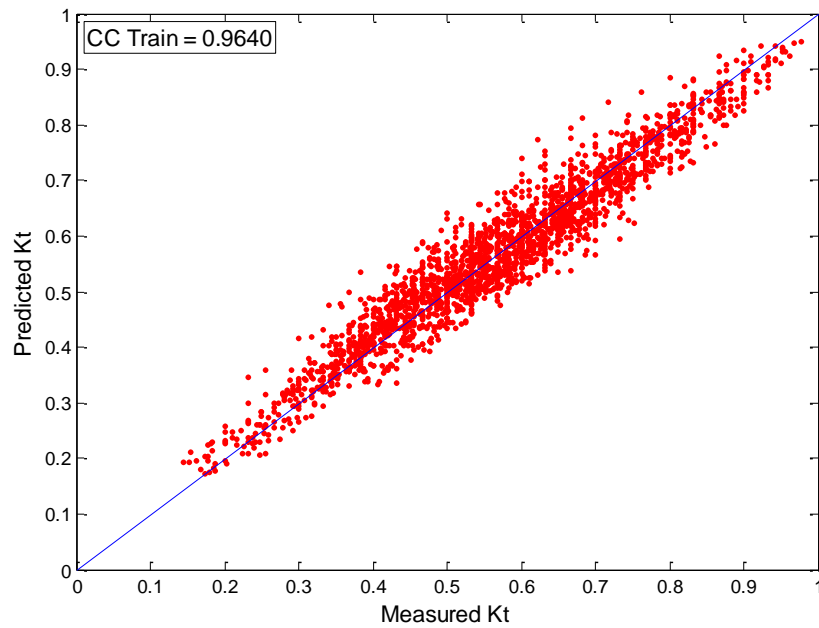


(a) Train Data

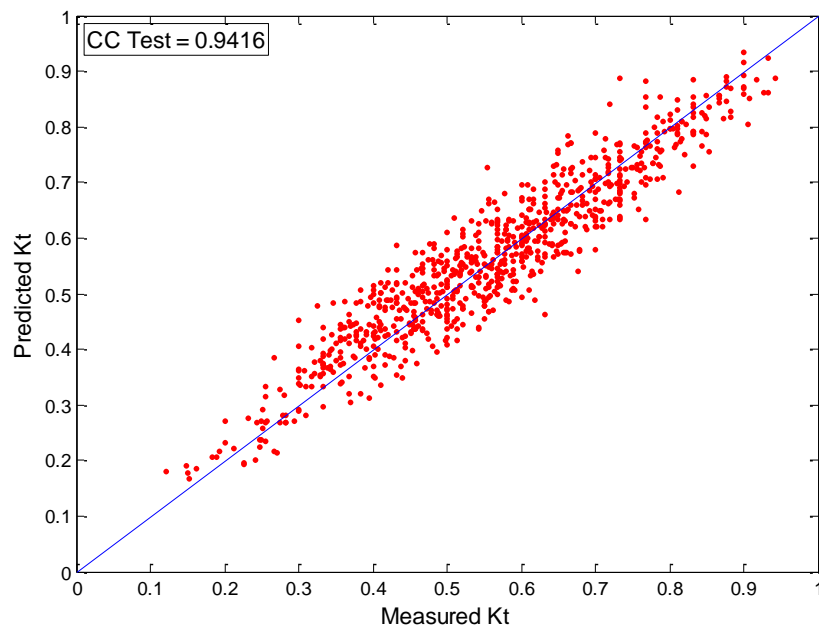


(b) Test Data

Fig. 5.23 Comparison of predicted and measured K_t for GA-SVMR (rbf) model

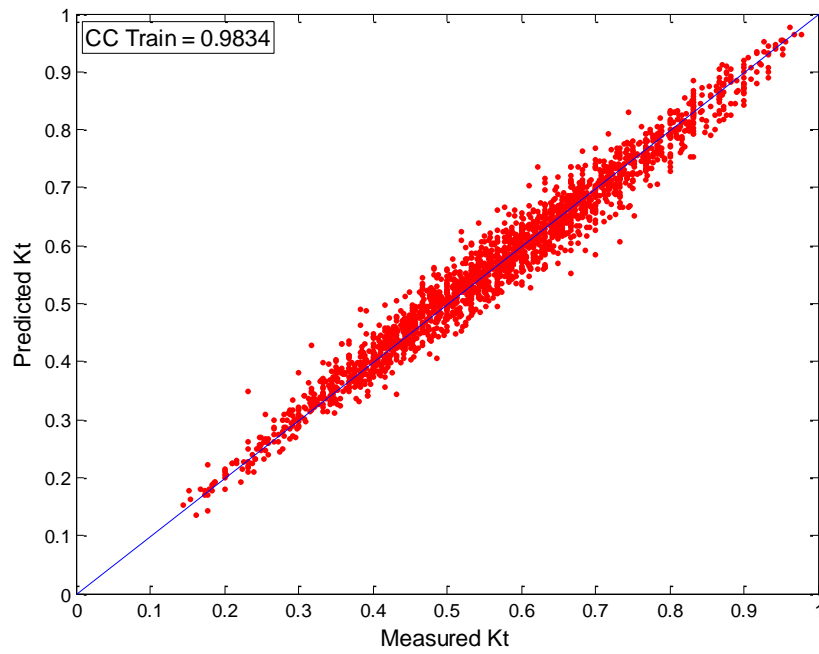


(a) Train Data

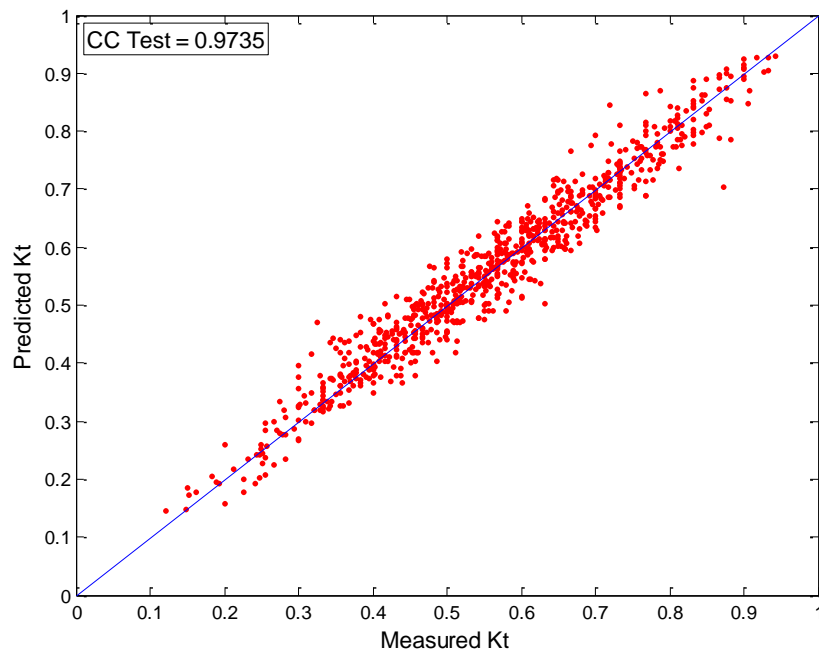


(b) Test Data

Fig. 5.24 Comparison of predicted and measured K_t for GA-SVMR (erbf) model

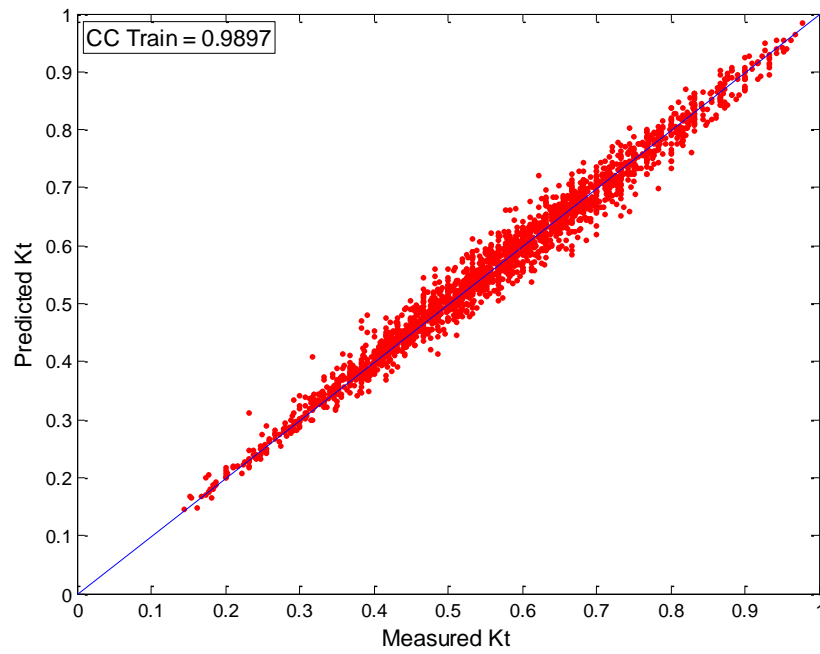


(a) Train Data

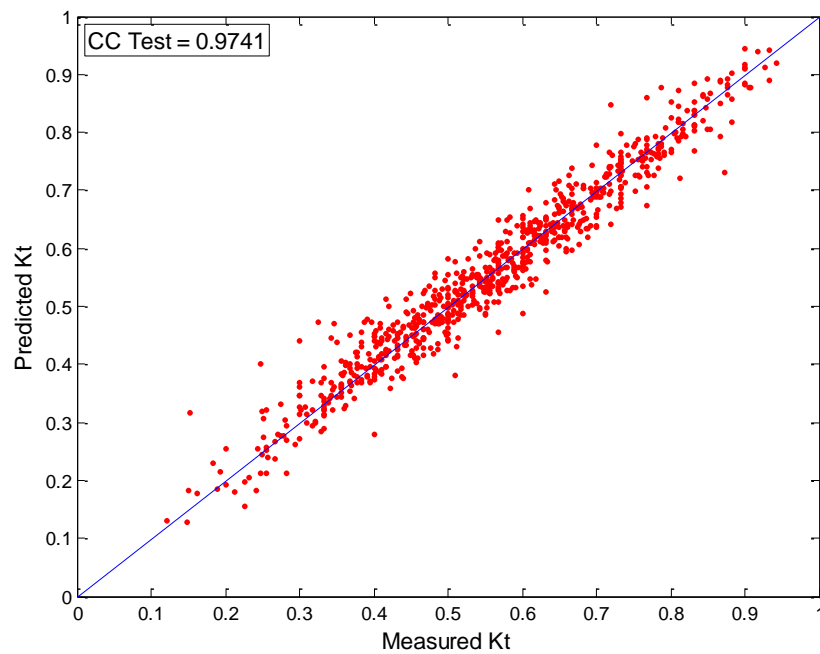


(b) Test Data

Fig. 5.25 Comparison of predicted and measured K_t for GA-SVMR (spline) model



(a) Train Data



(b) Test Data

Fig. 5.26 Comparison of predicted and measured K_t for GA-SVMR (b-spline) model

5.6 SUMMARY

In the present research work, An Artificial Neural Network (ANN) method has been applied for wave transmission prediction of multilayer floating breakwater. Two neural network models are constructed based on the parameters, which influence the wave transmission of floating breakwater. Training and testing of the network models are carried out for different hidden nodes and epochs. The results of network models are compared with the measured values. To study the performance of SVMR, six models were constructed. Effectiveness of these models are estimated using statistical measures such as *CC*, *SI* and *RMSE*. Further, six ANFIS models were developed to improve the results of ANN models. it is observed that there is an improvement in prediction of wave transmission through HIMMFPB over ANN models. Performance of SVMR models depends on the good settings of SVM and Kernel parameters. To optimize these parameters GA is hybridized with SVMR. Efficiency GA-SVMR with b-spline kernel function is excellent compared to ANN, ANFIS and SVMR.

CHAPTER 6

CONCLUSIONS

6.1 GENERAL

To solve real-world problems, like hydrodynamic performance of prediction of HIMMFPB by considering all the boundary conditions and extracting knowledge from large amount of experimental or in-situ data is extremely difficult as they are typically ill-defined systems and complex to model. In such cases, precise models are impractical, too expensive, or non-existent. Furthermore, the relevant available information is usually in the form of empirical prior knowledge and input-output data representing instances of the system's behavior. Therefore, we need an approximate reasoning system capable of handling such imperfect information. In this context CI models are developed, such as, ANN, ANFIS, SVMR and GA-SVMR. Each of these technologies provides us with complementary reasoning and searching methods to solve complex, real-world problems like wave transmission through HIMMFPB.

6.2 CONCLUSIONS

Based on the results of the present investigations and discussion thereon, following conclusions are arrived at:

- A high correlation coefficient (CC) is obtained at epoch equal to 200 with hidden nodes equal to four for ANN1 model with optimal S/D equal to five, whereas, ANN2 model has shown the similar trend with hidden nodes equal to five. In both models, non-linear transfer function *tansig* and linear transfer function *purelin* are used.

- K_t is better with increase in S/D values. ANN models show same trend. However, it is noticed that the CCs between measured and predicted K_t increase with S/D for ANFIS1, ANFIS2 and ANFIS3 models, whereas it is not true in case of ANFIS4 model. Increase or decrease in S/D ratio does not show a clear relation in increase or decrease of CCs while developing ANFIS models.
- Considering S/D as an input parameter there is a better CC between measured and predicted K_t . Compared with ANFIS1 and ANFIS2, S/D plays an important role as observed from ANFIS5. ANFIS5 model predictions are very realistic when compared with the measured values.
- Based on the PCA study, it is observed that S/D and W/L are the most significant parameters. Whereas, H_i/L is the least influencing parameter and variation of correlations coefficients (ANFIS5 and ANFIS6) is negligible. It is also concluded that S/D and W/L play an important role as inputs for training ANFIS.
- It is observed that hybrid models, such as ANFIS and GA-SVMR perform better than ANN and SVMR.
- Results also revealed that the efficiency of the ANFIS models depends on the number of membership functions associated with each input data. Highest correlation coefficient was obtained using the three bell shaped membership function.
- The performance of GA-SVMR appears to be highly influenced by the choice of its kernel function, and the good setting of kernel and SVM parameters. The b-spline kernel function performed superior than other kernel. It is also concluded that parameter selection in the case of GA-SVMR has a significant

effect on the performance of the model.

- GA-SVMR with b-spline kernel function performs better than ANN, SVMR and ANFIS models. Hence, it can replace the ANN, SVMR and ANFIS for wave transmission prediction of HIMMFPB.
- GA-SVMR can be utilized to provide a fast and reliable solution in prediction of the wave transmission for HIMMFPB, thereby making GA-SVMR as an alternate approach to map the wave structure interactions of HIMMFPB.

6.3 SUGGESTIONS FOR FUTURE WORK

There is scope for carrying out further research in developing computational intelligence models for designing the HIMMFPB. In this regard, the following suggestions may be considered for further study.

- Performance characteristics of Horizontal Interlaced Multi-layer Moored Floating Pipe Breakwaters with random waves may be studied.
- Studies on the influence of pipe diameter and spacing between the pipes on the performance characteristics of Horizontal Interlaced Multi-layer Moored Floating Pipe Breakwaters may be carried out.
- Studies on hybridizing latest computational intelligence techniques, such as, swarm intelligence, kernel principal component analysis, genetic programming etc., could be carried out for predicting the wave transmission of Horizontal Interlaced Multi-layer Moored Floating Pipe Breakwater.

6.4 SUMMARY

In this chapter, conclusions have been drawn regarding the performance of CI techniques in predicting wave transmission through HIMMFPB. Every care is taken to bring out all the conclusions that can be possibly drawn.

APPENDIX**MATLAB CODES FOR DEVELOPING CI MODELS**

(In the present work MATLAB 7 Release 14 was used to write the codes)

A-1 PROGRAM TO DEVELOP THE NETWORK MODEL ANN1 (ANN 3-4-1)

% Code for predicting K_t using network model 1

% (ANN 3-4-1) for $N = 5$ and $S/D = 5$

% Loading train data

Load E:\NITK\data\N5SD5\train\HID.txt

Load E:\NITK\data\N5SD5\train\HIL.txt

Load E:\NITK\data\N5SD5\train\WL.txt

Load E:\NITK\data\N5SD5\train\KT.txt

% Loading test data

Load E:\NITK\data\N5SD5\test\THID.txt

Load E:\NITK\data\N5SD5\test\THIL.txt

Load E:\NITK\data\N5SD5\test\TWL.txt

Load E:\NITK\data\N5SD5\test\TKT.txt

% Loading the ranges for train and test data

Load E:\NITK\data\N5SD5\range\RHID.txt

Load E:\NITK\data\N5SD5\range\RHIL.txt

Load E:\NITK\data\N5SD5\range\RWL.txt

% Train input vector

TRAIN_INPUT = [HID'; HIL'; WL'];

% Train output vector

TRAIN_OUTPUT = KT';

```
% Test input vector
TEST_INPUT = [THID'; THIL'; TWL'];

% Range matrix
RANGE = [RHID; RHIL; RWL];

% Creating a feedforward network
NET = newff (RANGE, [4,1], {'tansig', 'purelin'}, 'trainlm');

% Network parameters
NET.trainparam.show = 5;
NET. trainparam.epochs = 200;
NET. Trainparam.min_grd = 1.0e-3;
NET. Trainparam.goal = 1.0e-3;

% Training of network
NET = train (NET, TRAIN_INPUT, TRAIN_OUTPUT);

% Simulate the network with train data
SIMULATED_TRAINED_OUTPUT = sim(NET, TRAIN_INPUT);

% Simulate the network with test data
SIMULATED_TEST_OUTPUT = sim(NET, TEST_INPUT);

% Coefficient of correlation for training
ctrain = corrcoef (SIMULATED_TRAINED_OUTPUT', TRAIN_OUTPUT)
cTRAIN = ctrain (1,2)

% Coefficient of correlation for testing
ctest = corrcoef (SIMULATED_TEST_OUTPUT', TKT)
cTEST = ctest (1,2)
```

A-2 PROGRAM TO DEVELOP THE NETWORK MODEL ANN2 (ANN 4-5-1)

% Code for predicting K_r using network model 2

% (ANN 4-5-1) for $N = 5$ with combined data for S/D ratio 2, 3, 4 and 5.

% Loading train data

Load E:\NITK\data\N5SD5\train\SD.txt

Load E:\NITK\data\N5SD5\train\HID.txt

Load E:\NITK\data\N5SD5\train\HIL.txt

Load E:\NITK\data\N5SD5\train\WL.txt

Load E:\NITK\data\N5SD5\train\KT.txt

% Loading test data

Load E:\NITK\data\N5SD5\test\TSD.txt

Load E:\NITK\data\N5SD5\test\THID.txt

Load E:\NITK\data\N5SD5\test\THIL.txt

Load E:\NITK\data\N5SD5\test\TWL.txt

Load E:\NITK\data\N5SD5\test\TKT.txt

% Loading the ranges for train and test data

Load E:\NITK\data\N5SD5\range\RSD.txt

Load E:\NITK\data\N5SD5\range\RHID.txt

Load E:\NITK\data\N5SD5\range\RHIL.txt

Load E:\NITK\data\N5SD5\range\RWL.txt

% Train input vector

TRAIN_INPUT = [SD'; HID'; HIL'; WL'];

% Train output vector

TRAIN_OUTPUT = KT';

```
% Test input vector
TEST_INPUT = [TSD'; THID'; THIL'; TWL'];

% Range matrix
RANGE = [RSD'; RHID; RHIL; RWL];

% Creating a feedforward network
NET = newff (RANGE, [5,1], {'tansig', 'purelin'}, 'trainlm');

% Network parameters
NET.trainparam.show = 5;
NET. trainparam.epochs = 200;
NET. Trainparam.min_grd = 1.0e-3;
NET. Trainparam.goal = 1.0e-3;

% Training of network
NET = train (NET, TRAIN_INPUT, TRAIN_OUTPUT);

% Simulate the network with train data
SIMULATED_TRAINED_OUTPUT = sim (NET, TRAIN_INPUT);

% Simulate the network with test data
SIMULATED_TEST_OUTPUT = sim (NET, TEST_INPUT);

% Coefficient of correlation for training
ctrain = corrcoef (SIMULATED_TRAINED_OUTPUT', TRAIN_OUTPUT)
cTRAIN = ctrain (1,2)

% Coefficient of correlation for testing
ctest = corrcoef (SIMULATED_TEST_OUTPUT', TKT)
cTEST = ctest (1,2)
```

A-3 PROGRAM TO PLOT CORRELATION COEFFICIENT GRAPHS FOR 'KT'

% program to plot test CC graph for 'measured versus predicted' data

X = TKT; % Measures Kt

Y= SIMULATED_TEST_OUTPUT; % Predicted Kt

% Plots the measured values on the 'y' axis and the predicted on the 'x' axis

Plot (X, Y, 'r.');

hold on

% Plot a 45 degree line

Plot ([0:1], [0:1], 'b');

% axis ([xmin xmax ymin ymax])

% Sets the limits for the x and y axis of the current axes.

axis([0 1 0 1])

% Label on the X-axis

XLABEL ('Measured Kt')

% Label on the Y-axis

YLABEL ('Predicted Kt')

% Title for the Graph

title ('Correlation Coefficient between Predicted and Measured Kt')

% Display legend on the graph (CC % should be entered accordingly)

Legend ('CC test = xx.xx%');

% program to plot train CC graph for ‘measured versus predicted’ data

```
X = TKT; % Measures Kt
Y= SIMULATED_TRAINED_OUTPUT; % Predicted Kt

% Plots the measured values on the ‘y’ axis and the predicted on the ‘x’ axis
Plot (X, Y, ‘r.’);
hold on
% Plot a 45 degree line
Plot ( [0:1], [0:1], ‘b’);

% axis ( [xmin xmax ymin ymax] )
% Sets the limits for the x and y axis of the current axes.
axis( [0 1 0 1])

% Label on the X-axis
XLABLE (‘Measured Kt’)

% Label on the Y-axis
YLABLE (‘Predicted Kt’)

% Title for the Graph
title (‘Correlation Coefficient between Predicted and Measured Kt’)

% Display legend on the graph (CC % should be entered accordingly)
Legend (‘CC train = xx.xx%’);
```

% Plot of actual and measured Kt along x axis for training

% where x axis contains the number of data sets

%datasets should be set to total data sets minus one

Datasets = 2131

% Plot of Actual Kt along X axis

Plot ([0 : Datasets], KT, 'b x');

hold on

% Plot of Predicted Kt along X axis

Plot ([0 : Datasets], SIMULATED_TRAINED_OUTPUT, 'r.')

%axis ([xmin xmax ymin ymax])

%Sets the limits for the x and y axis of the current axes.

axis ([0 Datasets 0 1])

%Label on the Y-axis

YLABEL ('y-axis')

%Label on the X-axis

XLABEL ('x-axis')

%Display legend on the graph

Legend ('Predicted kt', 'Actual kt');

% Plot of actual and measured Kt along x axis for testing

% where x axis contains the number of data sets

%datasets should be set to total data sets minus one

Datasets = 812;

% Plot of Actual Kt along X axis

Plot ([0 : Datasets], KT, 'b x');

hold on

% Plot of Predicted Kt along X axis

Plot ([0 : Datasets], SIMULATED_TEST_OUTPUT, 'r.')

%axis ([xmin xmax ymin ymax])

%Sets the limits for the x and y axis of the current axes.

axis ([0 Datasets 0 1])

%Label on the Y-axis

YLABEL ('y-axis')

%Label on the X-axis

XLABEL ('x-axis')

%Display legend on the graph

Legend ('Predicted kt', 'Actual kt');

A-4 PROGRAM TO DEVELOP ANFIS 1-5 MODELS

% Code for predicting K_t using ANFIS1 (Same program is used for ANFIS2, ANFIS3, ANFIS4 by changing $S/D = 3, 4$ and 5 respectively and taking $S/D =$ Total

% (ANFIS1) for $N = 5$ and $S/D = 2$

% (ANFIS2) for $N = 5$ and $S/D = 3$

% (ANFIS3) for $N = 5$ and $S/D = 4$

% (ANFIS4) for $N = 5$ and $S/D = 5$

% (ANFIS5) for $N = 5$ and $S/D =$ Total

% Loading train data

Load E:\NITK\data\N5SD5\train\HID.txt

Load E:\NITK\data\N5SD5\train\HIL.txt

Load E:\NITK\data\N5SD5\train\WL.txt

Load E:\NITK\data\N5SD5\train\KT.txt

% Loading test data

Load E:\NITK\data\N5SD5\test\THID.txt

Load E:\NITK\data\N5SD5\test\THIL.txt

Load E:\NITK\data\N5SD5\test\TWL.txt

Load E:\NITK\data\N5SD5\test\TKT.txt

% Train input vector

Train1 = [HID'; HIL'; WL' 'KT'];

Train2 = [HID'; HIL'; WL'];

% Train output vector

mtrainoutput = KT';

% Test input vector

```
Test2 = [HID'; HIL'; WL'];
```

```
% Test output vector
```

```
mtestoutput = KT';
```

```
% anfis uses a hybrid learning algorithm to identify parameters of Sugeno-type fuzzy inference systems. It applies a combination of the least-squares method and the back- propagation gradient descent method for training FIS membership function parameters to emulate a given training data set.
```

```
%Number of Membership Functions and epochs are assigned to anfis function
```

```
% Here 3 is the number of membership function and 200 is the number of Epochs
```

```
% membership function and epochs vary depending on problem
```

```
anfis1=anfis (train1, 3,200,[0,0,0,0]);
```

```
% output1 is the predicted testoutput
```

```
output1=evalfis (test2, anfis1);
```

```
% Correlation coefficient between predicted test output and mtestoutput
```

```
cctest=corrcoef(output1,mtestoutput);
```

```
% output2 is the predicted train output
```

```
output2=evalfis(train2,anfis1);
```

```
% Correlation coefficient between predicted train output and mtrainoutput
```

```
cctrain=corrcoef(output2,mtrainoutput);
```

```
% plot of membership function for SD
```

```
plotmf (anfis1,'input',SD);
```

```
% plot of membership function for WL
plotmf (anfis1,'input',WL);

% plot of membership function for HID
plotmf (anfis1,'input',HID);
% plot of membership function for HIL
plotmf (anfis1,'input',HIL);

% Surface graph
gensurf(anfis1,[SD WL],KT);
gensurf(anfis1,[SD HIL],KT);
gensurf (anfis1,[SD HID],KT);
gensurf (anfis1,[WL HIL],KT);
gensurf (anfis1,[WL HID],KT);
gensurf (anfis1,[HIL HID],KT);

% Plot of predicted Kt versus Actual Kt for test and train data
plot (cctest, 'DisplayName','cctest', 'YDataSource', 'cctest'); figure(gcf)
plot (mtrainoutput,output2,'r. ');
hold on
plot ([0:1],[0:1],'b');
plot (mtestoutput,output1,'r. ');
hold on
plot([0:1],[0:1],'b');
```

A-5 PROGRAM TO DEVELOP ANFIS 6 MODELS

```
% Code for predicting  $K_r$  using ANFIS6 with  $S/D = \text{Total}$ 
% (ANFIS5) for  $N = 5$  and  $S/D = \text{Total}$ 

% Loading train data
Load E:\NITK\data\N5SD5\train\HID.txt
Load E:\NITK\data\N5SD5\train\WL.txt
Load E:\NITK\data\N5SD5\train\KT.txt

% Loading test data
Load E:\NITK\data\N5SD5\test\THID.txt
Load E:\NITK\data\N5SD5\test\TWL.txt
Load E:\NITK\data\N5SD5\test\TKT.txt

% Train input vector
Train1 = [HID'; WL' 'KT'];
Train2 = [HID'; WL'];

% Train output vector
mtrainoutput = KT';

% Test input vector
Test2 = [HID'; WL'];

% Test output vector
mtestoutput = KT';

% anfis uses a hybrid learning algorithm to identify parameters of Sugeno-type fuzzy
inference systems. It applies a combination of the least-squares method and the
back- propagation gradient descent method for training FIS membership function
parameters to emulate a given training data set.
```

```
%Number of Membership Functions and epochs are assigned to anfis function
% Here 3 is the number of membership function and 200 is the number of Epochs
% membership function and epochs vary depending on problem
anfis1=anfis (train1, 3, 200,[0,0,0,0]);

% output1 is the predicted testoutput
output1=evalfis (test2, anfis1);

% Correlation coefficient between predicted test output and mtestoutput
cctest=corrcoef(output1,mtestoutput);

% output2 is the predicted train output
output2=evalfis(train2,anfis1);

% Correlation coefficient between predicted train output and mtrainoutput
cctrain=corrcoef(output2,mtrainoutput);

% Plot of predicted Kt versus Actual Kt for test and train data
plot (cctest, 'DisplayName','cctest', 'YDataSource', 'cctest'); figure(gcf)
plot (mtrainoutput,output2,'r. ');
hold on
plot ([0:1],[0:1],'b');
plot (mtestoutput,output1,'r. ');
hold on
plot([0:1],[0:1],'b');
```

A-6 PROGRAM TO DEVELOP SVMR MODEL

% Code for predicting K , using SVMR $S/D = \text{Total}$

% (ANFIS1) for $N = 5$ and $S/D = 2$

% Loading train data

Load E:\NITK\data\N5SD5\train\HID.txt

Load E:\NITK\data\N5SD5\train\HIL.txt

Load E:\NITK\data\N5SD5\train\WL.txt

Load E:\NITK\data\N5SD5\train\KT.txt

% Loading test data

Load E:\NITK\data\N5SD5\test\THID.txt

Load E:\NITK\data\N5SD5\test\THIL.txt

Load E:\NITK\data\N5SD5\test\TWL.txt

Load E:\NITK\data\N5SD5\test\TKT.txt

% Train input vector

Train1 = [HID'; HIL'; WL' 'KT'];

Train2 = [HID'; HIL'; WL'];

% Train output vector

mtrainoutput = KT';

% Test input vector

Test2 = [HID'; HIL'; WL'];

% Test output vector

mtestoutput = KT';

```
% Initially assign the kernel function that is used, we have experimented with six
% kernel functions
ker='bspline';

% Here the kernel parameters are assigned
global p1 p2;
p1=2;

%SVR Support Vector Regression, here 15 is capacity factor, and 0.001 is error tube
% Performance of SVMR depends on good setting of SVM and Kernel parameters
[nsv, beta, bias] = svr (train1, mtrainoutput, ker, 15,'quadratic', 0.001);

% SVMR model give the predicted test output
ptestoutput = svroutput (train1, test2, ker, beta, bias);

% SVMR model give the predicted test output
ptrainoutput = svroutput (train1, train1, ker, beta,bias);

% Plot of predicted Kt versus Actual Kt for test and train data
plot (cctest, 'DisplayName','cctest', 'YDataSource', 'cctest'); figure(gcf)
plot (mtrainoutput, ptrainoutput,'r. ');
hold on
plot ([0:1],[0:1],'b');
plot (mtestoutput,ptestoutput,'r. ');
hold on
plot([0:1],[0:1],'b');
```

A-7 PROGRAM TO DEVELOP GA-SVMR MODEL

```

Clear
% assign the range of SVM and kernel parameters with lower and upper limits
dl=10; du=25; el=0; eu=1; fit_sum=0; prob_cross=0.8; prob_mut=0.1; incri=1;
gbest_obj=100000;
gen_no=input('Enter the number of generations ');
pop_size=input('Enter the population size ');
%nvar=input('Enter number of variables ');

% Initialization
d=round(dl+(du-dl)*rand(pop_size,1));
e=round(el+(eu-el)*rand(pop_size,1));
init_pop=[d,e];
pop=init_pop;
for i=1:gen_no; % Generation loop

% Fuction Evaluation
for i=1:pop_size,
    for j=1:2,
        ker='bspline';
        global p1 p2;
        p1=2;
        d1=pop(i,1);
        e1=pop(i,2);

%SVR Support Vector Regression
        [nsv, beta, bias] = svr(train1,mtrainoutput,ker,d1,'quadratic',e1);
        ptestoutput = svroutput(train1,test1,ker,beta,bias);
        cctest=corrcoef(ptestoutput,mtestoutput);
        c(i)=mtestoutput-ptestoutput;
    end
end
end

```

```
%Best solutions (pbest)
[pbest_obj,idx]=min(c);
pbest_a=pop(idx);
pbest_b=pop(idx,2);

%gbest
if pbest_obj<gbest_obj;
    gbest_obj=pbest_obj;
    gbest_a=pop(idx);
    gbest_b=pop(idx,2);
else
end

% Visualization
    %Fitness Evaluation
for i=1:pop_size,
    fit(i)=c(i);
end

%Calculation of Probability of selection
for i=1:pop_size,
    fit_sum=fit_sum+fit(i);
end
for i=1:pop_size,
    prob_sel(i)=fit(i)/fit_sum;
end
cum_prob=cumsum(prob_sel);

%Selection
rand_no=rand(pop_size,1);
for i=1:pop_size,
    for j=1:pop_size,
```

```
if rand_no(i)<cum_prob(j);
    m=j-1;
    if m>0;
        n=m;
    else
        n=1;
    end
    mat_pool(i,1)=pop(n,1);
    mat_pool(i,2)=pop(n,2);
    break
else

end

end

end

end

%Crossover
rand_no=rand(pop_size,1);
for i=1:pop_size,
    for j=1:2,    %Number of variables has to be used
        m=i;
        n=i+1;
        o=mod(n,2);
        if o==1;
            p=n-2;
        else
            p=n;
        end
    end
    if rand_no(i)<prob_cross;
        scal_fact=rand(pop_size,1)/10;
```

```

        off_spri(m,j)=round(mat_pool(m,j)+scal_fact(m)*(mat_pool(m,j)-
mat_pool(p,j)));
    else
        off_spri(i,j)=mat_pool(i,j);
    end
end
end
end

```

```

%Check for constraints

```

```

buffer=off_spri;

```

```

for i=1:pop_size,

```

```

    if (buffer(i,1)>=al)&(buffer(i,1)<=au);

```

```

        off_spri(i,1)=buffer(i,1);

```

```

    else

```

```

        off_spri(i,1)=mat_pool(i,1);

```

```

    end

```

```

    if (buffer(i,2)>=bl)&(buffer(i,2)<=bu);

```

```

        off_spri(i,2)=buffer(i,2);

```

```

    else

```

```

        off_spri(i,2)=mat_pool(i,2);

```

```

    end

```

```

end

```

```

% Mutation

```

```

rand_no=rand(pop_size,1);

```

```

for i=1:pop_size,

```

```

    for j=1:2,

```

```

        if rand_no(i)<prob_mut;

```

```

            mut_site=randint(1,1,[1,2]);

```

```

            rand_sign=rand();

```

```

            if j==mut_site;

```

```

                if rand_sign<0.5;

```

```

        pop(i,mut_site)=round(off_spri(i,mut_site)+incri);
    else
        pop(i,mut_site)=round(off_spri(i,mut_site)-incri);
    end
else
    pop(i,j)=off_spri(i,j);
end
else
    pop(i,j)=off_spri(i,j);
end
end
end

%Check for constraints
buffer=pop;
for i=1:pop_size,
    if (buffer(i,1)>=al)&(buffer(i,1)<=au);
        pop(i,1)=buffer(i,1);
    else
        pop(i,1)=off_spri(i,1);
    end
    if (buffer(i,2)>=bl)&(buffer(i,2)<=bu);
        pop(i,2)=buffer(i,2);
    else
        pop(i,2)=off_spri(i,2);
    end
end
end
gbest_obj
gbest_a
gbest_b

```

A-8 PROGRAM TO PERFORM PCA FOR A GIVEN DATA SET

```
function [signals, PC, V] = pca1(data)
% PCA1: Perform PCA using covariance.
% data - MxN matrix of input data
% (M dimensions, N trials)
% signals - MxN matrix of projected data
% PC - each column is a PC
% V - Mx1 matrix of variances
[M,N] = size (data);

% subtract off the mean for each dimension
mn = mean(data,2);
data = data - repmat(mn,1,N);

% calculate the covariance matrix
covariance = 1 / (N-1) * data * data';

% find the eigenvectors and eigenvalues
[PC, V] = eig(covariance);

% extract diagonal of matrix as vector
V = diag(V);

% sort the variances in decreasing order
[junk, rindices] = sort(-1*V);
V = V(rindices);
PC = PC(:,rindices);

% project the original data set
signals = PC' * data;
```


- Adee, B.H. and Martin, W. (1974). "Theoretical analysis of floating breakwater performance." *Proc., of the floating breakwater conference, Rhode Island*, 21-40.
- Altunkaynak, A. (2008). "Adaptive estimation of wave parameters by Geno-Kalman filtering." *Ocean Engineering*, 35, 1245-1251.
- Arunachalam, V.M. and Raman, H. (1980). "Discussion of design criteria for floating tire breakwater." *Journal of Waterway, Port, Coastal, and Ocean Engineering*, ASCE, 106(2), 296 - 298.
- Aydogan, B., Ayat, B., Ozturk, M. N., Cevik E.O. and Yuksel, Y. (2010). "Current velocity forecasting in straits with artificial neural networks, a case study: Strait of Istanbul." *Ocean Engineering*, 37, 443 – 453.
- Azm –A, A.G. and Gesraha, M.R. (2000). "Approximation to the hydrodynamics of floating pontoons under oblique waves." *Ocean Engineering* 27, 365–384.
- Bateni, S.M. and Jeng, D.S. (2007). "Estimation of pile group scour using adaptive neuro-fuzzy approach." *Ocean Engineering*, 34, 1344-1354.
- Bazartseren, B. (2005). "Applicability of artificial neural networks for investigating short-term developments of near shore morphology." PhD thesis, Lehtuhl Bauinformatil, BTU Cottbus (Germany).
- Beltrami, G.M. (2008). "An ANN algorithm for automatic, real-time tsunami detection in deep-sea level measurement." *Ocean Engineering*, 35, 572-587.
- Bezdek, j. (1996). "Computational intelligence defined–by everyone." *in: Computational Intelligence: Soft Computing and Fuzzy-Neuro Integration with Applications*, O. Kaynak et al. (Eds.), Springer Verlag, Germany.
- Bishop, T.C. (1982). "Floating tire breakwater design comparison." *Journal of Waterway, Port, Coastal, and Ocean, Engineering*, ASCE, 108(3), 421-426.

- Brebner, A. and Ofuya, A.O. (1968). "Floating breakwaters." *Proc., 11th Coastal Engineering Conference*, London, 1055–1094.
- Briggs, M., Ye, M., Demirbilek, Z. and Zhang, J. (2002). "Field and numerical comparisons of the RIBS floating breakwater." *Journal of Hydraulic Research*, 40(3), 289 – 301.
- Browne, M., Castelle, B., Strauss, D., Tomlinson, R., Blumenstein, M. and Lane, C. (2007). "Near-shore swell estimation from a global wind-wave model: spectral process, linear and artificial neural network." *Coastal Engineering*, 54, 445-460.
- Carr, J.H. (1951). "Mobile breakwaters." *Proc., 2nd Conference on Coastal Engineering*, Houston, 281- 294.
- Chang, H.K and Lin, L.C. (2006). "Multi-point tidal prediction using artificial neural network with tide-generating forces." *Coastal Engineering*, 53, 857-864.
- Chang, H.K. and Chien, W.A. (2006). "A fuzzy neural hybrid system of simulating typhoon waves." *Coastal Engineering*, 53, 737-748.
- Chen, K. and Wiegel, R.L. (1970). "Floating breakwaters for reservoir marinas." *Proc., 12th Coastal Engineering Conference*, Washington D.C, 647–1666.
- Cherkassky, V.Ma.Y. (2004). "Practical selection of SVM parameters and noise estimation for SVM regression." *Neural networks*, 17, 113-126.
- Deepak, J.C. (2006). "Laboratory investigations on horizontal interlaced multi-layer moored floating pipe breakwater." MTech thesis, Department of Applied Mechanics and Hydraulics, National Institute of Technology, Surathkal, Karnataka, India.
- Deo, M.C. and Jagdale, S.S. (2003). "Prediction of breaking waves with neural networks." *Ocean Engineering*, 30, 1163-1178.
- Deo, M.C. and Kumar, K.N. (2000). "Interpolation of wave heights." *Ocean Engineering*, 27, 907-919.

- Deo, M.C. and Naidu, S.C. (1999). "Real time wave forecasting using neural networks." *Ocean Engineering*, 26, 191-203.
- Deo, M.C., Jha, A., Chaphekar A.S. and Ravikant, K. (2001). "Neural networks for wave forecasting." *Ocean Engineering*, 28, 889-898.
- Drimer, N., Agnon, Y. and Stiassnie, M. (1992). "A simplified analytical model for a floating breakwater in water of finite depth." *Applied Ocean Research* 14, 33-41.
- El-bisy, M.S. (2007). "Bed changes at toe of inclined seawalls." *Ocean Engineering*, 34, 510-517.
- Fousert, M. W. (2006). "Floating Breakwater – A theoretical study of a dynamic wave attenuating system." Master thesis, Delft University of Technology, Faculty of Civil Engineering and Geosciences, section of Hydraulic Engineering.
- Gaur, S. and Deo, M.C. (2008). "Real-time wave forecasting using genetic programming." *Ocean Engineering*, 35, 1166-1172.
- Gesraha, R.G. (2006). "Analysis of Π shaped floating breakwater in oblique waves: I. Impervious rigid wave boards." *Applied Ocean Research* 28, 327–338.
- Gunaydin, K. (2008). "The estimation of monthly mean significant wave heights by using artificial neural network and regression methods." *Ocean Engineering*, 35, 1406-1415.
- Gunaydin, K. and Kabdashli, M.S. (2006). "Performance of solid and perforated U-type breakwaters under regular and irregular waves." *Ocean Engineering* 31, 1377–1405.
- Gunaydina, K. and Kaddasli, M.S. (2007). "Investigation of P-type breakwaters performance regular and irregular waves." *Ocean Engineering* 34, 1028–1043.
- Gunn, S.R. (1998). "Support vector machines for classification and regression." University of Southampton, Technical report, Image speech and intelligent Systems group.

- Guven, A., Azamathulla, H.Md. and Zakaria, N.A. (2009). "Linear genetic programming for prediction of circular pile scour." *Ocean Engineering*, 36, 985-991.
- Hagan, M. and Menhaj, M. (1994). "Training feedforward networks with the Marquardt algorithm." *IEEE Transactions on Neural Networks*, 5, pp. 989–993.
- Han, D., Chan, L. and Zhu, N. (2007). "Flood forecasting using support vector machines." *Journal of Hydroinformatics*, 09(4), 267-276.
- Harms, V.W. (1979). "Design criteria for floating tire breakwater." *Journal of Waterway, Port, Coastal, and Ocean Engineering, ASCE*, 106(2), 149-170.
- Harris, A.J. and Webber, N.B. (1968). "A floating breakwater." *Proc., 11th Coastal Engineering Conference*, London, 1049-1054.
- Hashemi M.R., Ghadampour Z. and Neill S.P. (2010). "Using an artificial neural network to model seasonal changes in beach profiles." *Ocean Engineering*, 37, 1345 – 1356.
- Headland, J.R. (1995). "Floating Breakwaters." *Marine structural engineering: specialized applications*, Gregory.P.Tsinker, Springer.
- Hegde, A.V., Kamath, K. and Magadam, A. S. (2007). "Performance Characteristics of Horizontal Interlaced Multilayer Moored Floating Pipe Breakwater." *Journal of Waterway, Port, Coastal and Ocean Engineering, ASCE*, 133(4), 275-285.
- Hermanson, M.W. (2003). "A physical modeling of floating breakwater with a membrane." M.S thesis report presented to the Civil and Coastal Engineering Department of University of Florida.
- Holland, J.H. (1975). "Adaption in natural and artificial system." The MIT Press, Massachusetts.

- Homma, M., Horikawa, K. and Mechizuki, H. (1964). “An experimental study on the floating breakwaters.” *Proc., 10th Annual Conference on coastal Engineering*, Japan, 44-149.
- Hong, D.C and Hong, S.Y. (2007). “Floating wave energy device with two Oscillating water columns.” *Proc., 26th International Conference on Offshore Mechanics and Arctic Engineering*, ASME, USA, Vol. 5, 425-432.
- Huang, W., Murray, C., Kraus, N. and Rosati, J. (2003). “Development of a regional neural network for coastal water level predictions.” *Ocean Engineering*, 30, 2275-2295.
- Huang, W., Murray, C., Kraus, N. and Rosati, J. (2003). “Development of a regional neural network for coastal water level predictions.” *Ocean Engineering*, 30, 2275-2295.
- Iglesias, G., Castro, A. and Fraguera, J.A. (2010). “Artificial intelligence applied to floating boom behaviour under waves and currents”. *Ocean Engineering*, 37, 1513 – 1521.
- Ippen, A.T. (1966). “Estuary and Coastal hydrodynamics.” *McGraw-Hill Book Company, Inc.*, New York.
- Ito, Y. and Chiba, S. (1972). “An approximate theory of floating breakwaters.” *Report of the Port and Harbor Research Institute, Ministry of Transport, Japan*, Vol. 11 (2), 138-213. (cross reference from Tsinker)
- Jagadisha, Y. S. (2007). “Laboratory investigations on horizontal interlaced multi-layer moored floating pipe breakwater model.” MTech thesis, Department of Applied Mechanics and Hydraulics, National Institute of Technology, Surathkal, Karnataka, India.
- Jang, J.S.R. (1993). “ANFIS: Adaptive–Networked–based Fuzzy Inference Systems.” *IEEE Transactions on Systems, Man, and Cybernetics*, 23(3), 665-685.
- Jang, J.S.R., Sun, C.T. and Mizutani, E. (1997). “Neuro-Fuzzy and Soft Computing.” PTR Prentice Hall.

- Jeng, D. S., Cha, D. and Blumenstein, M. (2004). "Neural network for the prediction of wave induced liquefaction potential." *Ocean Engineering*, 31, 2073-2086.
- Kalra, R. and Deo, M.C. (2007). "Derivation of coastal wind and wave parameters from offshore measurements of TOPEX satellite using ANN." *Coastal Engineering*, 54, 187-196.
- Kamat, K. (2010). "Hydrodynamics performance characteristics of horizontal interlaced multi-layer moored floating pipe breakwater – A Physical Model Study." Ph.D. thesis, Department of Applied Mechanics and Hydraulics, National Institute of Technology, Surathkal, Karnataka, India.
- Karatzoglou, A. and Meyer, D. (2006). "Support vectors machines in R." *Journal of statistical software*, 15, 1.
- Karla, R., Deo, M.C., Kumar, R. and Agarwal, V. K. (2005). "RBF network for spatial mapping of wave heights." *Marine Structures*, 18, 289-300.
- Kato, J., Noma, T., Uekita, Y. and Hagino, S. (1966). "Damping Effects of Floating Breakwaters." *Journal of Waterways and Harbors Division, ASCE*, 95(3), 337 – 344.
- Kazeminezhad, M. H., Etemad-shahidi, A. and Mousvi, S. J. (2005). "Application of fuzzy inference system in the prediction of wave parameters." *Ocean Engineering*, 32, 1709-1725.
- Kecman, V. (2001.) "Learning and Soft Computing, Support Vector Machines, Neural Networks, and Fuzzy Logic Models." The MIT Press, Cambridge, MA, USA.
- Kennedy, R. J. and Marsalek, J. (1968). "Flexible porous floating breakwater." *Proc., 11th Coastal Engineering Conference*, London, 1095-1103.
- Kim, D. H. and Park, W. S. (2005). "Neural network for design and reliability analysis of rubble mound breakwaters." *Ocean Engineering*, 32, 1332-1349.

- Kosko, B. (2003). "Neural Networks And Fuzzy Systems, A Dynamical System Approach to Machine Intelligence." *Prentice Hall of India Private Limited, New Delhi.*
- Leach, A.P., McDougal, G.W. and Solitt, K.C. (1985). "Hinged floating breakwater." *Journal of Waterway, Port, Coastal, and Ocean Engineering*, ASCE, 111(5), 895-920.
- Lee, T.L. (2004). "Back propagation neural network for long term tidal predictions." *Ocean Engineering*, 31, 225-238.
- Lee, T.L. (2006). "Neural network prediction of a storm surge." *Ocean Engineering*, 33, 483-494.
- Lee, T.L. and Jeng, D.S. (2002). "Application of artificial neural networks in tide forecasting." *Ocean Engineering*, 29, 1003-1022.
- Lee, T.L., Tsai, C.P., Lin, H.M. and Fang, C.J. (2009). "A combined thermographic analysis – neural network methodology for eroded caves in a sea wall." *Ocean Engineering*, 36, 1251-1257.
- Li, D., Panchang, V., Zhanxing, T., Demeribilek, J. and Ramdas, J. (2005). "Evaluation of an approximate method for incorporating floating docks in harbor wave prediction models." *Can. Journal of Civil Engineering* 32, 1082 – 1092.
- Liang, N., Huang, J. and Li, C. (2003). "A study of spar buoy floating breakwater." *Ocean Engineering Journal* 31, 43-60.
- Liang, S., Li, M. and Sun, Z. (2008). "Prediction models for tidal level including strong meteorologic effects using neural network." *Ocean Engineering*, 35, 666-675.
- Londhe, S.N. (2008). "Soft computing approach for real-time estimation of missing wave heights." *Ocean Engineering*, 35, 1080-1089.

- Londhe, S.N. and Deo, M.C. (2003). "Wave tranquility studies using neural networks." *Marine Structures*, 16, 419-436.
- Loukogeorgaki, E. and Agenlides, D.C. (2005). "Performance of Moored Floating Breakwaters." *International Journal of Offshore and Polar Engineering*, 15(4), 264–273.
- Macagno, E.O. (1953). "Fluid Mechanics experimental study of the effects of passage of a wave beneath a obstacle." *Proc., of Academic des Sciences, France*, 10-37.
- Magadum, A. S. (2005). "Laboratory investigations on horizontal interlaced multi-layer moored floating pipe breakwater model." MTech thesis, Department of Applied Mechanics and Hydraulics, National Institute of Technology, Surathkal, Karnataka, India.
- Mahjoobi, J. and Mosabbeb E.A. (2009). "Prediction of significant wave height using regressive support vector machines." *Ocean Engineering*, 36, 339-347.
- Mahjoobi, J. and Mosabbeb, E.A. (2009). "Prediction of significant wave height using regressive support vector machines." *Ocean Engineering*, 36, 339-347.
- Makarynskyy, O. (2004). "Improving wave predictions with artificial neural networks." *Ocean Engineering*, 31, 709-724.
- Makarynskyy, O., Piers-Silva, A.A., Markarynska, D. and Ventura-Soares. (2005). "Artificial neural networks in wave predictions at the west coast of Portugal." *Computers and Geosciences*, 31, 415-424.
- Malekmohamadi, I., Ghiassi, R. and Yazdanpanah, M.J. (2008). "Wave hindcasting by coupling numerical model and artificial neural networks." *Ocean Engineering*, 35, 417-425.
- Mandal, S. and Prabakaran, N. (2006). "Ocean wave forecasting using recurrent neural network." *Ocean Engineering*, 33, 1401-1410.

- Mandal, S., Rao, S. and Manjunatha, Y.R. (2007). “Stability analysis of rubble mound breakwater using ANN.” *Proc., Indian National Conference on Harbour and Ocean Engineering, INCHOE*, National Institute of Technology Karnataka, Surathkal, India, 551-560.
- Mandal, S., Rao, S. and Manjunatha, Y.R. (2008). “Stability prediction of berm breakwater using neural network.” *Proc., International conference on COPEDEC VII*, Dubai (UAE), 27, 1-11.
- Mandal, S., Rao, S. and Prabhakaran, N. (2001). “Wave forecasting using neural networks.” *Proc., International Conference in Ocean Engineering, ICOE*, Indian Institute of Technology, Madras, India, 103-108.
- Mandal, S., Rao, S. and Raju, D.H. (2005). “Ocean wave parameters estimation using back propagation neural network.” *Marine Structures*, 18, 301-318.
- Mani, J.S. (1991). “Design of Y-frame floating breakwater.” *Journal of Waterway, Port, Coastal, and Ocean Engineering*, ASCE, 117(2), 105-119.
- Mani, J.S. and Venugopal, C.R. (1987). “Wave transmission characteristics of floating barrier.” *Proc., 2nd National Conference on Dock and Harbour Engineering*, Madras, 54- 58.
- Mase, H. and Kitano, T. (1999) “Prediction model for occurrence of wave force.” *Ocean Engineering*, 26, 949–961.
- Mase, H., Sakamoto, M. and Sakai, T. (1995). “Neural network stability of rubble mound breakwaters.” *Journal of Waterway, Port, Coastal and Ocean Engineering*, ASCE, 121(6), 294-299.
- Masters, T. (1995). “Advanced Algorithms for Neural Networks: C++ Sourcebook.” John Wiley, Frankfurt, Germany.
- McCartney, L.B. (1985). “Floating breakwater design.” *Journal of Waterway, Port, Coastal, and Ocean Engineering*, ASCE, 111(2), 304-318.

- Mohandes, M., Halawani, T., Rehman, S. and Hussain. A.A. (2004). "Support vector machines for wind speed prediction." *Renewable Energy*, 29(6), 939–947.
- Msiza, I.S., Nelwamonda, F.V. and Marwala, T. (2008). "Water demand prediction using artificial neural networks and support vector regression." *Journal of computers*, 3, 1-8.
- Murali, K. and Mani, J.S. (1997). "Performance of cage floating breakwater." *Journal of Waterway, Port, Coastal, and Ocean Engineering ASCE*, 123(4), 172-179.
- Murlikrishna, I.N., Raman, H. and Sundar, V. (1987). "Performance of rigid floating breakwaters." *Indian National Conf., on Harbour and Ocean Engineering*, 67 - 79.
- Naithani, R. and Deo, M.C. (2005). "Estimation of wave spectral shapes using ANN." *Advances in Engineering Software*, 36, 750-756.
- Panizzo, A. and Briganti, R. (2007). "Analysis of wave transmission behind low crested breakwaters using neural networks." *Coastal Engineering*, 54, 643-656.
- Radhika, Y. and Shashi, M. (2009). "Atmospheric temperature prediction using support vector machines." *International journal of computer theory and engineering*, 1, 55-58.
- Rajasekaran, S., Gayathri, S. and Lee T.L. (2008). "Support vector regression methodology for storm surge prediction." *Ocean Engineering*, 35, 1578-1587.
- Rajasekaran, S., Gayathri, S. and Lee, T.L.(2008). "Support vector regression methodology for storm surge prediction." *Ocean Engineering*, 35, 1578-1587.
- Rajasekaran, S., Jeng, D.S. and Lee, T.L. (2005). "Tidal level forecasting during typhoon surge using functional and sequential learning neural networks." *Journal of Waterway, Port, Coastal and Ocean Engineering*, ASCE, 131(6), 321-324.

- Rajasekaran, S., Thiruvengataswamy, K. and Lee, T.L. (2006). "Tidal level forecasting using functional and sequential learning neural networks." *Applied Mathematical Modeling*, 30, 85-103.
- Rao, S. (2000). "Studies on performance of perforated pile breakwater." *Doctoral dissertation*, Mangalore University, Mangalore, India.
- Rao, S. and Mandal, S. (2005). "Hind casting of storm waves using neural networks." *Ocean Engineering*, 32, 667-684.
- Reikard, G. (2009). "Forecasting ocean wave energy: Tests of time-series models." *Ocean Engineering*, 36, 348-356.
- Ruol, P., Martinelli, L. and Zanuthigh, B. (2008). "Loads on floating breakwaters: effect of layout under irregular waves." *Proc., of Coastal Engineering conference*, 3875 -3887.
- Sannasiraj, S. A., Sundar, V. and Sundaravadivelu, R. (1998). "Mooring forces and motion response of pontoon-type floating breakwaters." *Ocean Engineering Journal* 25, 27-48.
- Sastry, J.S., Narasimhan, S. and Vethamony, P. (1985). "Model studies on tethered float breakwater system." *Proc., 11th Dock and Harbor Engineering*, Bombay, 1985, 273-286.
- Seymour, R. J. (1976). "Tethered float breakwaters a temporary wave protection system for open ocean construction." *Proc., Offshore Technology Conference*, Texas, 253-258.
- Shahidi, E.A. and Mahjoobi, J. (2009). "Comparison between M5' model tree and neural network for prediction of significant wave height in Lake Superior." *Ocean Engineering*, 36, 1175-1181.
- Shlens, J. (2009). "A Tutorial on Principal Component Analysis." Center for Neural Science, New York University New York City, NY 10003-6603 and Systems Neurobiology Laboratory Salk Institute for Biological Studies La Jolla, CA 92037.

- Smola, A. (1996). "Regression estimation with support vector learning machines." Technische Universitat Munchen.
- Stiassnie, M. and Drimer, N. (2003). "On a freely floating porous box in shallow water waves." *Applied Ocean Research* 25, 263-268.
- Sundar, V., Sundaravadivelu, R. and Purushotham, S. (2003). "Hydrodynamic characteristics of moored floating pipe breakwater in random waves." *Proc., Institution of Mechanical Engineers, J. Engrg. Maritime Environment*, 217(M), 95-108.
- Sylaios, G., Bouchette, F., Tsihrintziz, V.A. and Denamiel C. (2009). "A fuzzy inference system for wind wave modeling." *Ocean Engineering*, 36, 1358-1365.
- Takagi, T. and Sugeno, M. (1985). "Fuzzy Identification of Systems and Its Applications to Modeling and Control." *IEEE Transactions on System, Man, and Cybernetics*, 5(1), 116-132.
- Tay, Z.Y, Wang, C.M. and Utsunomiya, T. (2009). "Hydro elastic responses and interactions of floating fuel storage modules placed side-by-side with floating breakwaters." *Marine Structures*, 22, 633–658.
- Tsai, C.P., Lin, C. and Shen, J. N. (2002). "Neural network for wave forecasting among multi stations." *Ocean Engineering*, 29, 1683-1695.
- Tsay, T.-K. and Liu, P.L.-F. (1983). "A finite element model for wave refraction and diffraction." *Applied Ocean Research*, 5, 30–37.
- Tseng, C.M., Jan, C.D., Wang, J.S. and Wang, C.M. (2007). "Application of artificial neural networks in typhoon surge forecasting." *Ocean Engineering*, 34, 1757 – 1768.
- Ultsch, A., and Roske, F. (2002). "Self-organizing feature maps predicting sea levels." *Information Sciences*, 144(1-4), 91-125.

- Valioulis, I.A. (1990). "Motion Response and Wave Attenuation of Linked Floating Breakwaters." *Journal of the Waterway, Port, Coastal and Ocean Division*, ASCE, 116(5), 558-574.
- Vapnik, V. (1998). "Statistical Learning Theory." John Wiley and Sons, New York.
- Verhaeghe, H., Rouk, J.D. and Meer, J.V.D. (2008). "Combined classifier-quantifier model: A 2-phases neural model for prediction of wave overtopping at coastal structures." *Coastal Engineering*, 55, 357-374.
- Vethamony, P. (1995). "Wave attenuation characteristics of a tethered float system." *Ocean Engineering*, 22, 111-129.
- Wang, L.X. (1994). "Adaptive Fuzzy Systems and Control, Design and Stability Analysis". PTR Prentice Hall.
- Wang, L.X. (1997). "A Course in Fuzzy Systems and Control." PTR Prentice Hall.
- Wilamoski, B.M., Iplikci, S., Kaynak, O. and Efe, O.M. (2001). "An algorithm for fast convergence in training neural networks." *IEEE on Neural Network*, 1778-1782.
- William, A.N. and Abul-Azm, A.H. (1997). "Dual pontoon floating breakwater.", *Ocean Engineering Journal* 27, 465-478.
- Williams, A.N, Lee, H.S. and Huang, Z. (2000). "Floating pontoon breakwaters." *Ocean Engineering*, 27, 221-240.
- Williams, A.N. and McDougal, W.G. (1996). "A Dynamic Submerged Breakwater." *Journal of Waterway, Port, Coastal, and Ocean Engineering*, ASCE, 122(6), 288-296.
- Williams, A.N., Geiger, P.T. and McDougal, W.G. (1991). "Flexible Floating Breakwater." *Journal of Waterway, Port, Coastal and Ocean Division*, ASCE, 117(5), 429-449.

- Yagci, O., Mercan, D. E., Cigizoglu and Kabdasli, M. S. (2005). “Artificial intelligence methods in breakwater damage ratio estimation.” *Ocean Engineering*, 32, 2088-2106.
- Yamamoto, T., Yoshida, A. and Ijima, T. (1980). “Dynamics of elastically moored floating objects.” *Applied Ocean Research*, 2, 85 – 92.
- Yoon, H., Jun, S-C., Hyun, Y., Bae, G-O. and Lee, K-K. (2011). “A comparative study of artificial neural networks and support vector machines for predicting groundwater levels in a coastal aquifer”. *Journal Hydrology*, 396, 128–138.
- Zadeh, L. (1998). “Roles of soft computing and fuzzy logic in the conception, design and deployment of information/intelligent systems.” in: *Computational Intelligence: Soft Computing and Fuzzy-Neuro Integration with Applications*, O. Kaynak et al. (Eds.), Springer Verlag, Germany, 1-9.
- Zadeh, L.A. (1965). “Fuzzy Sets” *Information and Control*, 8, 338-353.
- Zamani, A., Solomatine, D., Azimian, A. and Heemink, A. (2008). “Learning from data for wind-wave forecasting.” *Ocean Engineering*, 35, 953-962.

PUBLICATIONS FROM PRESENT WORK

International Journals

1. **Patil, S.G.**, Mandal, S., Hegde, A. V. (2012). “Genetic algorithm based support vector machine regression in predicting wave transmission of horizontally interlaced multi-layer moored floating pipe breakwater”, *Advances in Engineering Software*, Vol. 45, pp. 203-212.
2. **Patil, S. G.**, Mandal, S., Hegde, A.V., and Srinivasan Alavandar (2011). “Neuro-Fuzzy based Approach for Wave Transmission Prediction of Horizontally Interlaced Multilayer Moored Floating Pipe Breakwater”, *Ocean Engineering*, Vol. 38, pp. 186-196.


International Conferences

3. **Patil, S. G.**, Mandal, S., Hegde, A. V. and A. Muruganandam. “Hybrid Genetic Algorithm Tuned Support Vector Machine Regression for Wave Transmission Prediction of Horizontally Interlaced Multilayer Moored Floating Pipe Breakwater”, *In: Proceedings of the 13th International Conference on International Association for Computer Methods and Advances in Geomechanics, IACMAG, Melbourne, Australia.* 9-11 May 2011, Vol. 1, pp. 557-563.
4. Mandal, S., Vishal Kumar, Hegde, A. V. and **Patil, S. G.** “Estimating transmitted waves of floating breakwater using support vector regression model”, *In: Proceedings of the 3rd International Congress on Computational Mechanics and Simulation, IIT-Bombay, Powai, Mumbai India.* 1-5 December. 2009, pp. 173-174.
5. Mandal, S., **Patil, S. G.** and Hegde, A. V. “Wave transmission prediction of multilayer floating breakwater using neural network”, *In: Proceedings of the 3rd*

International Conference in Ocean Engineering, ICOE, at IIT Madras, Chennai, India. 1-5 February 2009, pp. 574-585.

6. Mandal, S., **Patil, S. G.**, Manjunatha, Y. R. and Hegde, A. V. “Application of neural networks in coastal engineering- an overview”, *In: Proceedings of the 12th International Conference on International Association for Computer Methods and Advances in Geomechanics, IACMAG, Goa, India. 1-6 October 2008, pp. 1639-1645.*

Resume

Name : Sanjay Govind Patil 

Date of Birth : 31 - 08 - 1973

Address : Department of Built and Natural Environment,
Caledonian College of Engineering, Muscat,
PB No 2322, CPO Seeb-111,
Sultanate of Oman.

Telephone : (91-832) 2444602; 00919420818782

Email : sanras5@gmail.com

Designation : Deputy Head of Department

Qualification : B.E (Civil Engineering), M.Tech (Structures)

Area of Specialization : Structural Engineering

No. of years of Teaching Experience : 10 years

No. of years of Industrial Experience : 02 years

Membership of recognized
professional organizations : CIOB, ASCE

Journal Publication : 02

No. of Conference Presentations : International: 04

No. of UG Dissertations guided : 11